STUDY OF POLAR ORDERING IN ORDERED AND PARTIAL DISORDERED FERROELECTRIC SYSTEMS

Nikola Novak

Doctoral Dissertation
Jožef Stefan International Postgraduate School
Ljubljana, Slovenia, March, 2013

Evaluation Board:

Prof. Dr. Boštjan Zalar, Chairman, Jožef Stefan Institute, Jamova 39, Ljubljana, Slovenia

Asst. Prof. Vid Bobnar, Member, Jožef Stefan Institute, Jamova 39, Ljubljana, Slovenia

Prof. Dr. Horst Beige, Member, Martin-Luther-Universität Halle-Wittenberg, Von-Danckelmann-Platz 3, Halle, Germany

MEDNARODNA PODIPLOMSKA ŠOLA JOŽEFA STEFANA
JOŽEF STEFAN INTERNATIONAL POSTGRADUATE SCHOOL

Nikola Novak

STUDY OF POLAR ORDERING IN ORDERED AND PARTIAL DISORDERED FERROELECTRIC SYSTEMS

Doctoral Dissertation

ŠTUDIJA POLARNEGA UREJANJA V UREJENIH IN DELNO NEUREJENIH FEROELEKTRIČNIH SISTEMIH

Doktorska disertacija

Supervisor: Prof. Dr. Zdravko Kutnjak

Ljubljana, Slovenia, March 2013

Index

Abstract

This work presents experimental studies of ordering phenomena, electromechanical and electrocaloric properties in single crystal, ceramic and solid solution relaxor ferroelectrics and single crystal ferroelectric materials. The main aim of investigations is to prove the existence of a liquid-vapor critical point in these systems and to verify its impact on physical properties, such as electromechanical and electrocaloric response.

In the first part, the study of relaxor ferroelectric single crystal $Pb(Mg_{1/3}Nb_{2/3})O_3$ (PMN) oriented along the [110] direction performed via polarization and calorimetric measurements is presented. Motivated by the long-standing unresolved enigma of the relaxor ferroelectric ground state, a high-resolution heat capacity and polarization experiments were performed in the vicinity of the field-induced ferroelectric phase transition in the relaxor ferroelectric single crystal PMN. It is shown that the discontinuous evolution of the polarization as a function of the electric field or temperature is a consequence of a true first-order transition from a glassy to ferroelectric state, which is accompanied by an excess heat capacity anomaly and released latent heat. It is also shown that in a zero field, there is no ferroelectric phase transition in bulk PMN at any temperature, indicating that the nonergodic dipolar glass phase persists down to the lowest temperatures. Furthermore, the detailed study of the latent heat reveals that the first-order phase transition line ends in the liquid-vapor critical point. In addition, the presented calorimetric results are shown to be in a good agreement with the upgraded version of the spherical random bond random field model developed by R. Pirc. The presence of the critical point is tested also in a relaxor ceramic $Pb_{(1-x)}La_x(Zr_yTi_{(1-y)})_{(1-x/4)}O_3$ (PLZT) with relaxor composition 9/65/35 and ferroelectric single crystal $BaTiO_3$ oriented in [001] direction. The heterogeneity, typical for the ceramic material, plays an important rule in the observed smeared position of the critical point. On the other hand, a cubic to tetragonal first-order phase transition line in $BaTiO_3$ ferroelectric clearly ends in a sharply defined critical point.

The second part of the work is devoted to the influence of the critical point on electromechanical and electrocaloric response in solid solution $Pb(Mg_{1/3}Nb_{2/3})O_3$-$0.26PbTiO_3$ (PMN-0.26PT) oriented in [100] direction and ferroelectric single crystal $BaTiO_3$ oriented in [001] direction. Special attention is paid to the mechanism responsible for the enhancement of the piezoelectric coefficient in PMN-0.26PT and $BaTiO_3$, material with and without morphotropic phase boundary, respectively. The results obtained in both materials suggest that the proximity of the critical point is a driving mechanism for the enhancement of piezoelectric responses and not the presence of the morphotropic phase boundary. In addition, the influence of the proximity of critical point on the electrocaloric (EC) response in the $BaTiO_3$ ferroelectric single crystal was investigated. In particular, the temperature change related to the released latent heat at the first-order cubic to tetragonal phase transition and the temperature change related to the continuous variation of the polarization due to the applied electric field were studied. The experimental results show the shift of EC responsivity maximum away from the critical point. It is suggested that the shift of the EC responsivity maximum is directly related to the ratio between two electrocaloric contributions, i.e., the relatively large amount of the released latent heat at the paraelectric to ferroelectric phase transition and the contribution related to the

continuous variation of the polarization. The amount of the released latent heat decreases fast when approaching the critical point and accordingly the corresponding electrocaloric contribution cannot be compensated by the electrocaloric contribution stemming from continuous variations of the polarization. This results in decreasing of the EC responsivity when approaching the critical point and consequently in the shift of the EC responsivity maximum away from the critical point.

The main purpose of the doctoral dissertation is to better understand critical physical mechanisms responsible for the enhancement of certain physical properties of advanced ferroelectric and relaxor materials which are important for the engineering of new high technology devices, such as novel advanced sensors, actuators, temperature controlling elements, ultrasound generators etc.

Povzetek

V doktorski disertaciji so predstavljeni eksperimentalni rezultati študije štirih različnih materialov: relaksorskega feroelektričnega kristala, keramike in trdne raztopine ter feroelektričnega kristala. Študija je posvečena potrditvi obstoja kritične točke v teh snoveh in njenem vplivu na elektromehanski in elektrokalorični odziv.

Prvi del predstavlja raziskave obstoja kritične točke v kristalu relaksorskega feroelektrika $Pb(Mg_{1/3}Nb_{2/3})O_3$ (PMN), orientiranega vzdolž [110] smeri, relaksorski keramiki $Pb_{(1-x)}La_x(Zr_yTi_{(1-y)})_{(1-x/4)}O_3$ (PLZT) z relaksorsko sestavo 9/65/35 in feroelektričnem kristalu $BaTiO_3$, orientiranem vzdolž [001] smeri. Osrednji del raziskav prvega dela je namenjen reševanju vprašanja narave osnovnega relaksorskega stanja v PMN relaksorju. Predstavljene polarizacijske in kalorimetrične meritve sovpadajo med seboj in podpirajo tezo, da je osnovno relaksorsko stanje steklasto in ne nanodomensko feroelektrično stanje, zamrznjeno pod vplivom slučajnih polj. Ključen dokaz za podporo omenjene trditve predstavlja anomalija, ki jo kaže toplotna kapaciteta na mestu feroelektričnega prehoda, induciranega z električnim poljem. Anomalija se pojavi samo v primeru če je električno polje dovolj veliko, da inducira feroelektrično fazo, medtem ko pri nizkih električnih poljih ali pri polju nič anomalija izgine. Drugi dokaz, ki podpira obstoj steklastega osnovnega stanja v relaksorjih je prisotnost latentne toplote. Sproščena latentna toplota je znak, da gre za fazni prehod prvega reda med steklasto in feroelektrično fazo in je v primeru prehoda iz nanodomenske v mikrodomensko feroelektrično stanje s slučajnimi polji ne bi opazili. Nadaljna natančnejša študija latentne toplote je še pokazala, da se linija faznega prehoda prvega reda v [110] PMN konča v kritični točki. Predstavljeni rezultati so prav tako v skladu s teoretičnim sferičnim modelom naključnih vezi in naključnih polj (SRBRF), ki ga je razvil Raša Pirc. Njegova nadgradnja modela je pokazala, da izračunano obnašanje toplotne kapacitete kvalitativno opiše eksperimentalno obnašanje. Poleg relaksorskega kristala smo študirali tudi relaksorsko keramiko in obstoj kritične točke v tem materialu. Meritve latentne toplote so pokazale, da ta sicer počasi izginja, vendar ne izgine popolnoma tudi pri višjih temperaturah. To nakazuje dejstvo, da kritična točka v keramiki ni ostro določena, ampak je razmazana v določenem področju faznega diagrama električnega polja in temperature. Predpostavljamo, da je za razmazanost kritične točke odgovorna izotropnost keramike. Obstoj ostro določene kritične točke pa je bil dokazan v študiji linije faznega prehoda iz kubične v tetragonalno fazo feroelektričnega kristala $BaTiO_3$.

Drugi del disertacije zajema študijo elektromehanskega in elektrokaloričnega odziva ter vpliv bližine kritične točke na te lastnosti. Elektromehanski odziv je bil raziskan v dveh sistemih $Pb(Mg_{1/3}Nb_{2/3})O_3$-$_{0.26}PbTiO_3$ (PMN-$_{0.26}$PT) relaksorju ter feroelektriku $BaTiO_3$. Pri tem je relaksor blizu morfotropne fazne meje, feroelektrik $BaTiO_3$ pa sploh nima morfotropne meje. Posebna pozornost je bila tako namenjena raziskavi vpliva morfotropne fazne meje na piezoelektrični odziv. Analiza piezoelektričnega odziva PMN-0.26PT kristala kaže na to, da je ojačitev piezoelektričnega odziva povezana s kritičnim obnašanjem enega izmed višjih faznih prehodov. Da je ojačitev piezoelektričnega odziva povezana s prisotnostjo kritične točke in fluktuacijami v bližini le-te ter posledično divergence susceptibilnosti, potrjujeo meritve piezoelektričnega koeficienta v $BaTiO_3$, ki kažejo maksimum te količine v bližini kritične točke. Obe študiji nakazujeta na to, da za

ojačitev piezoelektričnega odziva ni nujna prisotnost MPB ter da je mehanizem ojačitve povezan z bližino kritične točke. Poleg vpliva kritične točke na ojačitev piezoelektričnega odziva nas je zanimal tudi vpliv na elektrokalorični odziv. V preteklosti je bilo že pokazano za različne inorganske relaksorske in organske feroelektrične ter relaksorske materiale, da je elektrokalorična (EC) odzivnost največja v bližini kritične točke. Zelo malo raziskav je bilo narejenih na feroelektričnih kristalih, kot na primer $BaTiO_3$, za katerega je znano, da ima feroelektrični fazni prehod prvega reda, pri katerem se sprosti znatno večja količina latentne toplote kot v relaksorskih sistemih. Pri raziskavi EC odzivnosti smo se tako osredotočili na vpliv razmerja med spremembo temperature, povezane z latentno toploto, in spremembo temperature, povezane z vlečenjem polarizacije zaradi povečevanja električnega polja. Meritve so pokazale, da se vrh EC odzivnosti odmakne od kritične točke. Vzrok za ta zamik pripisujemo količini sproščene latentne toplote, ki hitro pada, ko se približujemo kritični točki, medtem ko drugi del, povezan z zveznim spreminjanjem polarizacije, ne uspe kompenzirati spremembe temperature.

Namen doktorske disertacije je, da prispeva k boljšemu razumevanju naprednih relaksorskih in feroelektričnih materialov in fizikalnih mehanizmov, ki so odgovorni za ojačitev določenih fizikalnih lastnosti, pomembnih za razvoj novih visokotehnoloških izdelkov, kot so napredni senzorji, aktuatorji, elementi regulacije temperature, izvori ultrazvoka itd.

Abbreviations

BT	=	barium titanate $BaTiO_3$
CP	=	critical point
CSDG	=	compressible spherical dipolar glass
C	=	cubic
Cu	=	cupper
DSC	=	differential scanning calorimetry
DMM	=	digital multimeter
DG	=	dipolar glass
ECE	=	electrocaloric effect
FC	=	field cooled
FH	=	field heated
LGD	=	Landau-Ginzburg-Devonshire
M_B	=	monoclinic B
M_C	=	monoclinic C
MPB	=	morphotropic phase boundary
NMR	=	nuclear magnetic resonance
O	=	orthorhombic
PMN	=	lead magnesium niobate $Pb(Mg_{1/3}Nb_{2/3})O_3$
PLZT	=	lead lanthanum zirconate titanate $Pb_{(1-x)}La_x(Zr_yTi_{(1-y)})_{(1-x/4)}O_3$
PMN-PT	=	lead magnesium niobate-lead titanate $Pb(Mg_{1/3}Nb_{2/3})O_3$-$PbTiO_3$
PT	=	lead titanate $PbTiO_3$
PVDF	=	polyvinylidene fluoride
P-FE	=	paraelectric-ferroelectric
Pt	=	platinum
PNRs	=	polar nanoregions
PRT	=	platinum resistor thermometer
RF	=	random field
R	=	rhombohedral
SRBRF	=	spherical random bond random field model
TEM	=	transmission electron microscopy
T	=	tetragonal
ZFC	=	zero field cooled

1 Introduction

Ferroelectrics are polar materials that possess at least two equilibrium orientations of the spontaneous polarization vector in the absence of an external electric field, and in which the spontaneous polarization vector may be switched between those orientations by an electric field. The era of ferroelectricity began in the early 1940s when Wainer and Solomon published their pioneering work on mixed oxide ceramic barium titanate, $BaTiO_3$ (BT) with perovskite structure. Immediately, $BaTiO_3$ became a focus of interest due to its unusual high dielectric constant and polarization which have brought new possibilities of using this material in various electronic applications like high storage capacitors, transducers and thermistors. Between 1950 and 1960, more than 100 new ferroelectrics were discovered, e.g., lead titanate (PT), lead zirconate titanate (PZT), lead lanthanum zirconate titanate (PLZT), lead magnesium niobate (PMN), potassium niobate ($KNbO_3$), potassium sodium niobate (KNN), and potassium tantalate niobate (KTN), etc. [1, 2]. Some of these new ferroelectric materials were characterized by unusual dielectric and polarization response, high piezoelectric coefficient and good electro-optical properties. Characterization and study of these extraordinary physical properties of these materials accelerated rapidly, especially because of the competition for military and technological superiority during the Cold War. Like always, first applications were used for military purposes, in ultrasound sensors on submarines to track the movement of enemy's submarines and vessels. Some years later, the technology emerged into civil life and various applications were developed like medicine ultrasound devices, micro manipulators, micro pumps, data storage devices, etc., which have significantly influenced the everyday lives of people.

Today, one of the most important things in the technological industry is to make devices which are faster, more powerful, smaller, and thinner with low costs. This can be achieved by developing new materials, which is usually related to a lot of costs, or to improve the properties of these known materials, which should be cheaper due to the already established technological procedure of fabrication. To make this possible, we have to understand the origin and driving mechanism of these properties in a material. Our research is focused on the basic understanding of physical properties of a subgroup of ferroelectric materials called ferroelectric relaxors. We hope that our research results, which are partially presented in this thesis, will contribute to a better understanding of relaxors unusual large dielectric properties and maybe to advance the progress in engineering new advanced materials with even more improved ferroelectric and electromechanical properties.

1.1 Ferroelectrics

Ferroelectric properties were observed in different classes of materials, i.e., in hydrogen-bonded materials, oxide solid solutions with perovskite or tungsten bronze structure, triglycine sulphate (TGS) family or in ferroelectric polyvinylidene fluoride (PVDF) polymers [3, 4, 5]. In this work, we will limit ourselves on perovskite structured ferroelectric materials. The ABO_3 perovskite oxides constitute the most technologically

important class of ferroelectric materials whose relatively simple chemical and crystallographic structures have contributed significantly to our understanding of ferroelectric and antiferroelectric phenomena [3, 4]. The structure of an ideal cubic perovskite with a space group $Pm\bar{3}m$ is shown in Figure 1. In perfect perovskite structure, the A cations are placed at the corners of the cube, and the B cation at the center with X anions at the face-centered position. Alternatively, another view on this structure is regarded to regular octahedron formed by X anions with B cation at the center. The array of such octahedral linked at their corners build a cubic network with B cations at the corners with large holes which are occupied by A cations.

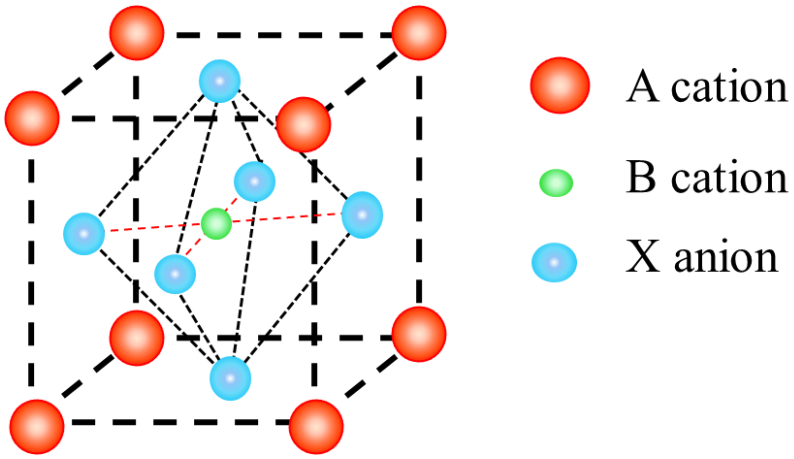

Figure 1: *Perovskite structure.* Typical ideal cubic perovskite structure with a space group $Pm\bar{3}m$.

A cations are usual monovalent to trivalent metal ions and are bigger than B cations which can be trivalent to hexavalent. The X anion in perovskite oxides is oxygen but in general it can also be fluorine or chlorine ions. In the case of BT the bigger A cation is Ba^{2+}, smaller B cation is Ti^{4+} and X anion is O^{2-} [3-6].

According to the origin of ferroelectricity, the ferroelectric transitions can be classified in two main groups, order-disorder or displacive. Order-disorder type of ferroelectric transition is usually associated to the hydrogen bonded crystals. Potassium dihydrogen phosphate, KH_2PO_4 (KDP), is the classic example of ferroelectric order-disorder transition. The order-disorder transition is triggered by movements of hydrogen protons between two energetically equivalent potential minimums. At high temperature, the proton has enough thermal energy to overcome the potential barrier and the possibility to occupy one of these two minimums is equally probable. The arbitrary distribution of protons represents disorder of system which results in symmetrical distribution of elongation of hydrogen bonds found with neutron diffraction measurements and zero net polarization. Below the critical temperature, i.e., Curie temperature, T_C, the overcoming of proton between the potential minimums becomes blocked. Proton gets trapped in one of the potential minimums and the system becomes ordered and exhibits a nonzero net polarization [6, 7, 8, 9, 10].

The displacive class of ferroelectrics usually includes perovskite structured crystals. BT is treated as a classic example of displacive ferroelectric transition associated with the shift of ions from their original position. BT is at high temperature in a paraelectric state with cubic structure and zero polarization. By cooling it below T_C, Ba and Ti ions shifts from their original positions due to the oxygen ions and structural phase transition appears from the cubic to tetragonal structure. Because of the shift of ions, the centers of positive and negative charges do not coincide anymore which results in appearing of spontaneous

dipole moments and polarization typical for ferroelectric materials. Some of ferroelectrics like BT undergo several phase transitions into successive ferroelectric phases whereby each of these ferroelectric phases has lower symmetry [3, 4, 6]. The nature of the particular ferroelectric transition can be either first order with discontinuous change of the spontaneous polarization or second order with continuous change of the spontaneous polarization. The macroscopic view of ferroelectric transition is given by Landau-Ginzburg-Devonshire (LGD) thermodynamic theory [3, 4, 11]. LGD consider the expansion of the free energy density, f in terms of polarization P,

$$f(T,P,E) = f_0 + gP + \frac{1}{2}a(T)P^2 + \frac{1}{3}h(T)P^3 + \frac{1}{4}b(T)P^4 + \cdots - EP. \quad (1)$$

f_0 is a density of a free energy in paraelectric state, E is applied external electric field and g, a, h, b are coefficients of expansion which can be smooth functions of temperature or other physical parameters, such as pressure (etc.). Usually in mean-field approximation and generally for simplicity people assume temperature dependence only in the leading coefficient a, whereas other coefficients like b and c are treated as temperature independent. It should be stressed that not all terms in expansion of free energy are allowed. If crystal is centrosymmetric in the paraelectric state, i.e., has a center of inversion, then odd terms are not allowed. Taking this into account and that the external electric field is zero, then the expansion can be written as

$$f(T,P) = f_0 + \frac{1}{2}a(T)P^2 + \frac{1}{4}b(T)P^4 + \frac{1}{6}c(T)P^6 + \cdots. \quad (2)$$

The polarization P in the ferroelectric phase yields spontaneous polarization P_S. To estimate value of P_S in thermal equilibrium, we have to minimize the density of free energy as a function of P, which leads to the equation of state,

$$\left(\frac{\partial f}{\partial P}\right)_{P_S} = a(T)P_S + b(T)P_S^3 + c(T)P_S^5 = 0. \quad (3)$$

In the case of the first-order transition, the second coefficient in equation (3) is negative, $b(T) < 0$ and we get two minima in the free energy density function at $T \leq T_C$ shown in Figure 2(a). First solution $P_S = 0$ is trivial and corresponds to the paraelectric phase. The nontrivial solution of equation (3) with negative second coefficient which is valid for ferroelectric phase is

$$P_S = \pm\sqrt{\frac{-b(T) + \sqrt{(b(T))^2 - 4c(T)a_0(T - T_0)}}{2c(T)}}, \quad (4)$$

where it is assumed that $a = a_0(T - T_0)$ around Curie point. T_0 is a Curie-Weiss temperature which represents a divergence of the dielectric constant at the ferroelectric phase transition. The temperature evolution of the spontaneous polarization at first-order ferroelectric transition is shown in Figure 2(b). At T_C, a discontinuous jump in spontaneous polarization is observed which corresponds to the onset of nontrivial minimum of f as a function of P (shown in Figure 2(a)). At the first-order ferroelectric transition, the temperature of the stable paraelectric and ferroelectric phase does not coincide, i.e., Curie transition temperature and Curie-Weiss temperature don't coincide, $T_C \neq T_0$. On the way from paraelectric to ferroelectric phase, a small temperature interval exists below transition temperature called paraelectric metastable range where paraelectric phase still exists. On the other hand, at the transition from ferroelectric to paraelectric phase, we have ferroelectric metastable range above transition temperature where ferroelectric phase is still present.

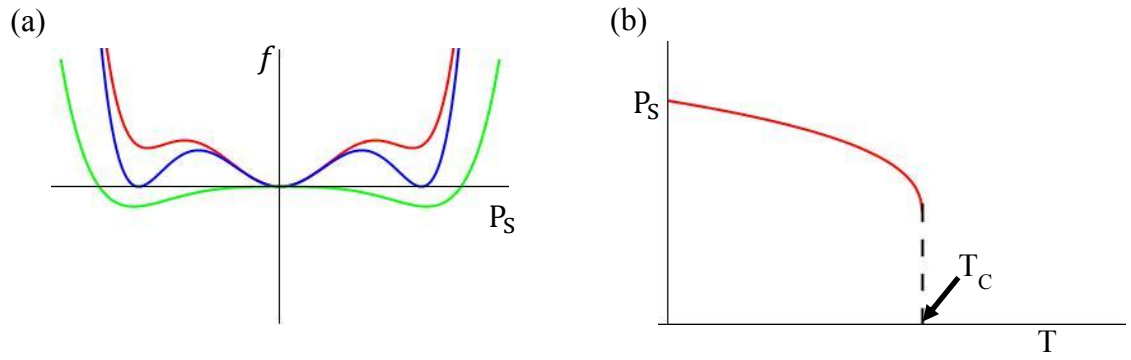

Figure 2: *First-order phase transition.* (a) Free energy as a function of the polarization at $T_1 > T_C$, $T_2 = T_C$, and $T_3 < T_C$, red, blue, and green line, respectively. (b) Spontaneous polarization P_S as a function of temperature.

In the case of the second-order transition the second coefficient in equation (3) is positive, $b(T) > 0$ and the higher term $\frac{1}{6}c(T)P^6$ can be neglected. The expression for the spontaneous polarization in the ferroelectric phase derived from the equation of state, $\frac{df}{dP} = 0$, can be written

$$P_S = \pm\sqrt{\frac{-a_0(T - T_0)}{b}}. \tag{5}$$

From the free energy density function shown in Figure 3(a) we can see that above T_0, the $f(P_S)$ has only one minimum at $P_S = 0$, which corresponds to the paraelectric phase, and below T_0 $f(P_S)$ has two minimums which solution is equation (5).

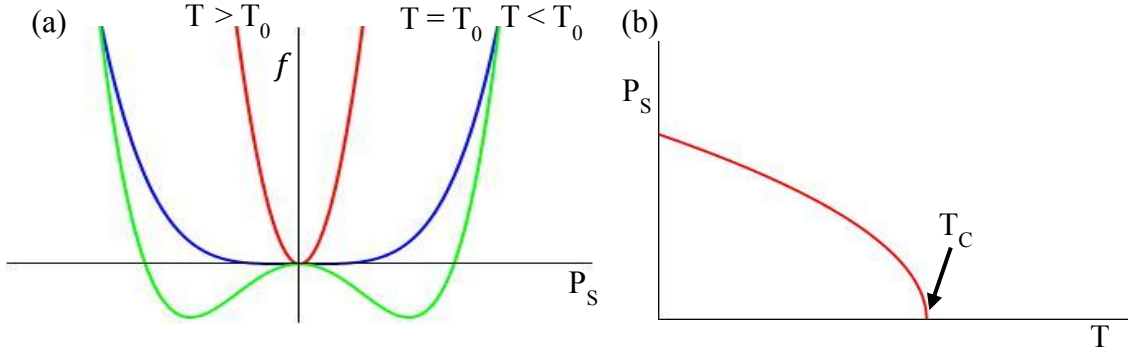

Figure 3: *Second-order phase transition.* (a) Free energy as a function of the polarization at $T > T_0$, $T = T_0$, and $T < T_0$, red, blue, and green line, respectively. (b) Spontaneous polarization P_S as a function of temperature.

The temperature evolution of the spontaneous polarization (see Figure 3(b)) in the case of the second-order ferroelectric transition is a continuous function which is zero at and above T_c. In both cases spontaneous polarization in ferroelectrics vanishes at and above transition temperature in the absence of the external electric field. But this is just one typical feature of ferroelectrics; another important characteristic of these materials is the response of the dielectric susceptibility, χ or the dielectric constant, $\varepsilon = 1 + \chi$. The second derivative of the free energy density is equal to inverse value of the dielectric susceptibility,

$$\left(\frac{\partial^2 f}{\partial P^2}\right)_{P_S} = \left(\frac{\partial E}{\partial P}\right) = a(T) + 3b(T)P_S^2 + 5c(T)P_S^4 = \chi^{-1}. \quad (6)$$

The dielectric susceptibility response of ferroelectrics with the first-order ferroelectric transition shows a sharp discontinuous drop of χ at the ferroelectric transition. If the ferroelectric transition is second order, the dielectric susceptibility diverges, as shown in Figure 4(a) and 4(b), respectively.

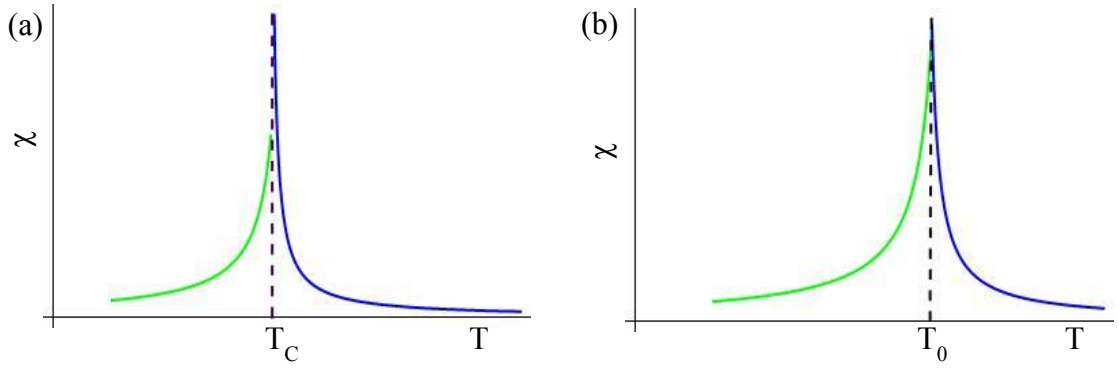

Figure 4: *Linear dielectric susceptibility*. Schematic presentation of linear dielectric susceptibility as a function of temperature at (a) first-order discontinuous and (b) second-order continuous phase transition.

The temperature dependence of the dielectric susceptibility in the paraelectric phase close to the phase transition can be estimated from equation (6). By taking into account that above T_C, $P_S = 0$ and $a_0 = \frac{1}{C}$, where C stands for the Curie constant, we get a following relationship

$$\chi = \frac{C}{T - T_0}, \quad (7)$$

which is known as Curie-Weiss law. The Curie-Weiss behavior of χ for $T > T_0$ is observed in most ferroelectrics and provides also additional support for the linear temperature ansatz for a.

Next typical property of ferroelectrics is polarization reversal or switching by an external electric field. By plotting the change of polarization with electric field, a hysteresis loop resembling the magnetic hysteresis loop is obtained [12, 13, 14]. The appearing of hysteresis is a consequence of switching polarization, i.e., ferroelectric domains which are present in ceramics and single crystal materials. Ferroelectric domain is a region in the material with uniformly oriented spontaneous polarization. Domains forms to minimize the electrostatic energy of depolarizing fields and the elastic energy associated to the mechanical stress to which the ferroelectric material is subjected at the paraelectric-ferroelectric transition [15, 16, 17]. The separations between domains are called domain walls which can be 180° or 90° domain walls depending on the polarization orientation of neighboring domains. As already mentioned, by applying the cycled electric field a broad ferroelectric hysteresis loop is observed, as shown in Figure 5. The relation between the polarization and the applying electric field can be described by a power series of E,

$$P(E) = P(E=0) + E\frac{\partial P}{\partial E} + \frac{E^2}{2!}\frac{\partial^2 P}{\partial E^2} + \frac{E^3}{3!}\frac{\partial^3 P}{\partial E^3} + \frac{E^4}{4!}\frac{\partial^4 P}{\partial E^4} + \cdots, \quad (8)$$

$$P(E) = \varepsilon_0(\chi_1 E + \chi_2 E^2 + \chi_3 E^3 + \chi_4 E^4 + \cdots), \quad (9)$$

which contains a higher order non-linear terms of susceptibility, $\chi_2, \chi_3, \chi_4, \ldots$ At small electric fields, the polarization obeys linear relationship and higher terms can be neglected. In this region the field is too weak to switch the domains with unfavorable polarization. With increasing electric field domains start to switch and order along directions that are crystallographic as close as possible to the direction of the electric field. This results in a non-linear increasing of polarization which gets saturated at high enough fields where all domains are switched and aligned. By decreasing the electric field the polarization starts slowly decreasing because polarization of some domains are not perfectly aligned anymore and some even switch back to initial state. But not all domains switch back, some of them stay in field direction and due to this, the polarization is still present at zero field. The value of polarization at zero field is called remanent polarization, P_R. To eliminate the polarization the field has to be reversed. Application of the reversed field results in the decay of the polarization to zero by switching the polarization in opposite direction. A further increase of the electric field in negative direction causes a new negative alignment of polarization and saturation. To complete the circle the field is first reduced to zero and then again increased in the positive direction. The field necessary to reduce the polarization to zero is called coercive field, E_C.

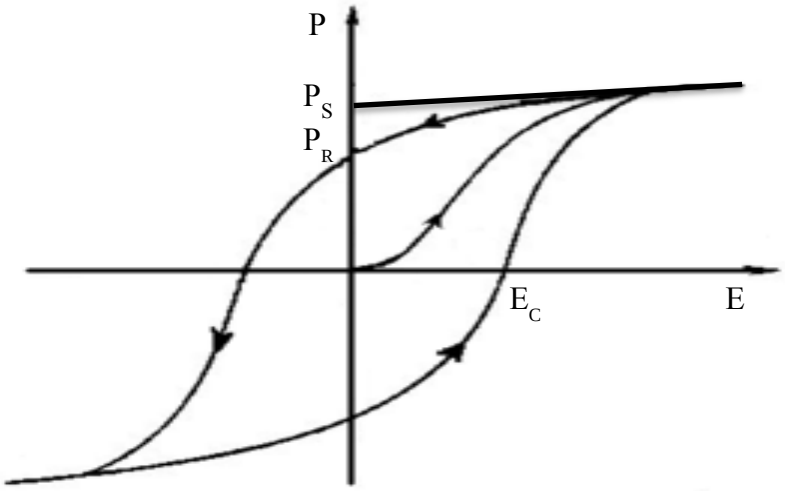

Figure 5: *Hysteresis loop.* Schematic presentation of ferroelectric hysteresis loop observed at and below phase transition with illustrated coercive field E_C, remanent polarization P_R, and spontaneous polarization P_S.

The last and also frequently studied dielectric property is the nonlinear dielectric response of ferroelectrics. By substituting equation (3) into equation (8) we get relationship between P and E, which gives us linear and nonlinear terms of the dielectric susceptibility. At the first-order phase transition b is negative and differentiation of equation (3) with respect to P_S gives following linear, second-order and third-order term of the dielectric susceptibility:

$$\chi_1 = \frac{1}{a_0(T - T_0) + 3bP_S^2 + 5cP_S^4}, \quad (10)$$

$$\chi_2 = -(3b + 10cP_S)\chi_1^2 P_S, \tag{11}$$

$$\chi_3 = -(3b + 30cP_S^2 - \chi_1(6bP_S + 20cP_S^3)^2)\frac{1}{6}\chi_1^2. \tag{12}$$

The behavior of the linear dielectric susceptibility at the first-order phase transition was shown in Figure 4(a). Always negative second-order term of the dielectric susceptibility is nonzero only in noncentrosymmetric systems where the odd terms of the free energy are present and below Curie transition temperature where $P_S \neq 0$. Slightly different is third term which is always present and little bit more complicated. To see the temperature behavior of the third-order term below T_C we substitute the expression for P_s obtained in equation (4) into equation (12) and rewrite it

$$\chi_3 = \frac{c^2(71b^2\left(-b-\sqrt{b^2-4ca_0(T-T_0)}\right)+28ca_0(T-T_0)(-9b+5\sqrt{b^2-4ca_0(T-T_0)}))}{6(4ca_0(T-T_0)+b(-b+\sqrt{b^2-4ca_0(T-T_0)}))^3}. \tag{13}$$

The expression of χ_3 above T_C is less complicated due to the fact that all components which contains P_S are zero and thus we get

$$\chi_3 = -\frac{b}{2\left(a_0(T-T_0)\right)^2}. \tag{14}$$

Temperature dependence of the third-order nonlinear dielectric susceptibility for the first-order phase transition is shown in Figure 6. We can see that χ_3 is in the whole temperature range positive and shows a peak at T_C.

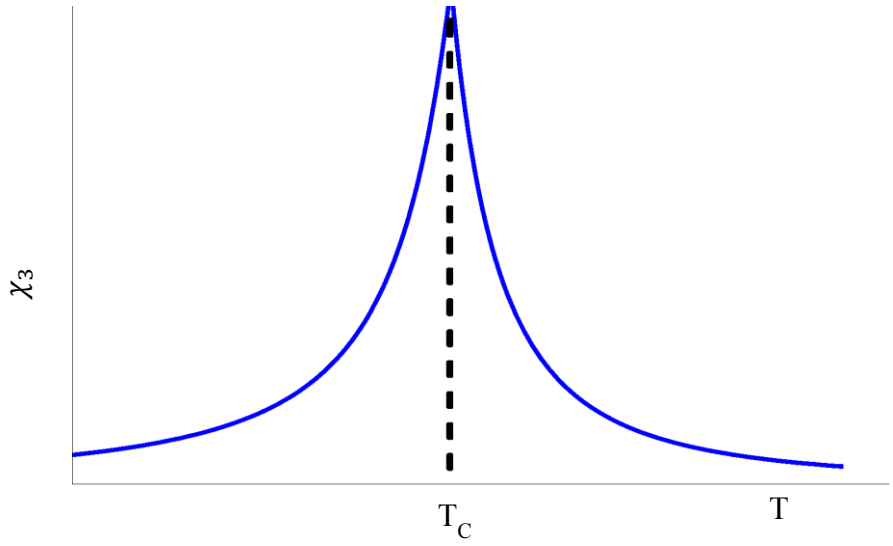

Figure 6: *Nonlinear dielectric susceptibility.* The nonlinear dielectric susceptibility remains positive in paraelectric and ferroelectric temperature range at first-order phase transition.

In the case of the second-order transition, the b coefficient is positive and the third term of equation (3) can be neglected. The expressions for the first three coefficients of the dielectric susceptibility are

$$\chi_1 = \frac{1}{a_0(T - T_0) + 3bP_S^2}, \tag{15}$$

$$\chi_2 = -3bP_S^2\chi_1^2, \tag{16}$$

$$\chi_3 = 12b^2P_S^2\chi_1^3 - b\chi_1^2. \tag{17}$$

The situation is the same as in the first-order phase transition. The second-order coefficient is always negative below T_C and zero above. To get temperature dependence of the third-order nonlinear susceptibility, we repeat the calculation steps used in the first-order phase transition and obtain the expression for below and above T_C, respectively

$$\chi_3 = \frac{b(-a_0(T - T_0) - 9a_0(T - T_0))}{2(a_0(T - T_0) - 3a_0(T - T_0))^3}, \tag{18}$$

$$\chi_3 = -\frac{b}{2\left(a_0(T - T_0)\right)^2}. \tag{19}$$

From equations (18) and (19) it becomes clear that the third-order dielectric susceptibility is positive below and negative above T_C, as shown in Figure 7. The sign of χ_3 is thus a sensitive probe for the discrimination between continuous and discontinuous ferroelectric phase transitions.

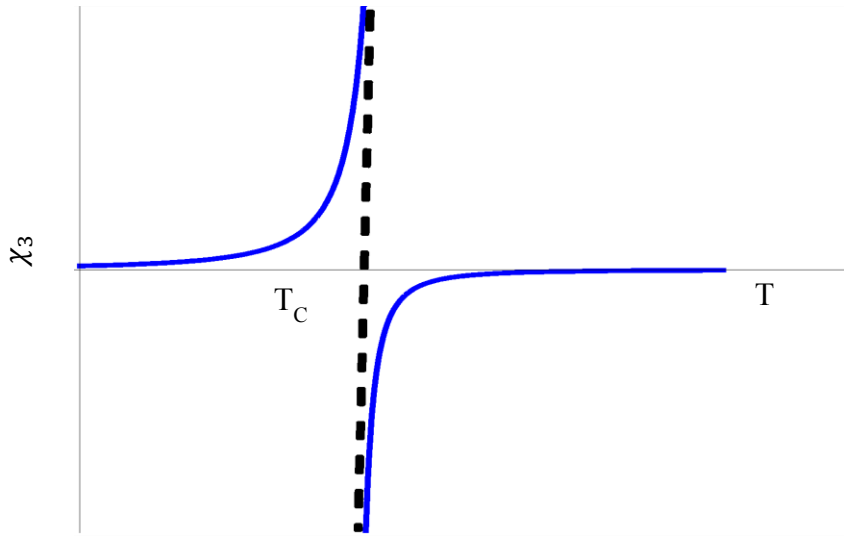

Figure 7: *Nonlinear dielectric susceptibility*. Thus, the LGD model predicts a change of sign of χ_3 at continuous phase transition.

1.2 Relaxor ferroelectrics

Another class of dielectrics is relaxor ferroelectrics. Relaxor properties can be found in differently structured materials similar as ferroelectric properties but again we will limit our-self on perovskite structured compounds [18, 19]. Perovskite relaxors have the same ABO_3 structure as classical ferroelectrics apart of one difference, relaxors have a substituted cations on A, B or both sites of the structure [20]. Depending on which site the cation is substituted we have A-site substituted relaxors, typical example is bismuth strontium titanate, $(Bi_xSr_{1-x})TiO_3$ (BST), B-site substituted relaxors such as, lead

magnesium niobate $Pb(Mg_{1/3}Nb_{2/3})O_3$ (PMN), and AB-site substituted relaxors like, lead lanthanum zirconate titanate $Pb_{(1-x)}La_x(Zr_yTi_{(1-y)})_{(1-x/4)}O_3$ (PLZT). It has to be noted that in the A-site substituted relaxors x must be above a certain critical value for relaxor properties to manifest [4, 18, 21, 22].

The first disordered relaxor ferroelectric, discovered by Smolensky group was PMN in early 1959 [20]. In the last half a century, PMN became a prototypical relaxor and one of the most studied relaxor systems. The general formula for B-site disordered relaxors like PMN can be written as $A(B'_{1/3}B''_{2/3})O_3$, where B'' represents the substituted ion. A universal signature of the ferroelectric relaxor is a broad frequency dependent peak in real and imaginary part of temperature dependent dielectric susceptibility (see Figure 8(a)) [20, 22]. In contrast to normal ferroelectrics where the temperature dependent dielectric susceptibility or dielectric constant (ε') exhibits a sharp frequency independent response, relaxors exhibit a very broad $\varepsilon'(T)$ peak and strong frequency dispersion in the peak temperature (T_m). As shown in Figure 8(a), the peak temperatures of dielectric constant increase with increasing frequency. As noted earlier, the dielectric constant of normal ferroelectrics follows the Curie-Weiss law at high temperatures, i.e., in a wide temperature range of the cubic paraelectric phase [3]. However, $\varepsilon'(T)$ of relaxors shows large deviation from this law for temperatures above T_m, as shown schematically in Figure 8(b) [20, 22, 23, 24].

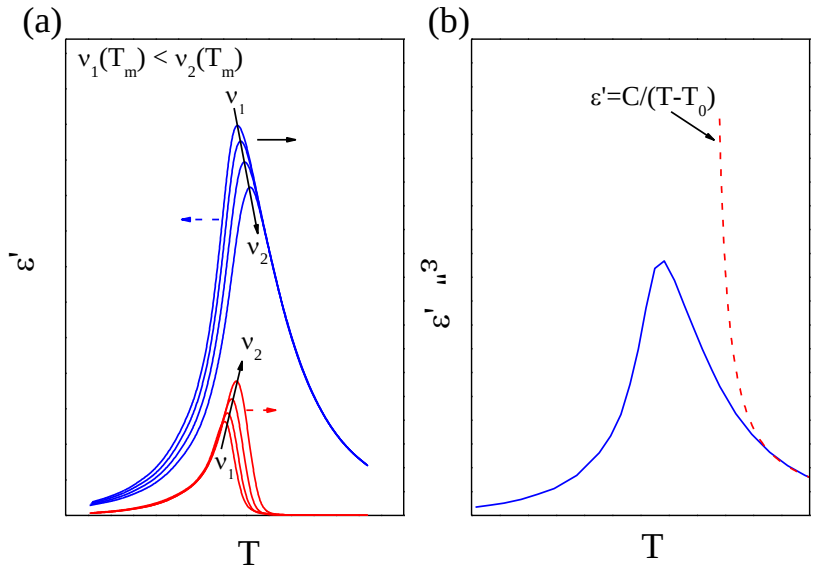

Figure 8: *Relaxor ferroelectrics.* (a) A strong frequency dispersion of complex dielectric constant typical for relaxor ferroelectrics. (b) Large deviation of $\varepsilon'(T)$ from the Curie-Weiss law.

A broad $P-E$ hysteresis loop (Figure 5) typical for normal ferroelectric can be observed at and below T_C, i.e., in the low temperature FE phase. Relaxor, on the other hand, exhibits so-called slim hysteresis loop, shown in Figure 9, around T_m which gets broader below freezing temperature, T_f[20, 22, 25, 26]. A small remanent polarization, obtained on removing the electric field is a consequence of short range polar order within so called polar nanoregions (PNRs) [27].

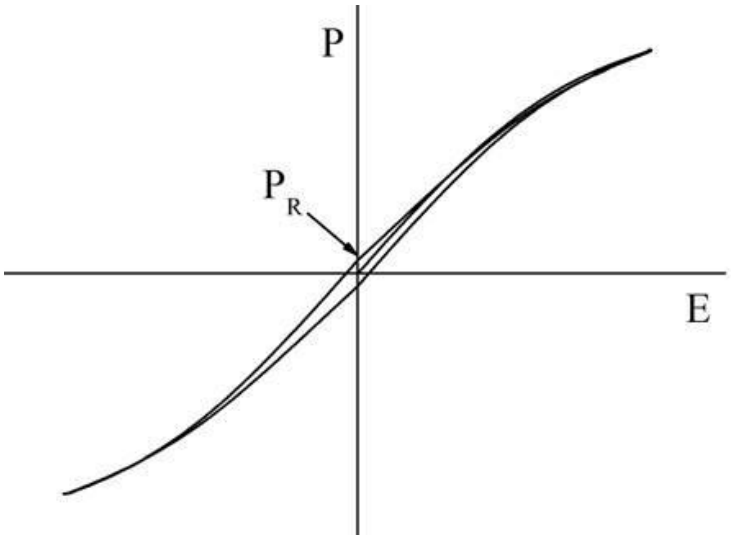

Figure 9: *Slim hysteresis loop.* A slim hysteresis loop typical for relaxor ferroelectric observed below T_m.

An interesting thing on relaxor material is that the remanent polarization doesn't disappear at the dielectric peak temperature, but persist well above T_m (see Figure 10), whereas in normal ferroelectrics P_R disappear at T_C similar as spontaneous polarization shown in Figure 2(b) and Figure 3(b) [13, 14, 22, 27, 28, 29].

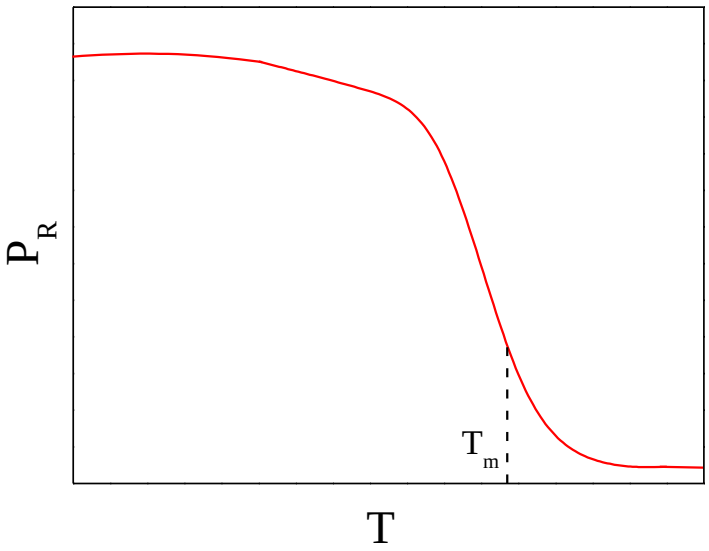

Figure 10: *Polarization in relaxor ferroelectrics.* The remanent polarization in relaxor ferroelectrics persist well above T_m.

The above discussion makes it very clear that the properties of relaxors are very different from those of normal ferroelectrics. It is interesting that relaxors show more similarity with spin glasses and dipolar glasses as with ferroelectrics [30, 31, 32, 33, 34]. Especially the dispersed dielectric response of relaxors is very similar to observed magnetic susceptibility response of spin glasses or to dielectric response of dipolar glasses which exhibit also a slim hysteresis loop [30, 31, 32, 35]. Because of this

similarity, it is believed that relaxors provide a conceptual link between ferroelectrics and dipolar glasses. However, it is clear that the physical background is different and even more complicated as in the case of normal ferroelectrics.

1.3 Review of physical concepts for relaxor PMN

In terms of chemical interpretation, PMN is perhaps the simplest and well-defined compound of mixed perovskite, but its physics is far from simple. The unusual dielectric and polarization response of relaxor materials attract a lot of interest in the ferroelectric community whose aim was to explore these properties and to interpret them. In last half a century a number of different concepts have been proposed for PMN to finally find a physical picture which would give a good description of the relaxor properties.

The unusual relaxor properties of PMN were first discovered and studied extensively by Smolensky research group [20]. Smolensky and coworkers originally introduced concept of the "diffuse phase transition" based on compositional fluctuations on a microscopic scale that are caused by the statistical distribution of heterovalent ions in the same crystallographic position [36]. The compositional fluctuations are treated as polar entities or polar regions which emerge and agglomerate into clusters with varying composition. The ferroelectric phase transition occurs in separate regions of crystal independent of one another with varying local T_C, depending on the composition of the individual region. Thus, the dielectric response was interpreted as switching of the local spontaneous polarization between states with different orientation. They assume, that at given temperature T, only regions of which the local T_C is near T contribute to macroscopic dielectric response.

Cross proposed for PMN so-called superparaelectric concept in analogy to a superparamagnetic state [22]. He considers relaxor as consisting from small non-interacting polar regions which are created as a consequence of the composition fluctuations. The idea is based on Burns and Dacol's study of the temperature dependence of the refractive index [27]. They show that the refractive index in relaxor material deviate from the linear behavior with decreasing temperature. The deviation was interpreted as a result of the existence of local polar clusters which nucleate at particular temperature. For PMN the temperature of nucleation was found to be at so-called Burns temperature, $T_B \cong 616$ K, which is much higher as T_m. Cross postulated that ferroelectricity is a cooperative phenomenon and due to this the energy involved with every polar region is scaled with the volume. This means that for domain of macroscopic volume the required energy for overcoming the energy barrier which separate alternative domain state is much larger than the thermal energy of the crystal, kT, and domain is stable. By domain volume reduction the energy barrier decrease and become compatible to kT and the polar region become unstable against thermal agitation. Thus, the local polarization in each region can fluctuate under thermal agitation. This results in the frequency dependence of the dielectric response and slowing down of the local polarization fluctuation.

Viehland et al. follow the idea of Cross superparaelectric concept and show in addition to this a dipolar glass-like character of PMN [26, 28]. In contrast to Cross they proposed the interaction between the polar nanoregions which leads to the dipolar glass behavior. They believe that correlation between polar nanoregions control the kinetic of the fluctuations and freezing processes as the deviation of $\varepsilon'(T)$ from Curie-Weiss behavior above T_m. Specifically, they showed evidence for a freezing temperature of thermally activated polarization fluctuations, by modeling the dielectric relaxation using the Vogel-Fulcher relationship. The dispersion in the fluctuation frequency is a reflection of the cluster size dispersion and leads to a relaxation time distribution. The suggested model of

a temperature dependent relaxation time spectrum show broadening of the spectrum at T_f, where the average relaxation time approaches macroscopic time period [28]. In addition, Levstik et al. later show that the longest characteristic relaxation time in relaxation spectrum diverge below freezing temperature [37]. All this findings are similar to that observed in spin glasses and additional support came also from Colla et al., who observed very slow dynamics and a logarithmic decay of the long-time relaxation of the $\varepsilon'(T)$ response of PMN [35, 38]. Viehland and coworkers adopt Cross concept and upgrade it in a dipolar glass concept, where the ground state of PMN in zero electric field is a kind of short-range ordered dipolar glass state which transforms by applying high enough electric field into long-range ordered ferroelectric state [26]. The support to this idea was given by the prior work of different research groups who studied the dielectric and polarization properties of relaxors under the influence of applying electric field [20, 22, 25, 27, 29, 35].

Parallel to Viehland's dipolar glass concept, Westphal et al. developed so-called random field concept which is based on random field Ising model used in ferromagnetic systems and refers to the original idea of Imry and Ma, who pointed out the stability of domain states due to the local fluctuations of quenched microscopic fields [39, 40]. Compositional fluctuations which are present in PMN create space charges and, hence, electric field fluctuations on atomic length scales and negatively charged ordered domains which give rise to additional quenched random electric fields. They believe that the present random fields in PMN have a strong influence on the phase transition and destroy the macroscopic long-range ordered ferroelectric phase. The ground state of PMN in zero electric field is, hence, a ferroelectric nanodomain state which can be switched into long-range ordered ferroelectric state if the applied electric field is high enough and prevails over the RF's. In support to RF mechanism they present the discontinuous jumps of the optical birefringence interpreted as Barkhausen jumps. The discontinuous jumps were explained as a result of the alignment process where the nanodomains are switched into ordered long-range macroscopic domains by applying high enough external electric field. An addition argument which was used in favor of the RF concept is the observation of ferroelectric symmetry breaking by X-ray and neutron diffraction and observation of nanodomains by high resolution TEM [41, 42].

The last and maybe a little bit less known and used concept to describe the relaxor nature is a reorienting polar clusters concept proposed by Vugmeister et al. [43, 44]. The proposed concept was developed from the studies of the influence of dipolar impurities in highly polarizable dielectric crystals. They show that the onset of ferroelectric or dipolar glass state is strongly dependent on the dipole-dipole interaction energy which is determined by the polarization correlation radius and impurity concentration. If the impurity concentration is too low, the separation between dipoles is greater as the characteristic polarization correlation length of the system and dipolar impurities form a dipolar glass state at low temperatures. On the other hand, if the concentration is high enough and the characteristic polarization correlation length of the system is greater as the dipolar separation, a ferroelectric phase is established. They assume that the present disorder in ferroelectric relaxors can be treated as impurities and the origin of clusters in the crystal which are characterized by the cluster dipole moment. This makes the relaxors for incipient ferroelectrics. According to this, they apply the theory of order-disorder ferroelectrics for describing the polarization relaxation of each cluster. By finding the equation to perform the average over the distribution of relaxation times and the distribution of the local fields they were able to calculate the frequency dependent linear dielectric constant as a function of the temperature [44].

From the discussion above it is clear that over the decades different concepts were proposed which attempted to describe the physical properties of relaxors. However, over

the years the physical picture based on polar nanoregions emerged and gets widely accepted. In general it is accepted that a polar nanoregions formed at Burns temperature ($T_B \cong 600\ K$) are responsible for unusual relaxor behavior [27]. Let us first take a look what is going on in relaxor system if it is cooled down in the zero electric field. In relaxors, it is clear that chemical substitution and lattice defects are at the origin of dipolar entities. At very high temperatures these dipolar entities are not present in the system either because of the large thermal fluctuations or simply because the local displacive transition at which the dipolar entities are formed did not take place yet. On cooling the system below the Burns temperature the dipolar entities get stabilized and regions with chemical disorder form polar clusters, i.e., polar nanoregions (PNRs) which were observed by NMR and neutron diffraction scattering experiments [45, 46, 47]. These PNRs have random polar orientation which can be easily reoriented down to the freezing temperature T_f. The range of temperatures of reorientable PNRs with finite relaxation times is called ergodic dipolar glass phase [37, 48]. On cooling below the freezing temperature the PNRs freeze randomly and form nonergodic dipolar glass phase where the relaxation times gets longer. The transition from the ergodic to nonergodic phase is characterized by the divergence of the longest relaxation time [37]. By applying a sufficiently high electric field which is equal or higher as a threshold or critical electric field, E_C, of the system a phase transition from a short-range order dipolar glass state into a long-range ferroelectric state is induced [25, 29, 38, 49, 50]. The relaxor properties of PMN like NMR line shape with associated probability distribution of local polarization [45] and nonlinear dielectric response [37, 50] can be well described by the Spherical Random-Bond Random-Field (SRBRF) model [51]. SRBRF model takes into account not only the influence of random fields present in the disordered system but also the influence of the random bonds/interaction between the polar clusters. Depending on the ratio between the strength of random fields and random bonds a dipolar glass like state or a ferroelectric state is established. In relaxors, the random fields are too small to induce the locally ordered ferroelectric phase, for these reasons an external electric field has to be applied [51]. The electric field temperature $(E-T)$ phase diagram obtained by SRBRF model is in a good agreement with experimentally obtained $E-T$ phase diagram [29, 48 52, 53, 54]. In $E-T$ phase diagram the ergodic and nonergodic dipolar glass phase are separated from ferroelectric phase by a ferroelectric transition line. The schematic $E-T$ phase diagram for PMN is shown in Figure 11.

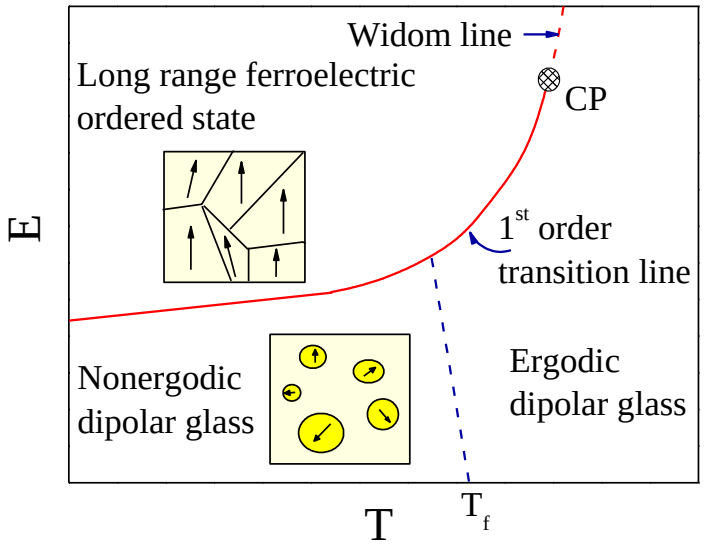

Figure 11: *Electric field-temperature phase diagram.* The solid line in the schematic $E-T$ phase diagram separates the dipolar glass state from the field-induced ferroelectric phase.

Kutnjak et al. show on single crystal ferroelectric relaxor system $Pb(Mg_{1/3}Nb_{2/3})O_3$-$x$$PbTiO_3$ (PMN-xPT) oriented in [111] direction with $x = 0.295$ that the low temperature dipolar glass state and ferroelectric state are separated by a first-order transition line which ends in a liquid-vapor type of critical point [55]. The same was shown also for the PMN single crystal oriented in [111] direction and just recently for [110] direction [56, 57]. The critical point is the only second-order transition point above which the difference between the different phases disappears and a continuous supercritical evolution in various physical quantities can be observed [58, 59, 60].

1.4 The nature of the relaxor ground state: open issues

In all this years a number of different optical, dielectric, polarization, X-ray, TEM and other studies under various conditions and different relaxor systems were presented and most of them are in favor of the above presented physical picture [18- 29, 35, 37- 42, 45, 48, 50, 52- 57, 61, 62]. However, some studies in contrast to the glassy picture have suggested that glassiness should be excluded in favor of the random field mechanism driving the system to freeze into a domain state on a nanometric length scale [40- 42, 61, 62]. Westphal et al. performed optical measurement under external electric fields. The measured linear birefringence show discontinues jumps known as a Barkhausen jumps under applied external electrical field. This jump authors interpreted as a consequence of depinning of microdomains [40]. The interpretation of polar clusters as ferroelectric nanodomains in low temperature relaxor phase is based on the X-ray and neutron diffraction results presented by de Mathan et al. [41]. In contrast to Bonneau et al. [63], who performed X-ray studies on PMN single crystal and found that the obtained data fit the best the model corresponding to the cubic symmetry, de Mathan et al. found better reliably factors by fitting the data with rhombohedra model. Here, it should be noted that he presented results from de Mathan et al. were obtained at 5 K, whereas Bonneau et al. performed the measurement in a broad temperature range, between 800 and 5K [41, 63].

Another argument which has been used to consolidate the proposal that the relaxor ground state is a ferroelectric nanodomain state was based on TEM observations [42]. Husson et al. reported the observation of a superstructure along [111] direction in PMN ceramic. The problem of TEM experiments is that the thickness of sample plays important role. For instant, if we want to get some information about atomic arrangement with TEM the thickness has to be as small as possible ($t < 100nm$), at larger thickness only the information from the surface can be evaluated. Another problem is that with decreasing thickness the size effects start to play an important role. Thus, we can observe a different picture in thin films than in the case of bulk samples. Recent x-ray diffraction measurements on relaxor ferroelectric $Pb(Zn_{1/3}Nb_{2/3})O_3$ (PZN) by Xu et al., found the low temperature unit cell near the surface to be rhombohedral where the bulk was found to be cubic in shape [64]. Investigations of the strain as a function of crystal depth by using a diffraction technique commonly applied to study spatially resolved strain in industrial materials demonstrated that large strain indicating a large lattice distortion can be found in the surface region in the relaxor PMN. Large strain near the surface region can induce different phase within the surface region as in the bulk [65]. As we can see, neither the X-ray nor TEM studies could provide a final answer whether the relaxor ground state is truly a ferroelectric nanodomain phase. Besides the structural studies some of the dielectric spectroscopy measurements were also interpreted in support to the ferroelectric nanodomain state at low temperatures. The linear and nonlinear dielectric response of PMN ceramics at high ac and dc electric fields have shown that the observed dynamics in the ergodic phase may be explained as a domain wall motion process [61, 62, 66].

Therefore, despite a long and intensive research history of relaxors especially PMN relaxor, the question about the nature of the relaxor ground state still remain unsolved. In the present work we will present some new findings which should help to find an answer to the question of the relaxor ground state. For better understanding of the relaxor ground state, a series of dielectric, polarization and calorimetric experiments were devised in order to study the polar ordering in a PMN single crystal, i.e., to check the E-T phase diagram of a canonical relaxor compound. Here the calorimetric studies are of special importance since except some pioneering work of Gorev et al. and Tachibana et al. no detailed calorimetric measurements especially under the electric bias field were performed in relaxor materials [67, 68 69]. The calorimetric investigation should reveal thermodynamic aspects of the polar ordering and the relaxor ground state and should help to determine the nature of the transition lines in the $E - T$ phase diagram [57].

1.5 Electromechanical and electrocaloric properties of relaxors

Rediscovery of the large electromechanical response in single crystal relaxor ferroelectric solid solutions and recently reports of large electrocaloric effect (ECE) rise again the interest on relaxor systems due to the application possibility in cooling devices [70, 71, 72, 73, 74, 75].

Let us first discuss the electromechanical response. Electromechanical response is the conversion of mechanical energy into electrical and vice versa. Applying the stress to a crystal will result in a small displacement of charges and consequently changes of polarization. Accordingly, the electric field applied to a crystal would change its shape. In order to describe the conversion of energy, we have to understand coupling between the electrical and mechanical parameters. This can be done by considering the thermodynamic relations between the mechanical and electrical parameter and writing down the Gibbs free energy G of the crystal as a function of mechanic stress X and electrical field E, or the mechanical strain x and polarization P. The expansion of the free energy in terms of the strain and polarization adds to the equation (1) three new terms:

$\frac{1}{2}\sum_1^3 s_{ijkl}^P x_{ij}x_{kl}$ represents elastic compliance (Hook's law), $\sum_1^3 g_{ijk} x_{ij}P_k$ linear electromechanical response and $\frac{1}{2}\sum_1^3 Q_{ijkl} x_{ij}P_kP_l$ quadratic electromechanical response. Here, s_{ijkl}^P represents the tensor of the elastic compliance at constant polarization, g_{ijk} is the tensor of linear electromechanical or piezoelectric effect and $Q_{ijkl}$is the tensor of the quadratic electromechanical or electrostriction effect [3]. By considering the Maxwell relations [4, 17]

$$S = -\left(\frac{\partial G}{\partial T}\right)_{X,E} \qquad x_{ij} = -\left(\frac{\partial G}{\partial X_{ij}}\right)_{T,E} \qquad D_i = -\left(\frac{\partial G}{\partial E_i}\right)_{T,X}, \tag{20}$$

it is possible to the relation between the strain and electric field

$$x_{ij} = \alpha_{ij}\Delta T + s_{ijkl}X_{kl} + d_{kij}E_k + M_{klij}E_kE_l. \tag{21}$$

Here, $\alpha_{ij}\Delta T$ is thermal expansion and the piezoelectric and electrostrictive tensors are denoted with d_{kij} and M_{klij}, respectively. As we can see from equation (21), the electrostriction is proportional to the square of the electric field which makes it independent from the field direction, whereas the piezoelectric response is linearly proportional to the electric field which makes it sensitive to the direction of the applied electric field or stress (see Figure 12).

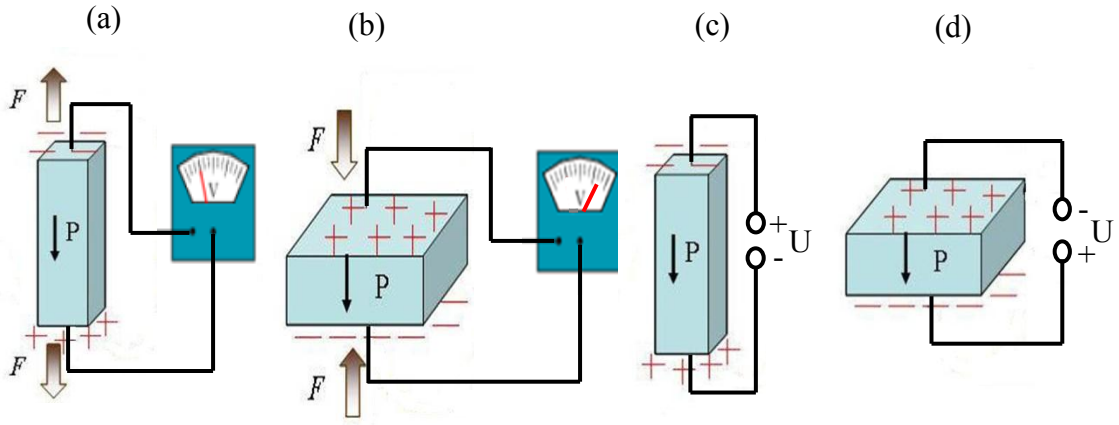

Figure 12: *Reaction of piezoelectric element to applied stimuli.* (a) and (b) shows a direct piezoelectric effect where applied stress generates charge on the surface. (c) and (d) shows a converse piezoelectric effect where the applied electric field changes the size of the piezoelectric element. The change of the size and the sign of the accumulated charge depend on the direction of the applied stimuli.

The expression $x_{ij} = d_{kij}E_k$ stands for the so-called *converse* piezoelectric effect shown in Figure 12 c and d. The converse piezoelectric effect describes the strain that is developed in a piezoelectric material due to the applied electric field. On the other hand, the applied mechanical stress X_{ik} creates charge on the surface of the piezoelectric material and is known as *direct* piezoelectric effect and can be written as $D_i = d_{ijk}X_{jk}$ where D_i stands for charge density. The tensors of the direct and converse piezoelectric effect are identical, $d_{ijk}^{direct} = d_{kij}^{converse}$ because the strain and stress are symmetrical tensors [17, 76]. The piezoelectric tensor is a third rank tensor of piezoelectric coefficients, but the number of independent coefficients is reduced to 18, due to the symmetry of direct and converse piezoelectric tensors. The number of independent piezoelectric coefficients is further reduced by the symmetry of the material. The absence

of piezoelectric effect in materials with centrosymmetric point group symmetry reduces the number of piezoelectric coefficients in tensor as for example for tetragonal symmetry:

$$\begin{bmatrix} D_1 \\ D_2 \\ D_3 \end{bmatrix} = \begin{bmatrix} 0 & 0 & 0 & 0 & d_{15} & 0 \\ 0 & 0 & 0 & d_{24} & 0 & 0 \\ d_{31} & d_{32} & d_{33} & 0 & 0 & 0 \end{bmatrix} \begin{bmatrix} X_1 \\ X_2 \\ X_3 \\ X_{23} \\ X_{31} \\ X_{12} \end{bmatrix}. \quad (22)$$

The piezoelectric coefficient d_{ij} is relates the strain applied in the j axis and electric field applied along the i axis. The $d_{33}, d_{31} = d_{32}$ and $d_{15} = d_{25}$ are longitudinal, transverse, and share piezoelectric coefficients, respectively. These coefficients can be expressed as [76, 77]:

$$d_{33} = 2\varepsilon_0 \chi_{33} Q_{11} P_3, \quad (23)$$

$$d_{31} = 2\varepsilon_0 \chi_{33} Q_{12} P_3, \quad (24)$$

$$d_{15} = \varepsilon_0 \chi_{11} Q_{44} P_3. \quad (25)$$

The piezoelectric properties of ferroelectric materials are of great interest due to the numerous applications in ultrasonic and medical devices as well as in telecommunications [78]. Therefore, much effort has been invested to enhance the piezoelectric response in these materials. The enhancement of the piezoelectric response can be a result of several different interplaying factors: (i) proximity to the morphotropic phase boundary [70, 71, 72, 79, 80, 81, 82, 83], (ii) engineered domain configuration [70, 84, 85, 86, 87], and (iii) proximity of the critical point [55, 56, 88]. Studies of systems with the engineering domain configuration show that the application of the electric field in different direction as the polar direction enhances the piezoelectric response in single crystals. For instance, in the case of $BaTiO_3$ (BT) it was shown that the poling of crystal along [111] direction induces the formation of different domain structure and domain density which influences the strain inside the crystal and enhances the piezoelectric response [84, 86, 87]. For ferroelectric relaxor solid solutions single crystal like $Pb(Zn_{1/3}Nb_{2/3})O_3$-$x$$PbTiO_3$ (PZN-xPT) and $Pb(Mg_{1/3}Nb_{2/3})O_3$-$x$$PbTiO_3$ (PMN-xPT) the enhancement of piezoelectric response was observed at the morphotropic phase boundary (MPB) composition [70, 71, 72, 80]. Fu and Cohen show theoretically that the large piezoelectric response can be driven by the polarization rotation induced by an external electric field [81]. The concept of polarization rotation was proposed to be the driving mechanism for enhancement of piezoelectric response at the MPB [71, 77, 79]. MPB region represents the structural bridge between the tetragonal and rhombohedral phase (see Figure 13(a))[77, 83]. The X-ray diffraction studies by Noheda et al. and Xu et al. show a monoclinic distortion between the tetragonal and rhombohedral phase [79, 80]. It was experimentally and theoretically shown that when the electric field is applied along nonpolar direction (T, R or O) a polarization rotation over the intermediate monoclinic phases is induced (see Figure 13(b)) [71, 77, 79- 82, 89].

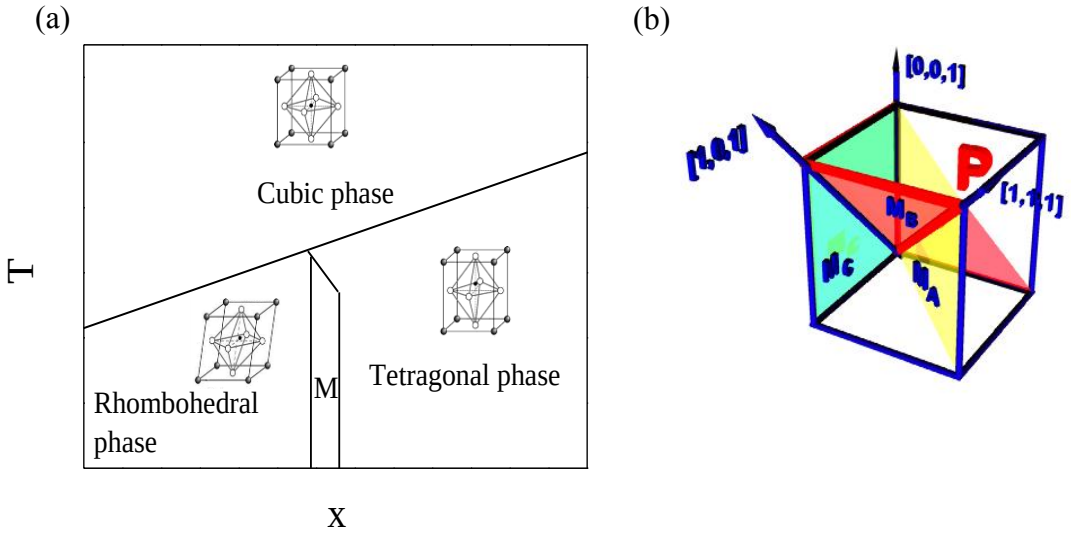

Figure 13: *Temperature composition phase diagram and polarization rotation.* (a) Schematic $x-T$ phase diagram shows the morphotropic phase boundary between the tetragonal and rhombohedral phase. (b) The polarization rotation over the intermediate monoclinic phase sequence.

Therefore, the polarization rotation via intermediate monoclinic phases causes the distortion of the lattice and it is suggested that this results in a large piezoelectric response. Another suggestion is that the dielectric susceptibility diverges at the tetragonal to monoclinic transition and this enhances the piezoelectric response [90]. The question whether the presence of the MPB is really a dominant reason for the enhancement of the piezoelectric response is even more important due to the reports of the large piezoelectric response in systems without MPB [3, 77, 91]. Recently, Kutnjak et al. show the existence of the electric field-induced liquid-vapor type of the critical point at the paraelectric to ferroelectric phase transition in PMN-PT system [55, 56]. The highest piezoelectric response was observed at the electric field corresponding to the electric field of the critical point [53]. The experiments show that the large piezoelectric response in solid solution PMN-PT can be found in the proximity of the line of critical points in the electric field-temperature-composition phase diagram $(E-T-x)$ of this system [55]. They also found in the same temperature range similar critical behavior of the dielectric constant as for the piezoelectric coefficient, which indicates that the divergence of the dielectric constant at the critical point is responsible for the large piezoelectric response [56]. This was later confirmed by theoretical calculations which show that the piezoelectric tensor diverges at the critical point due the divergence of the electric susceptibility, thus leading to the enhancement of the piezoelectric response [92]. The large piezoelectric response as a critical phenomenon reveals a new driving mechanism to enhance the piezoelectric coefficient and might be the central issue in the development and engineering of new advanced materials for electromechanical converters.

In this thesis, the previous studies of the piezoelectric response in PMN-PT system will be extended in order to verify the existence of the critical point in the PMN-0.26PT system oriented in [100] direction and the impact of the electric field on the monoclinic phase sequence and the critical behavior of the piezoelectric coefficient near the cubic-tetragonal-rhombohedral (C-T-R) triple point [88]. Besides the solid solution PMN-PT system which exhibits a MPB, a piezoelectric enhancement at the critical point was tested in canonical ferroelectric $BaTiO_3$ single crystal which does not exhibit the MPB [93].

Another important energy conversion which can be found in ferroelectric and relaxor

materials is the electrocaloric effect (ECE), i.e., the conversion of the electrical energy to the heat and vice versa. This is an important property of materials due to the possibility of broad range of applications ranging from sensors to heating and cooling devices of new generation, which would be more efficient and environmentally friendly. The effect has been known for some time, but it was not considered to be useful for commercial applications, due to its small magnitude in previously known materials [14]. The microscopic mechanism of the ECE is not yet fully established, but it is considered to be a direct consequence of the change of entropy S stimulated by an external electric field. Specifically, in the application of the external electric field induces change of the ferroelectric dipolar state, from the less ordered into a more ordered one (Figure 14) and vice versa, when the electric field is removed [73, 94]. The entropy of a system can be considered as a sum of the entropy related to the electric ordering, i.e., the entropy of the dipolar subsystem and the entropy related to lattice-vibration or phonon entropy, $S = S_{dip} + S_{ph}$ [95, 96]. An applied electric field induces dipolar ordering in electrocaloric materials and consequently reduction of the dipolar entropy S_{dip}. If this is done under adiabatic condition, the sample would release heat in order to satisfy the entropy condition $dS = 0$ or $dS_{dip} = -dS_{ph}$ (see the change from point $T_1(S_1, E_1)$ to point $T_2(S_2, E_2)$ in Figure 14). This is known as a heating part of ECE. After a while, when the system reaches the temperature equilibrium with the surrounding bath (from point $T_2(S_2, E_2)$ to point $T_1(S_3, E_2)$ in Figure 14) the applied field is removed. The dipolar subsystem gets disordered and the dipolar entropy of the system increases. To compensate the increasing of the dipolar entropy the phonon entropy is reduced resulting in a cooling of the system, i.e., system absorbs the heat from the surrounding which could be used in cooling devices (see the change from point $T_1(S_3, E_2)$ to point $T_3(S_4, E_1)$ in Figure 14). After some time the system reaches the initial temperature equilibrium with the surrounding bath and the electrocaloric cycle is completed (see the change from point $T_3(S_4, E_1)$ to point $T_1(S_1, E_1)$ in Figure 14).

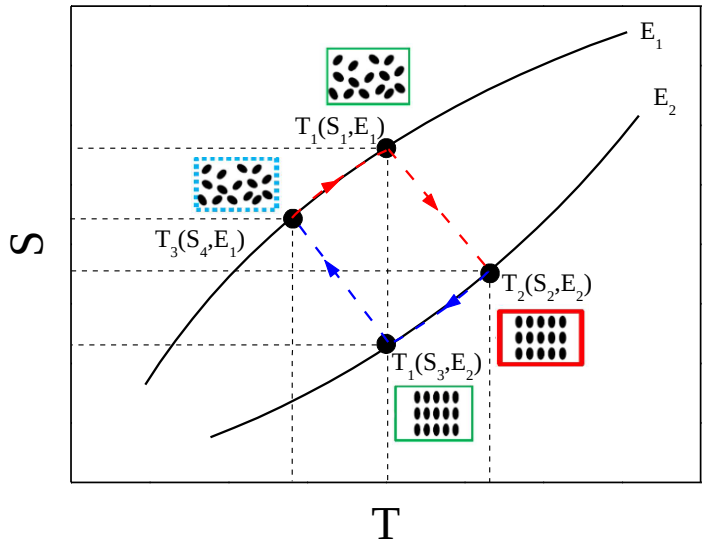

Figure 14: *Schematic representation of the electrocaloric cycle*. The schematic representation of the entropy during the electrocaloric cycle while the electric field is switched between the constant fields E_1 and E_2. The dashed blue and red lines represent cooling or heating parts in the cycle.

It is interesting to note that the so-called EC responsivity $\Delta T_{EC}/E$, i.e., a ratio between the ECE temperature change and the amplitude of the electric field was found to be the highest near the critical point in bulk relaxor ferroelectrics [75, 95, 97, 98]. This was found to be in good qualitative agreement with theoretical calculations based on the SRBRF model [95, 96]. Many ECE studies were done on relaxor ferroelectrics and polymers, but little on a ferroelectric single crystals [99, 100, 101, 102, 103]. In this thesis a study of the influence of the electric field on the paraelectric (P) to ferroelectric (FE) phase transition line in $BaTiO_3$ single crystal oriented along [001] direction will be presented. This transition is known to be of the first order at which relatively big amount of latent heat is released [3]. Within this thesis it was tested whether the P-FE transition line ends in a critical point and the influence of the critical point on the ECE behavior. The amount of the released latent heat in $BaTiO_3$ is much larger as in previous studied relaxor systems and it is expected that it could lead to additional enhancement of the EC responsivity, i.e., to the shift of the EC responsivity maximum with respect to the critical point in BT [93].

2 Experimental techniques and methods

2.1 Dynamic dielectric spectroscopy

Dielectric susceptibility, χ, or dielectric constant, ε, describes the response of material to the applied electric field and its ability to store charge. Let us take two parallel plates with a given area and plate separation held in vacuum, i.e., capacitor. By applying DC electric field the plates get charged which is described by a capacitance C_0. If we put a dielectric material between the plates the capacitance will increase to C since the electric field induces dipoles in the material which effectively cancel part of the charge on the plates (see Figure 15). The ratio of the capacitance between the charged and empty capacitor gives us the dielectric permittivity or dielectric constant of the material, $\varepsilon = \frac{C}{C_0}$. In terms of Maxwell's equation the influence of the electric field $\vec{E}$ on the dielectric material can be expressed by an electric displacement, $\vec{D}$:

$$\vec{D} = \varepsilon_0 \vec{E} + \vec{P}, \tag{26}$$

where ε_0 is a permittivity of vacuum ($8.85\times10^{-12}\ \frac{As}{Vm}$) and $\vec{P}$ is the electric polarization.

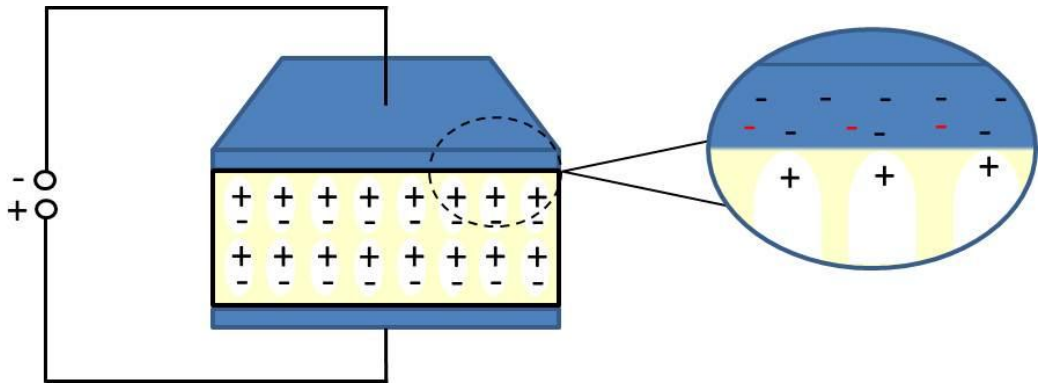

Figure 15: *Induced dipoles.* Applied electric field induces dipoles in the dielectric material. The enlarged picture of the layer between the electrode and the material shows the charge cancelation and addition charge acceptance (red minus).

By applying a sinusoidal voltage to the capacitor in vacuum, the charging current appears which is 90° shifted in phase in relation to the applied voltage. When the same alternating voltage is applied to the capacitor with dielectric material, the charging current is now less than 90° shifted in phase. This change in the phase is due to the fact that the dielectric materials do not have infinitely large resistivity and that some current leaks through the capacitor. This leaking current represents losses in the material.

Let us consider this situation in terms of E and D which are treated as a scalar for the reason of simplicity. The time varying electric field

$$E(t) = E_0 \cos(\omega t), \tag{27}$$

induces dipoles in material which can reorient themselves (switch) by following the direction of the electric field. In time interval, $[t,\ t+dt]$, in which the electric field is switched from one direction to another the electric displacement can be written as

$$D(t_1) = \varepsilon_\infty \varepsilon_0 E(t_1) + \varepsilon_0 \int_0^t E(t)\,\alpha(t_1 - t)dt,\ \ if\ t < t_1 < t + dt. \tag{28}$$

ε_∞ in the first term in equation (28) represents the response of dipoles which follow vary fast the time varying electric field, whereas the second term represents the part with delay, i.e., the phase shift $\frac{\pi}{2}$ and include simple decay function $\alpha(t_1 - t)$ [104, 105]. If the time period of the field switching is much longer $(t \to \infty)$ as the characteristic relaxation time (τ) in which the decay function falls to 0, then the dielectric displacement function is also periodic with the same period as the electric field and a phase shift

$$D(t) = \varepsilon_0 E_0 \cos(\omega t)\,(\varepsilon_\infty + \varepsilon') + \varepsilon_0 E_0 \sin(\omega t)\varepsilon''. \tag{29}$$

ε' and ε'' are the real and imaginary part of the complex dielectric constant

$$\varepsilon^* = \varepsilon' - i\varepsilon''. \tag{30}$$

The real part of the dielectric constant characterizes a material ability to store the charge and imaginary part is a measure of the heat related losses. By combining the equations (28) and (30) and assume that the decay function is a simple exponent function, $\alpha = \alpha(0)e^{-\frac{t}{\tau}}$, one get a Debye expression for the frequency dependent ε^*,

$$\varepsilon^*(\omega) = \varepsilon_\infty + \frac{\varepsilon_s - \varepsilon_\infty}{1 + i\omega\tau}. \tag{31}$$

The Debye expression describes the relaxation in the material with single relaxation time whereas in real materials a distribution of relaxation times can be found. Because the Debye function doesn't fit the dielectric response of most of the materials, an empirical ansatz called Cole-Cole ansatz was proposed [106]. The mean idea of this ansatz is that the complex dielectric constant can be described as a sum of Debye relaxations

$$\varepsilon^*(\omega) - \varepsilon_\infty = (\varepsilon_s - \varepsilon_\infty) \int_{\tau_1}^{\tau_2} \frac{g(\ln\tau)\,\mathrm{d}\ln\tau}{1 + i\omega\tau}, \tag{32}$$

where $g(\ln\tau)$ is the distribution of relaxation times [33, 35]. However the details of analysis of the dielectric response can be found in Refs. [104] and [105].

Now the question is how to measure the complex dielectric response of a material. As already mentioned above, the capacitor with the dielectric material between the plates is a non-ideal capacitor. Most of the dielectric materials have a large but not infinitive resistivity which means that material conduct electricity. Such leaky capacitor can be represented as an electric circuit with ideal capacitor in parallel with resistor, as shown in Figure 16.

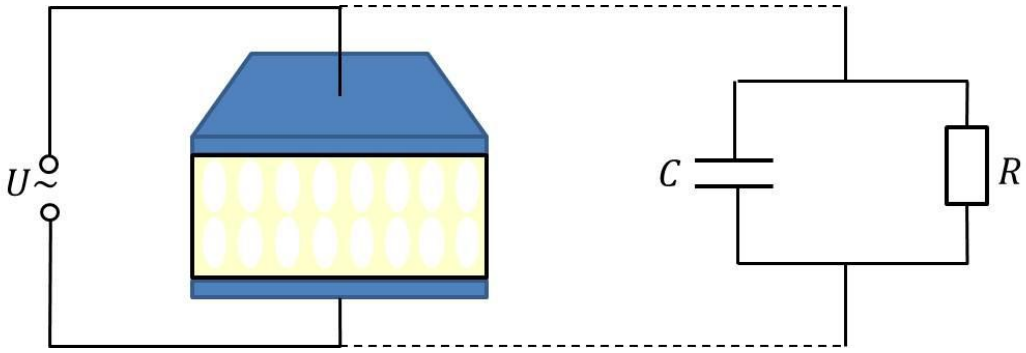

Figure 16: *Equivalent circuit.* The leaky capacitor with dielectric material can be represented by an equivalent circuit of parallel connected capacitor C and resistor R.

By applying an oscillating voltage probe signal on the sample one can measure the complex impedance, Z, of the sample

$$\frac{1}{Z} = i\omega C_0 \varepsilon^*. \tag{33}$$

Taking into account the above equivalent circuit from Eq. (33) expressions for ε' and ε'' are obtained

$$\varepsilon' = \frac{C}{C_0}, \tag{34}$$

$$\varepsilon'' = \frac{1}{RC_0\omega}. \tag{35}$$

The measurement method of impedance manly depends on the required frequency range. Most of the measurements of the complex dielectric constant are carried out in the frequency range from 20 Hz to 2MHz. Such frequency range can be covered by Agilent E4980A (4282A) Precision LCR Meter (LCR Meter) which belongs to standard equipment in our laboratory. LCR Meter uses auto balancing bridge method for measuring the impedance. The simplified schematic picture of auto balancing bridge is shown in Figure 17.

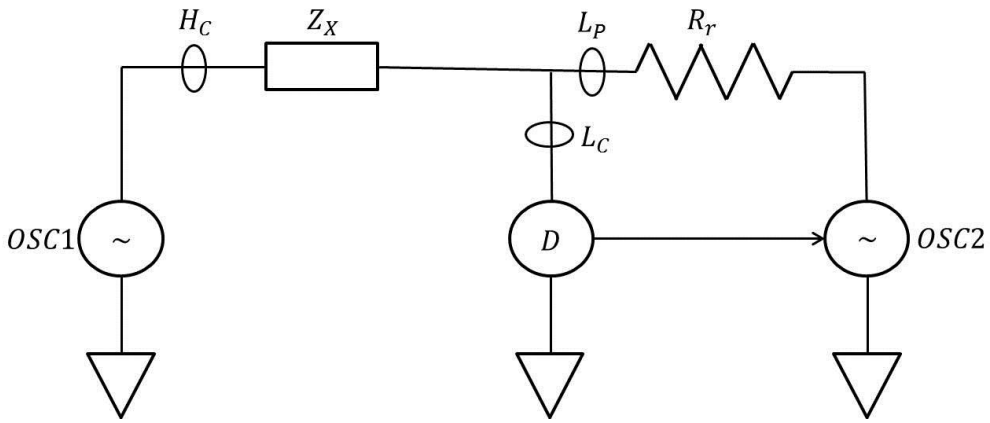

Figure 17: *Auto balancing bridge.* The schematic picture of auto balancing bridge which is used in LCR Meter. The bridge is in balance when the current detected by detector D is zero.

The OSC1 send a.c. probe signal to the sample with impedance Z_X. Because our sample represents non-ideal capacitor, some leakage current goes through the sample. On the other site OSC2 send a signal through a range resistor R_r. The detector D detects the

potential at the low terminal and if the potential is zero, the bridge is in balance. Actually we can say that detector measures the sum of leakage current of the sample and current which flow through R_r. If the currents are not equal, the sum is not zero and the detector detects an error current. In this case, the detector changes the output signal of OSC2 so that the error current goes to zero. When equilibrium is reached, the voltage on sample and resistor R_r is measured and since the resistivity of R_r is known, one can calculate the impedance of the sample and real and imaginary part of the dielectric constant [107]. The second part of our complex dielectric measurement setup represents the temperature stabilization unit. The core of the temperature stabilization unit is a Wheatstone bridge with two resistors of constant resistivity ($R_1 = R_2 = 500\ \Omega$), one variable decade resistor ($R_3 = 0 \rightarrow 5\ k\Omega$) and a platinum resistor ($R_{Pt} = 100\ \Omega\ at\ 20°C$). The platinum resistor is used as a temperature sensor and is placed in the measurement cell close to the sample, so that the temperature gradients are as small as possible. The Wheatstone bridge is connected to a phase detector and a power amplifier, as shown in Figure 18. The phase detector sends a reference signal to the bridge. The balance of the bridge, i.e., equality of R_3 and R_{Pt} is checked by lock-in detection of the voltage difference between the measuring points. When the bridge is unbalanced, the phase detector in combination with the power amplifier adjusts the current trough the heater in the measured cell and consequently changes the resistance of R_{Pt}. All processes such as setting the values of R_3 and measurement of R_{Pt} resistance by Keithley 196 System DMM are controlled via computer. This kind of temperature stabilization unit is capable to stabilize the temperature within accuracy of $\pm 1\ mK$ [108].

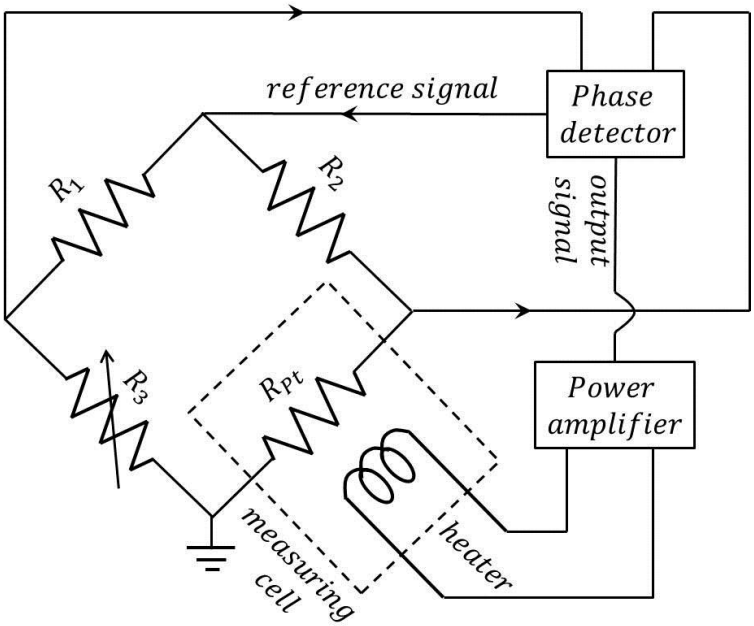

Figure 18: *Temperature stabilization unit.* The Wheatstone bridge is a hart of the temperature stabilization unit. The set temperature is given by the variable decade resistor R_3 and by heating the platinum resistor R_{Pt} the bridge is balanced and the temperature of the measuring cell changed.

2.1.1 Piezoelectric resonance measurements

The dielectric measurement setup can also be easily used for the so-called piezoelectric resonance measurements. Electromechanical effect or piezoelectric effect is the conversion of mechanical energy in electrical energy and vice versa. If we apply force on crystal it generates charge on its surfaces and by applying electric field the crystal changes its size. In the first case we talk about direct piezoelectric response and in second case about converse piezoelectric response. Both are very interesting for different applications in different fields like: robotics, telecommunications, ultrasonic devices, etc. The determination of the piezoelectric coefficient which is one of the important materials constant that characterize the material is relatively simple if large pieces of material are available. Namely, most of the commercially available methods today require relatively large samples prepared in a special geometry, apart of the interferometric method. Most of commercially available apparatuses operate only at the room temperature or at most in a very narrow temperature range about the room temperature. Thus the measurements of the piezoelectric response in a broad temperature range still represent a challenge. Here the resonance method represents a relatively simple method which can measure one component of the piezoelectric tensor d_{31} in a broad range of temperatures [109, 110]. If we apply electric field perpendicular to the length of the bar-shaped sample, this one acts like a resonator. The dielectric spectroscopy setup can be used to measure the admittance response as a function of the frequency at the constant temperature from which a transverse (d_{31}) piezoelectric coefficient can be determined. In the vicinity of the resonant frequency the admittance of such a resonator with a large piezoelectric loss can be expressed in terms of the complex dielectric constant $\varepsilon_{33}^{*} = \varepsilon_{33}' - i\varepsilon_{33}''$, the complex piezoelectric constant $d_{31}^{*} = d_{31}' - id_{31}''$, and the complex elastic compliance $s_{11}^{*} = s_{11}' - is_{11}''$, as [109, 110]

$$Y = i\omega\left(\varepsilon_{33}' - Re\left(\frac{{d_{31}^{*}}^{2}}{s_{11}^{*}}\right)\right)\frac{lw}{t} + \omega\left(\varepsilon_{33}'' + Im\left(\frac{{d_{31}^{*}}^{2}}{s_{11}^{*}}\right)\right)\frac{lw}{t} + i\omega\frac{8wl}{t\pi^2}\left(Re\left(\frac{{d_{31}^{*}}^{2}}{s_{11}^{*}}\right) + iIm\left(\frac{{d_{31}^{*}}^{2}}{s_{11}^{*}}\right)\right) \times \frac{\Omega - iM}{\Omega^2 - iM^2}, \tag{36}$$

where $M = \frac{s_{11}''}{s_{11}'}$, $\Omega = \frac{(\omega_0^2 - \omega^2)}{\omega_0^2}$ and ω_0 represents a resonant frequency. The parameters l, w and t are the length, width and thickness of a piezoelectric bar resonator, respectively. The admittance of the bar resonator with large piezoelectric losses can be analyzed by the analogy of the equivalent circuit introduced by Damjanović [109]. Equation (36) can be rewritten

$$Y = i\omega C_0 + \frac{1}{R_2} + \frac{1}{(i\omega C)^{-1} + i\omega L + R} + \frac{1}{(i\omega C_x)^{-1} + i\omega L_x + R_x}, \tag{37}$$

where R, C and L are the parameters of the equivalent circuit, and R_x, C_x and L_x describe piezoelectric losses. By expanding admittance Y as a sum of conductance G and susceptance B, $Y = G + iB$, expression for G and B can be derived

$$G = \frac{\omega^2 RC^2}{(1 - \omega^2 LC)^2 + \omega^2 R^2 C^2} - x\frac{\omega C - \omega^3 LC^2}{(1 - \omega^2 LC)^2 + \omega^2 R^2 C^2} + \frac{1}{R_2}, \tag{38}$$

$$B = \frac{\omega C - \omega^3 LC^2}{(1 - \omega^2 LC)^2 + \omega^2 R^2 C^2} + x\frac{\omega^2 RC^2}{(1 - \omega^2 LC)^2 + \omega^2 R^2 C^2} + \omega C_0. \tag{39}$$

By fitting the experimental data of G and B with equations (38) and (39) we obtain the parameters of the equivalent circuit which can be used to calculate the real and imaginary part of the complex piezoelectric coefficient. However, fitting experimental data with function which contains five fit parameters can sometimes represent a challenge. To avoid this problem one can use another approach to analyze the data. In this approach one transforms equations by replacing $G \to \varepsilon''$ and $B \to \varepsilon'$ whereby $\omega_0 = \frac{1}{\sqrt{LC}}$ and $\beta = \frac{RC}{LC}$. In the first approximation one can set the piezoelectric losses x to zero and with minimization of the function $\varepsilon'(\omega)$ one can find maximum and minimum of the function which corresponds to ω_1 and ω_2 frequencies in Figure 19, respectively. By using these two parameters one can calculate resonant frequency $\omega_0 = \sqrt{\frac{\omega_2^2+\omega_1^2}{2}}$ and parameters $\beta = \frac{\omega_2^2-\omega_1^2}{\sqrt{2(\omega_2^2+\omega_1^2)}}$ and $\Delta\varepsilon = \frac{\varepsilon''(\omega_0)\beta}{\omega_0}$. If $x = 0$, the following equation can be used to calculate the ratio

$$\frac{d_{31}''}{d_{31}'} = \frac{\beta}{\omega_0\left(1+\sqrt{1+2\left(\frac{\beta^2}{\omega_0^2}-1\right)^2}\right)}, \tag{40}$$

and the calculated value can be used to obtain

$$x = \frac{\frac{\beta}{\omega_0}\left(1-\frac{d_{31}''^{\,2}}{d_{31}'^{\,2}}\right)+2\frac{d_{31}''}{d_{31}'}}{1-\frac{d_{31}''^{\,2}}{d_{31}'^{\,2}}+2\frac{d_{31}''}{d_{31}'}\frac{\beta}{\omega_0}}. \tag{41}$$

Ones all the parameters are obtained one can calculate the real and imaginary part of the piezoelectric coefficient

$$d_{31}' = \pm\sqrt{\frac{\pi^4\varepsilon_0\Delta\varepsilon\left(\frac{1}{\omega_0^2}+\frac{\beta^2}{\omega_0^4}\right)\left(x-\frac{\omega_0}{\beta}\right)}{16\rho l^2\left(\frac{\beta^2}{\omega_0^2}-1\right)\frac{\omega_0}{\beta}}\left(1+\sqrt{1+2\left(\frac{\frac{\omega_0^2}{\beta^2}\left(\frac{\beta^2}{\omega_0^2}-1\right)^2\left(1-x\frac{\omega_0}{\beta}\right)^2}{\left(x-\frac{\omega_0}{\beta}\right)^2}\right)}\right)}, \tag{42}$$

$$d_{31}'' = \frac{\pi^4\varepsilon_0\Delta\varepsilon\left(\frac{1}{\omega_0^2}+\frac{\beta^2}{\omega_0^4}\right)\left(1-x\frac{\omega_0}{\beta}\right)}{16\rho l^2 d_{31}'\left(\frac{\beta^2}{\omega_0^2}-1\right)\frac{\omega_0}{\beta}}. \tag{43}$$

The calculated values of d_{31}' and d_{31}'' are obtained on the assumption that $x = 0$. To compensate this assumption one has to reiterate procedure by recalculating the x with new piezoelectric coefficients and repeat the procedure again to calculate the piezoelectric coefficients. The iteration procedure is repeated until x gets constant within required precision.

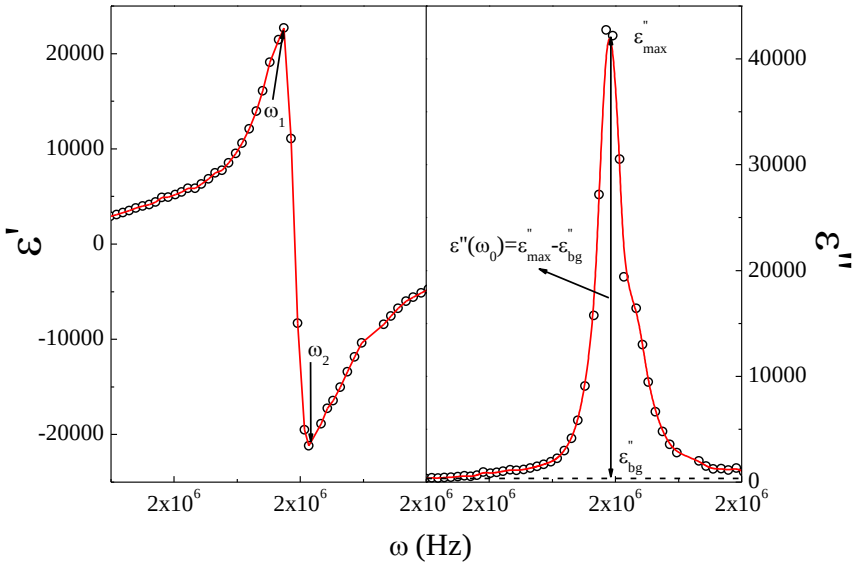

Figure 19: *Resonant response of the complex dielectric constant.* Left panel shows real part of the complex dielectric constant as a function of frequency from which a maximum and minimum frequency is deduced, ω_1 and ω_2, respectively. The right panel shows an imaginary part as a function of frequency from which the value of the dielectric background ε''_{bg} and maximum ε''_{max} at the resonant frequency is estimated.

2.2 Quasi-static polarization measurements via charge accumulation technique

Sawyer-Tower bridge is a standard method for measuring the polarization as a function of the electric field, i.e., hysteresis loop which is a most common measurement for analyzing the ferroelectric properties. The quasi-static polarization measurements were performed in a similar way just instead of oscilloscope we use Keithley 617 Programmable Electrometer in order to detect the accumulated charge related to the sample polarization. The measurement experimental time scale is on the order of 0.1 ms, hence quasi-static experiment. The sample is electrode in order to create a capacitor, C_X, which is then in series connected with another capacitor with known capacity, C_{00}. The capacity of known capacitor is usually much larger ($C_{00} \geq 100 \times C_X$) as the capacity of the sample capacitor. The circuit was supplied with the DC voltage signal from KEPCO power supply. Keithley 617 Programmable Electrometer is connected parallel to C_{00} to measure the voltage, U, on the known capacitor (see Figure 20). The measured voltage of C_{00} is linearly proportional with the polarization of the sample, P,

$$P = \frac{UC_{00}}{S}, \tag{44}$$

where S is a surface of electrodes on the sample. By using the same temperature stabilization unit as in the case of the dielectric measurements one can easily obtain a quasi-static polarization data as a function of temperature. To obtain a hysteresis loop the power supply was controlled via HP 3325B Synthesizer/Function Generator (Function Generator in Figure 20). Function Generator cycles the DC signal linearly between $\pm U_{DC}$, whereas electrometer measures the voltage of C_{00}. The advantage of this measurement is that the frequency of a DC signal can be easily controlled.

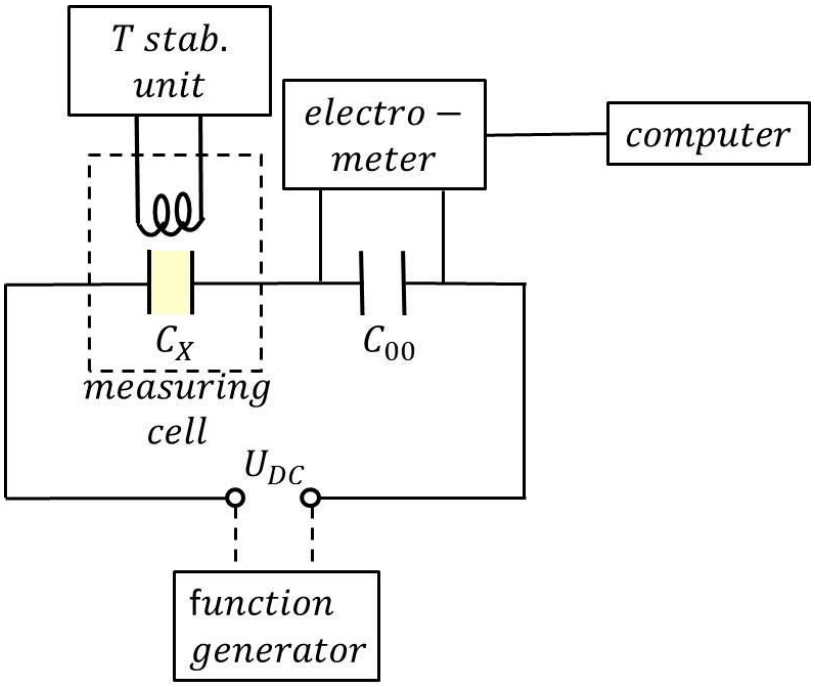

Figure 20: *Quasi-static polarization measurement setup.* Schematic representation of quasi-static polarization measurement setup used for the polarization measurements as a function of temperature and electric field.

2.3 High-resolution calorimetry

One way to obtain the value of thermodynamic quantities such as heat capacity, enthalpy, latent heat critical exponents and thus the information about nature of the particular phase transition and/or the thermodynamic state of the system is to employ a high-resolution calorimetric technique. Specifically, the high-resolution methods allow us a detailed study and characterization of the phase transitions which can occur in materials, the nature of critical energy fluctuations in the vicinity of the phase transitions and to distinguish between the first- and second-order phase transitions. In addition, it can provide information about the quantitative value of the released latent heat in the case of the first-order phase transition via measurements of the critical exponent α the information about the universality class to which the criticality belongs [111, 112, 113]. For this purpose different high-resolution experimental techniques were developed like traditional adiabatic calorimetry, differential scanning calorimetry (DSC) and ac and relaxation calorimetry [114]. Each of the techniques has his own advantages and disadvantages. For instant the traditional adiabatic method is very slow to get a really high resolution data and usually larger amount of a sample is needed. On the other hand a DSC method is faster with good sensitivity for detecting the enthalpy changes and needs smaller quantities of the sample. The main disadvantage of DSC is that one cannot make high resolution measurements near the phase transition due to the very fast scanning rates and thus one cannot determine the critical exponents and distinguish between the first- and second-order phase transitions [114]. In many cases it is almost insensitive to the second-order transitions with small enthalpy changes.

At the Jožef Stefan Institute, a full computerized home-made high-resolution calorimeter is used which can operate in a dual mode, ac and relaxation mode. The setup building block with used apparatuses is shown in Figure 21. In the ac and relaxation mode we apply power on the sample through the heater which is attached to the sample. The

heater on the sample is connected to the Krohn-Hite 5920 Function Generator which generates oscillating or linearly ramped input power, depending of the operating mode. Digital Multimeter Keithley 2002 measures the resistivity of the thermistor which is attached on the opposite site of the sample. The sample cell is closed by a cupper block, i.e., thermal shield 2 around which another heater is attached. The heater on the thermal shield 2 is connected to the LakeShore 340 Temperature Controller, which controls the stabilization of the bath temperature. To control the bath temperature two thermometers (a 100 Ω Platinum Resistor Thermometer or shortly PRT and a 1 kΩ or 500 kΩ thermistor) are placed in the cell block close to the sample to minimize the temperature gradients between the bath and the sample temperature. The PRT measures temperature T_{Pt}, which later serves for calibration of thermistor attached to the sample. The 1 or 500 kΩ thermistor is used to precisely measure the temperature of the bath T_b for the bath temperature stabilization purposes. The whole cell is then closed by another outer thermal shield 1. All the apparatuses are controlled by the computer who also stores the data measured during the experiment.

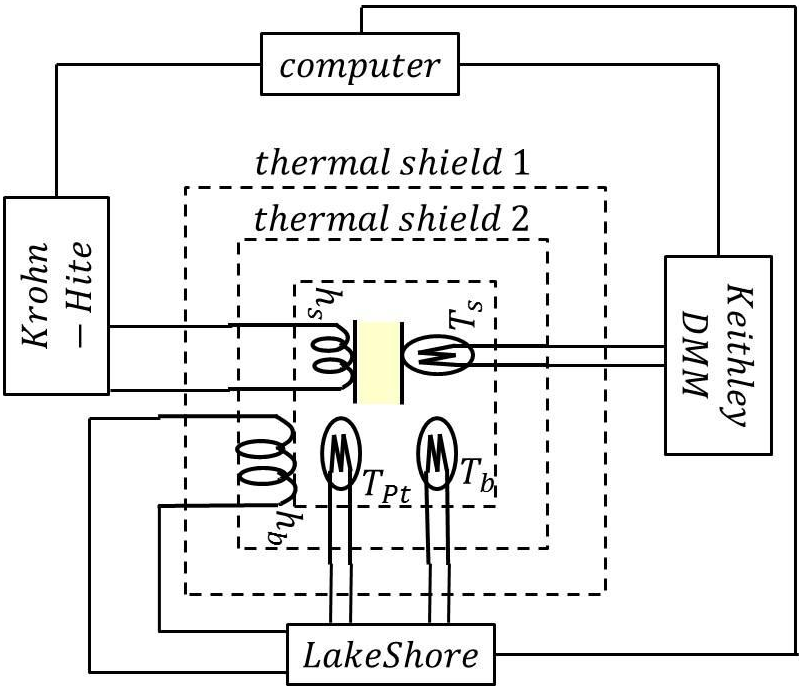

Figure 21: *Calorimetric setup.* The schematic representation of calorimetric setup used at IJS. For the measurement of the bath temperature are responsible platinum resistor thermometer and a bath thermistor T_{Pt} and T_b, respectively, whereas T_S measures the sample temperature. h_S and h_b are heaters attached to the sample and to the thermal shield 2, respectively.

For the analysis of the obtained data and the calculation of the heat capacity, C_p and the enthalpy, H a simple 'zero-dimensional' model of thermal analysis can be employed in all cases which will be presented in this thesis [114, 115]. It assumes that the internal relaxation time for achieving the internal temperature equilibrium of the sample, τ_{int}, is very short in comparison to the time scale of the variations of the sample temperature in order to avoid temperature gradients within the sample. Another simplification of the model is the assumption that the heat losses to the thermal bath can be represented by a single parameter, thermal resistance R of the gas in the cell and support wires that link the sample to a temperature controlled bath.

Now the basis for thermal analysis is the conservation of energy or first law of thermodynamics

$$dU = dQ + dW, \tag{45}$$

where dU is the internal energy of the system, dQ is the absorbed or released heat of the system and dW is the work done by the system or on the system. One can express the first law also in terms of enthalpy

$$dH = dU + Vdp = dQ + dW + Vdp, \tag{46}$$

where V is the volume and p is the pressure. For the processes at the constant pressure and by considering the time dependence we get

$$\frac{dH}{dt} = \frac{dQ}{dt} + \frac{dW}{dt}, \tag{47}$$

where $\frac{dQ}{dt}$ represents the heat flow between the sample and bath and can be written as $\frac{T-T_b}{R}$ with T as a sample temperature, whereas $\frac{dW}{dt}$ is the heat input power, P supplied over the attached heater. By taking into account also the relation between the enthalpy and the heat capacity, $dH = \left(\frac{\partial H}{\partial T}\right)_p dT = C_p^{sys} dT$, one can rewrite the equation (47) into

$$P = C_p^{sys} \frac{dT}{dt} + \frac{T - T_b}{R}. \tag{48}$$

C_p^{sys} is a total heat capacity of the sample and the cell, $C_p^{sys} = C_p + C_{p(cell)}$. Let us now take a look how can this model be used in systems exhibiting either first- or second-order phase transition. The major difference between the first- and second-order phase transition is the presence or absence of the latent heat L, respectively. The total enthalpy change of the first-order phase transition characterized by the latent heat is a sum of continuous δH and discontinuous changes of the enthalpy, where the released latent heat represents the discontinuous part, $\Delta H = \delta H + L$. The presence of the latent heat brings into equation (48) a new term, the conservation of energy yields

$$P = C_p^{sys} \frac{dT}{dt} + \frac{dL}{dt} + \frac{T - T_b}{R}, \tag{49}$$

where $dL = \bar{L} dm$ with $\bar{L}$ being the latent heat per gram and dm the mass of the material converted from one coexisting phase to another. Now one can calculate the heat capacity in the case of the first-order phase transition

$$C_p^{sys} + \frac{dL}{dT} = C_{eff}^{sys} = \frac{\frac{P - (T - T_b)}{R}}{\frac{dT}{dt}}, \tag{50}$$

where C_{eff}^{sys} denotes an effective heat capacity. In the case of the second-order phase transition (where $L = 0$)

$$C_p^{sys} = \frac{\frac{P - (T - T_b)}{R}}{\frac{dT}{dt}}. \tag{51}$$

2.3.1 Ac calorimetry

Let us discuss a little bit more in detail the ac calorimetric method. The ac calorimetry is based on an adiabatic scanning method with some modifications. The ac method uses the sinusoidal oscillating input power, $P = P_0 + P_0\cos(\omega t)$, and the thermal leakage $\frac{T-T_b}{R}$ is not negligible which makes the ac method a non-adiabatic scanning method. The frequency of the oscillating input power has to be chosen in the limited range $\frac{1}{\tau_{ext}} \ll \omega \ll \frac{1}{\tau_{int}}$, where τ_{ext} is the external relaxation time in which the sample temperature relaxes back to the bath temperature. In the case of our calorimeter at the Jožef Stefan Institute this frequency is typically $\omega = 0.0767$ Hz. If the bath temperature is constant during the measurement and the sample temperature is in thermal equilibrium $(T = T_b)$, then the sample temperature as a function of the time after switching on the input power is

$$T(t) = T_b + P_0 R\left(1 + \frac{\cos(\omega t)+\omega\tau_{ext}\sin(\omega t)}{1+(\omega\tau_{ext})^2} - \left(1 + \frac{1}{1+(\omega\tau_{ext})^2}\right)e^{-\frac{t}{\tau_{ext}}}\right). \tag{52}$$

After a long enough time, a steady state is reached and the exponential term can be neglected. Thus the sample temperature can be simplified as a sum of two components a dc and an ac component:

$$T(t) = T_{dc} + T_{ac}(t), \tag{53}$$

with

$$T_{dc} = T_b + P_0 R, \tag{54}$$

and

$$T_{ac}(t) = \frac{P_0 R}{1+(\omega\tau_{ext})^2}(\cos(\omega t) + \omega\tau_{ext}\sin(\omega t)) = \Delta T_{ac}\sin(\omega t + \varphi). \tag{55}$$

Here φ represent a phase shift between the input power oscillation and the temperature oscillation. By combining the expression (48) and (55) one can obtain the amplitude of temperature oscillations for the second-order phase transitions where $L = 0$

$$T_{ac}(t) = \frac{P_0}{\omega C_p^{sys}}\left(1 + \frac{1}{\omega^2 R^2 C_p^{sys\,2}}\right)^{-\frac{1}{2}}, \tag{56}$$

and the phase shift

$$\tan\varphi = \frac{1}{\omega R C_p^{sys}}. \tag{57}$$

The heat capacity is thus

$$C_p^{sys} = \frac{P_0}{\omega\Delta T_{ac}}\cos\varphi. \tag{58}$$

In the practice the phase shift is usually very small but not negligible $(\cos\varphi \neq 1)$. In such a case one can approximate the equation (58) by

$$\left(C_p^{sys}\right)^2 \approx \left(\frac{P_0}{\omega\Delta T_{ac}}\right)^2 - \frac{1}{\omega^2 R^2}, \tag{59}$$

where R can be estimated from the dc component of the sample temperature. The fact that the heat oscillations lag in phase behind the temperature oscillations brings another aspect of a dynamic behavior of the heat capacity into the discussion where the heat capacity is treated as complex function, similar as complex dielectric constant, $C_p^* = C_p'(\omega) + iC_p''(\omega)$. Combining this with equation (55) where $C_p^{sys} = C_p^*$ one obtains the expressions [59]

$$C_p' = \frac{P_0}{\omega T_{ac}} \cos\varphi, \tag{60}$$

and

$$C_p'' = \frac{P_0}{\omega T_{ac}} \sin\varphi - \frac{1}{\omega R}. \tag{61}$$

In most of the cases, the heat capacity is a purely real frequency-independent quantity: $C_p'(\omega) = C_p^* cos\varphi = C_p^{sys} cos\varphi$ and $C_p'' = 0$. The discussed method is known as classical ac method where by using the sufficiently precise experimental setup one can very accurate trace the sample temperature variation as a function of time while, achieving very good temperature stabilization. These allow very accurate determination of the sample heat capacity and the phase shift.

One can improve the classical ac method by slowly scanning the bath temperature which makes the method much faster. In this case the sample temperature is given

$$T(t) = T_{dc} + T_{ac}(t) + T_{exp}(t), \tag{62}$$

where $T_{ac}(t)$ is the same as before, $T_{exp}(t)$ is the exponential term of temperature which can be neglected in the steady state and dc component is

$$T_{dc}(t) = T_b(0) + \dot{T}_b(t - \tau_{ext}) + RP_0. \tag{63}$$

Now let us discuss how proper is the ac method in the case of first-order phase transitions where $L \neq 0$. At the first-order phase transition we have a coexisting range where the sample transforms from on phase into another. In the coexisting range the latent heat is released or absorbed depending whether the transformation occur from the phase with higher symmetry to the phase with lower symmetry or vice versa. The release or absorption of the latent heat can be observed in the anomalous variation of the sample temperature and the phase shift. The conversion from one phase to another can occur fast or slow which means that the release of latent heat can be quick or sluggish. In the case that the released latent heat is a smooth function of time the change of the sample temperature due to the released latent heat will not influence the T_{ac} oscillations but it will bring small changes to the $T_{dc}(t)$. In this case the analysis to obtain the heat capacity is the same as if there was no latent heat. However, if the release of latent heat is fast in comparison to the period of our sinusoidal temperature variations, this again does not affect the T_{ac} oscillations, but brings again changes to the $T_{dc}(t)$. In this case, the C_p^{sys} in equation (58) is substituted by the C_{eff}^{sys} which contains also a part of latent heat. Very often we deal with cases where the speed of the released latent heat is in between these two cases. In such cases the release of latent heat causes problems because it distorts the sinusoidal oscillations of the sample temperature. Because of the distortion one would get anomalous variation in the phase shift φ and an artificial large heat capacity response, $C_p^{sys} < C_p < C_{eff}^{sys}$. Therefore, the behavior of the phase shift carries additional

information about the nature of the phase transition. According to equation (57), the phase shift is inversely proportional to the heat capacity and the phase shift will exhibit a dip at the phase transition. At the first-order phase transition, the latent heat released in the coexistence range produces an anomalous peak instead of a dip in the phase response (see Figure 22(a)). However, if the amounts of the released latent heat at the first-order phase transition are small, then the phase shift exhibits a suppressed dip. On the other hand, at the second-order phase transition, the phase shift exhibits a sharp dip (see Figure 22(b)).

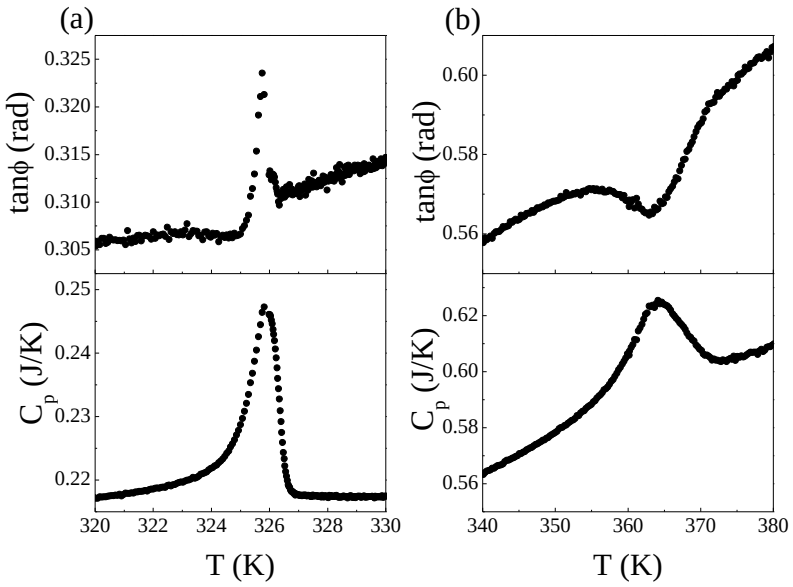

Figure 22: *Phase shift and heat capacity.* The phase shift and heat capacity as a function of temperature at: (a) first-order and (b) second-order phase transition. (a) In the upper panel the phase shift starts to decrease at the beginning of the coexistence range but the released latent heat produces a turnover into a peak. (b) In the second-order phase transition $L = 0$ and the phase shift exhibits a dip.

As we can see, the ac method is not the best suitable to study quantitatively the amount of latent heat released at the first-order phase transition because one gets only qualitative information about the latent heat existence. To get a quantitative value of released latent heat at the first-order phase transition, it is better to use the relaxation method which is much more sensitive to the released latent heat.

2.3.2 Relaxation calorimetry

As discussed in the last section the ac calorimetric method can be successfully used to study the heat capacity response of the materials. A constant scanning rate for the bath temperature used in the ac method is very useful in studying the nature of phase transitions. Nevertheless, ac method has also some disadvantages and one of them is its inability to quantitatively detect the latent heat released at the first-order phase transition. In such cases the relaxation method is much more convenient because of its sensitivity to the released latent heat. Another advantage of the relaxation method is its ability to measure small amount of the latent heat present at weakly first-order phase transitions [114- 116].

The original version of the relaxation method uses instead of sinusoidal oscillating

input power a step change of the input power. The relaxation method operates at constant bath temperature and is usually performed in a pair runs, heating part and cooling part or vice versa [114, 115, 116]. The step function of input power is switched from zero to P_0 in heating run whereas in cooling run the power is switched from P_0 to zero. Assuming for the moment that R and C_p are constant, then for the process without the latent heat the cell temperature relaxes exponentially:

$$T(t) = T_b + \Delta T_\infty \left(1 - e^{-\frac{t}{\tau_{ext}}}\right), \tag{64}$$

$$T(t) = T_b + \Delta T_\infty e^{-\frac{t}{\tau_{ext}}}, \tag{65}$$

for heating and cooling regime, respectively. ΔT_∞ is defined as $\Delta T_\infty = RP_0$ and represents the difference between the bath temperature and the equilibrium temperature reached after the P_0 is switched on. By fitting the cell temperature data with equation (64) or (65) one can determinate both R and τ_{ext} and calculate $C_p^{sys} = \frac{\tau_{ext}}{R}$.

If the process with latent heat occurs between T_b and $T(\infty)$, there will be an anomalous non-exponential variation of the $T(t)$. Yao et al. [115] solve this problem by introducing a time-dependent heat capacity

$$C_p(t) \equiv \frac{\dot{Q}}{\dot{T}}, \tag{66}$$

where $\dot{Q} = \frac{P_0 - (T - T_b)}{R}$ and $\dot{T}$ are time derivatives of the heat and temperature, respectively. But in the case of a step function for the input power we see that derivatives decay exponentially to zero which makes numerical calculation difficult at long times. To avoid this problem a linear function for the input power was introduced [115]. For a heating scan the power profile is

$$P(t) = \begin{cases} P = 0, & t < 0 \\ P = \dot{P}t, & 0 \le t \le t_1 \\ P = P_0 \equiv \dot{P}t_1, & t > t_1, \end{cases} \tag{67}$$

where $\dot{P} = \frac{dP}{dt}$ is a constant. In the cooling regime the power profile is reversed

$$P(t) = \begin{cases} P = P_0, & t < 0 \\ P = P_0 + \dot{P}t, & 0 \le t \le t_1 \\ P = 0, & t > t_1, \end{cases} \tag{68}$$

and $\dot{P}$ is negative. The variation of the cell temperature over the time interval $[0 \le t \le t_1]$ for linearly ramped power is

$$T(t) = T_b + R\dot{P}(t - \tau_{ext}) + \tau_{ext} R\dot{P} e^{-\frac{t}{\tau_{ext}}}, \tag{69}$$

$$T(t) = T_\infty + R\dot{P}(t - \tau_{ext}) + \tau_{ext} R\dot{P} e^{-\frac{t}{\tau_{ext}}}, \tag{70}$$

for heating and cooling regime, respectively. In this liner power mode the temperature varies almost linearly, $T(t) = T_b + R\dot{P}(t - \tau_{ext})$, which is much more convenient as exponential variation. In the process where $L = 0$ the C_p^{sys} is calculated with equation

(51) where $R = \frac{(T_\infty - T_b)}{P_0}$. In the case of the latent heat presence, R should be measured outside the two-phase coexisting range and interpolated within the coexistence region. For such cases the effective heat capacity was introduced which exhibit a strong peak in the coexisting range due to the anomalous variation of the time derivative of the temperature. By using equation (50) we calculate C_{eff}^{sys} which contains the continuous part C_p^{sys} and discontinuous part L. The difference between the C_{eff}^{sys} obtained in the ac and relaxation mode is in the accuracy of difference $\frac{P-(T-T_b)}{R}$ and the time derivative $\dot{T}$, which can be much more precisely determined in the relaxation than in the ac mode. The relaxation measurement is thus much more sensitive to the released latent heat and measures accurate the total change of enthalpy ΔH, whereas ac measurement does not detect quantitatively the released latent heat and measures only a continuous variation of the enthalpy, δH. The best method to obtain the value of the released latent heat at the phase transition is to combine both methods in order to calculate the difference between the total change of the enthalpy and continuous variation of the enthalpy δH

$$L = \Delta H - \delta H. \tag{71}$$

In practice we subtract the surface area obtained in the ac measurements from the surface area obtained in the relaxation measurement, as shown in Figure 23. The remaining surface area represents the released latent heat.

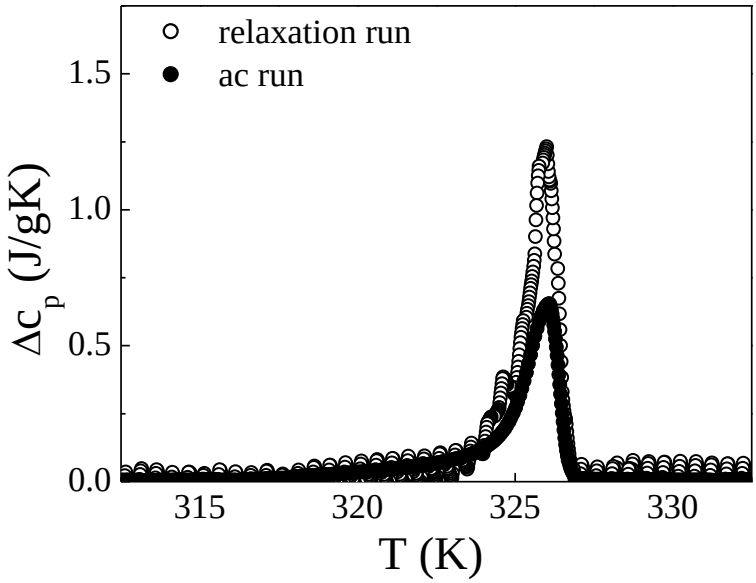

Figure 23: *Ac and relaxation measurements.* Comparison of the excess heat capacity obtained from the ac and relaxation measurements. The amount of released latent heat is equal to the difference of the integrals calculated for the relaxation and ac data.

More details related to the calorimetry with respects to specific problems studied in this thesis will be given in subsequent corresponding chapters.

2.3.3 Direct measurements of electrocaloric effect

The electrocaloric effect (ECE) is lately one of the hot topics in ferroelectric community due to the prediction of a giant ECE in some organic and inorganic materials [73, 74, 75, 94, 95]. These predictions were based on indirect ECE measurements of polarization as a function of temperature and electric field, $P(T,E)$ which are needed to calculate the magnitude of the ECE, ΔT_{EC}. By using Maxwell relation $\left(\frac{\partial P}{\partial T}\right)_E = \left(\frac{\partial S}{\partial E}\right)_T$, one can calculate ΔT_{EC} for a material with density ρ and the heat capacity C_p if the electric field changes from E_1 to E_2 [73, 74, 94, 96]

$$\Delta T_{EC} = -\frac{1}{\rho C_p}\int_{E_1}^{E_2} T\left(\frac{\partial P}{\partial T}\right)_E dE. \tag{72}$$

Another possible way to determinate the ΔT_{EC} is to measure it directly by using for instance so called electrocaloric thermometry [75, 95, 98]. In our case, the electrocaloric thermometry method is based on the same home-made high resolution calorimeter as for the ac and relaxation heat capacity measurements. Our setup allows us precise measurements of the sample temperature variation ΔT_{EC} produced by the change of the applied electric field and precise stabilization of the bath temperature which is crucial if ΔT_{EC} is small like in thin films on a substrate. The preparation of the sample for the direct ECE measurements is actually similar to that described in the calorimetric measurements with one difference, here we do not need heater (see Figure 24(a)).

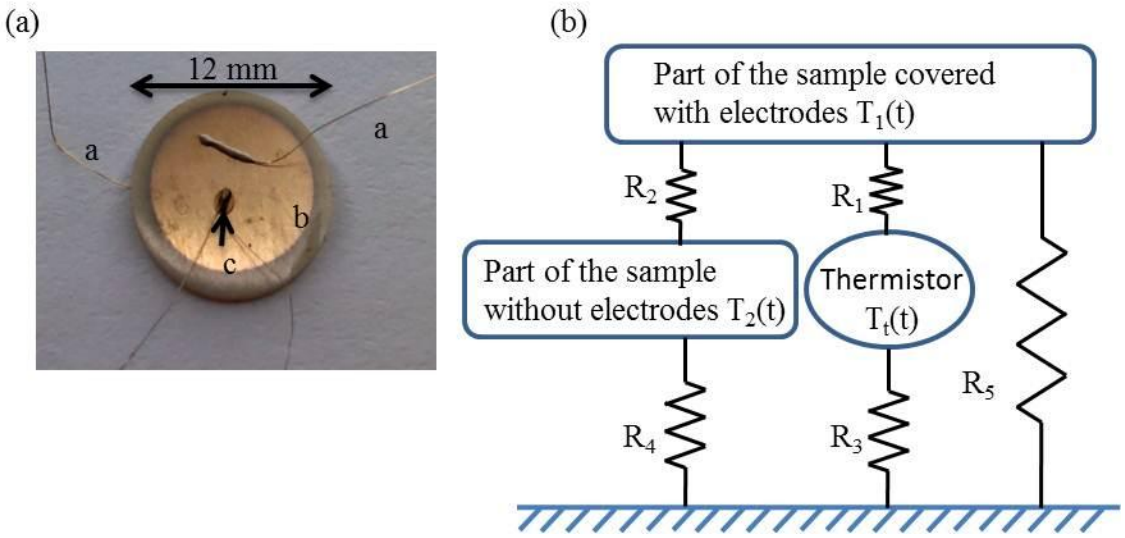

Figure 24: *Sample preparation.* (a) Photo of the sample prepared for the electrocaloric thermometry measurements. The wires for applying electric field are marked with a, gold electrode on the sample with b and c represents the thermistor attached to the sample. (b) Schematic representation of the typical sample thermal subsystems and their mutual coupling. Each subsystem has its own heat capacity C_p and the couplings are represented by the thermal resistances R_i, $i = 1, \ldots, 5$ [75].

As we can see in Figure 24(a), the whole system consists from different subsystems like parts of the sample with and without electrodes, attached wires and thermistor. These subsystems are thermally coupled together and finally linked with the bath. In order to analyze the sample temperature as a function of time, one has to take into account the presence of different subsystems and corresponding heat flow dynamics among them [75,

117]. By assuming that the internal thermal diffusion times of the sample are very short to avoid temperature gradients in the sample and also much smaller compared to the time scale of experimental data acquisition we can use again the physical zero-dimensional model. It has to be pointed out that the internal thermal diffusion times are very short in comparison to the external thermal time scale related to the coupling to the bath. Figure 24(b) represents a schematic diagram of the coupled subsystems linked to the bath. To get a solution of such a system one has to solve a system of three differential equations as it is shown in detail in Refs. [75] and [117]. The final solution is given as [117]

$$T_t(t) = T_{bath} + [(1 - A - C)\Delta T_{res} + (B + D)\Delta T_{EC}]e^{-\frac{t}{\tau_1}} + (A\Delta T_{res} - B\Delta T_{EC})e^{-\frac{t}{\tau_2}} + (C\Delta T_{res} - D\Delta T_{EC})e^{-\frac{t}{\tau_3}}, \quad (73)$$

where ΔT_{res} represents the additional Joule heating of the sample due to the finite electric conductivity and A, B, C and D are constants related to the thermal diffusion times and relation between them.

In the real systems it turns out that the internal thermal diffusion time is very fast and such a rigorous analysis is usually unnecessary and further simplification in the analysis can be employed. Such very fast transfer of heat through the whole sample allows very fast internal equilibration of the sample which now slowly loses the heat to the surrounding bath. In this case the system temperature change can be analyzed by consider only the external relaxation of the temperature

$$\Delta T(t) = T_{bath} + \Delta T e^{-\frac{t}{\tau_{ext}}}. \quad (74)$$

The final ECE temperature change of the subsystem covered with electrodes is then determined from

$$\Delta T_{EC}(t) = \Delta T(t)\frac{\sum_i C_p^i}{C_p^{EC}}, \quad (75)$$

where C_p^i stands for heat capacities of all subsystems involved in the fast internal equilibration and C_p^{EC} is the heat capacity of the sample part covered with electrodes where the ECE take place.

As already mentioned above, the setup for electrocaloric thermometry is the same as for the standard calorimetric measurements with only small modification of the tasks of the electronic devices. Digital multimeter (DMM) Keithley 2002 and LakeShore 340 Temperature Controller perform the same tasks as in calorimetric measurements, whereas the Krohn-Hite 5920 Function Generator is not any more used to apply an oscillatory or linearly ramped power, but it is used to generate the electric field step signal. The maximum output voltage of the generated signal is 15 V which does not give high enough electric fields to induce large ECE. For this reason the signal is amplified with a High Voltage Generator KEPCO to achieve desired electric fields. The duration of a step like pulses was chosen so that the sample could get into the thermal equilibrium with surrounding baths while the field remains still turned on. The measured resistance of the platinum resistor (PRT) and the microbead thermistor attached to the sample are collected by DMM and transferred to the computer. The example of a measured sample temperature response to the step-like electric field signal as a function of time is shown in Figure 25.

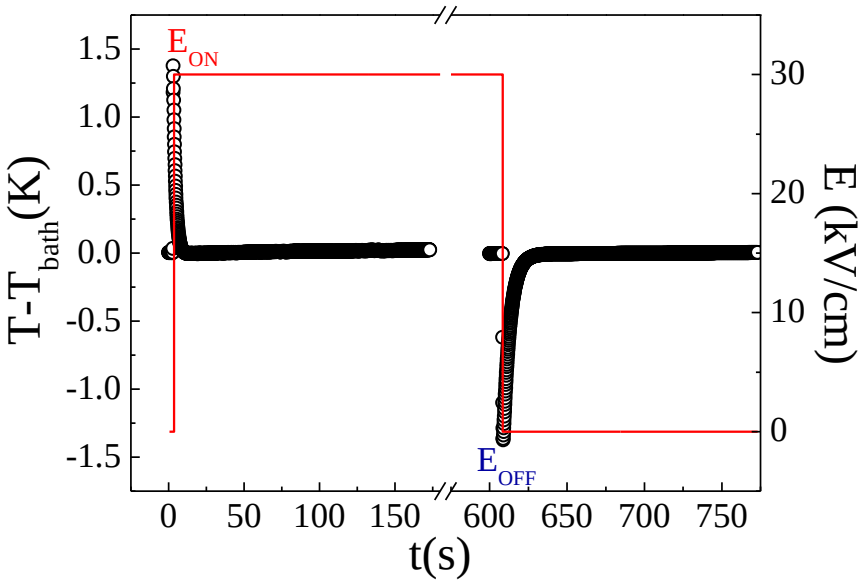

Figure 25: *Measured ECE data*. Open circles shows the sample temperature change during the electrocaloric measurement cycle. The solid line shows electric field step function typically used in the ECE measurements.

3 Liquid-vapor critical point in relaxors and ferroelectrics

As already mentioned in a subchapter, 1.3 a number of various concepts were proposed over the years to explain the physical picture of PMN relaxor system. Among them two phenomenological models emerge: (i) Random Field Ising model (RF) [40] and (ii) Spherical Random Bond-Random Field model (SRBRF) which is based on a mean field theory [51]. Both models agree that in the relaxor PMN system a long-range ordered ferroelectric phase is established if the applied electric field is high enough but they disagree in the description of the relaxor ground state. In this chapter we will compare these two models and we will try to give an answer to the long lasting question about the relaxor ground state. For this a series of experiments were performed such as polarization and heat capacity measurements as a function of bias electric field and temperature, quasi-isothermal measurements of the heat capacity under the linearly changing electric field, and quasi-isotherm measurements of the latent heat on a ferroelectric transition line induced by the linearly changing electric field. These experiments are designed to show thermodynamic properties of the phase transition line which should discern between two competing models.

3.1 Enigma of the PMN ground state nature

The main difference between the RF and SRBRF model is the interpretation of the relaxor ground state. According to the RF model the low temperature relaxor ground state is a ferroelectric state broken up into polarized nanodomains under the influence of quenched local random fields [40]. On the other hand SRBRF model does not take into account only the influence of random field but also the interaction between polar nanoregions (PNRs), so called random bonds. Depending on the strength of the random bonds a special kind of dipolar glass (DG) state appears [51]. This section will briefly describe predictions of both models so that later we could compare them with the experimental results.

Let us first reiterate some facts which are widely accepted for PMN relaxor. Lead magnesium niobate belongs to the group of B site disordered ferroelectric relaxors. In the absence of an external electric field, it can be well described at all temperatures by the cubic $Pm\bar{3}m$ space group with the same structure as the paraelectric structure of the ABO_3 perovskite ferroelectrics (see Figure 1) [63]. In the case of PMN the niobium ion is substituted with magnesium ion. Atomic disorder between Nb^{5+} and Mg^{2+} brings into the system difference in valence, ionic radium (0.64 Å vs. 0.74 Å) and electronegativity (1.6 vs. 1.2 on Pauling scale) [18]. The site and charge disorder seems to be the origin of relaxor properties [22, 118]. The X-ray and neutron diffraction studies show the statistical shift of the atoms from their ideal positions. The A site displacement of Pb ion was found to be 0.34 Å along the ⟨110⟩ or ⟨111⟩ directions, whereas O ions shift close to 0.20 Å in planes parallel to the faces of the cube and 0.06 Å in the perpendicular direction [63]. The displacement of the Nb/Mg ions could not be accurately evaluated because of too small displacement. However, the difference in the ionic radii and electronegativity between Mg and Nb results in different lengths of Nb-O and Mg-O bonds [63]. In PMN the B-sites contain a 1:2 distribution of divalent and pentavalent cations. The extensive studies that

have been conducted on the structures of the relaxors have led to the establishment and acceptance of the presence of regions with different compositional order on B site [49, 119, 120]. The ordered regions contain 1:1 distribution of different cation sites, whereas the disordered regions have 1:2 distributions [49, 119, 120]. On the mesoscopic level PMN is a structurally inhomogeneous material consisting of Nb-rich regions or polar clusters embedded in a quasiregular array of chemically ordered 1:1 regions or chemical clusters. The evidence for the existence of local polar clusters was provided from the study of the temperature dependence of the refractive index, n [27]. At high paraelectric phase the refractive index decrease linearly with decreasing temperature down to $T_B \cong 616\,K$, below which $n(T)$ deviates from linear dependence [27]. For the interpretation of the data they consider the quadratic electrooptic effect to relate the change in index, Δn and local polarization [27]

$$\Delta n = -\frac{(n^0)^3}{2}\left(\frac{g_{33}+2g_{13}}{3}\right)P_d^2. \tag{76}$$

n^0 is the index if there were no polarization and g_{33} and g_{13} are terms of the quadratic electrooptic tensor. The deviation is believed to be due to the formation of polar clusters with randomly oriented local polarizations, P_d. Because of the randomly oriented local polarizations the net polarization is zero, $\sum P_d = 0$, whereas $\sum P_d^2 \neq 0$ which means that the existence of polar clusters is manifested in properties that depend on P_d^2, like the quadratic electrooptic effect and electrostriction. Electrostriction describes the change of the crystal shape by applying of an electric field. The resulting strain remains unchanged on reversing the direction of E. Cross studied the thermal expansion of PMN and shows the deviation from linearity in strain temperature diagram sets at ~ 618 K [22]. An additional proof of the existence of PNRs brings the neutron diffraction scattering studies on PZN and PMN single crystals [46, 47]. The diffuse scattering appears around ~ 620 K, consistent with the Burns temperature $T_B \approx 616$ K for PMN, and increases almost exponentially with decreasing temperature [47]. These founding's strongly imply that the diffuse scattering in PMN results from the formation of PNRs at T_B. Nevertheless, the discussion about the formation of PNRs at Burns temperature is still ongoing and some studies give rise to doubt in the existence of fixed temperature at which the PNRs are formed [121, 122, 123]. The high-resolution dielectric studies show no anomaly in the dielectric constant between 500 and 750 K which would be related to the formation of PNRs [123]. These studies suggest that the actual Burns temperature is either well above the 750 K or the PNRs are continuously formed in a broad temperature range.

The difference between the RF and SRBRF model starts immediately after the PNRs are formed, with the interpretation of the nature and evolution of polar clusters. The site and charge disorder in PMN creates space charges and, hence, electric fields fluctuation on atomic length scales, i.e., random fields [40, 124]. The presence of random fields justifies the application of models that investigate the impact of random fields on low temperature ordering. A standard theoretical model used for the phenomenological RF description of relaxors is random field Ising model [40, 124, 125]. In this model the total energy or Hamiltonian is given by

$$\mathcal{H} = -\sum_{i,j} J_{ij} S_i S_j - \sum_i h_i S_i, \tag{77}$$

where J_{ij} is the strength of the nearest neighbor interaction energy at given site i or j and $S_{i,j} = \pm 1$ are the pseudospins [125, 126]. The second sum in equation (77) signifies the interaction of the pseudospins with quenched random field strength h_i. In the absence of random fields the Ising model will have an ordered ferromagnetic or ferroelectric phase in all dimensions $d > 1$ [125]. However, the additional RF term will act against the order. If

the random field strength is sufficiently large compared to the interaction strength, the pseudospins follow the orientation of the local field which results in disordered state. More interesting is the case where the random fields are weaker in comparison to the interaction strength but not zero. For this case Imry and Ma show that for $d \leq 2$ the ferromagnetic state becomes unstable with respect to the domain formation [127]. On the other hand this means that for the $d > 2$ long-range ordered state exists [128]. Westphal et al. applied the random field Ising model in order to explain the nature of the relaxor ground state and other observed properties of PMN [40, 124]. According to RF model the polar clusters in PMN are treated as ferroelectric nanodomain. By considering the random field Ising model, one would expect a formation of macroscopic long-range ordered ferroelectric domain state in PMN. But Westphal et al. proposed that the long-range order at low temperature is destroyed by the presence of the strong random fields and that the random fields are the origin of the slowing down of the polarization relaxation of PMN and its freezing into nanodomain state [40].

The interpretation of the relaxor ground state as a random-field-induced nanodomain state is based on the results of optical measurements. The zero linear birefringence as a function of temperature in a zero-field cooling/field heating (ZFC-FH) protocol was interpreted as a sign of a random distribution of spontaneously polarized domains and their complete immobility. Sufficiently large electric field applied to the crystal induces large linear birefringence in FH protocol. This indicates the formation of long-range ordered polarized state, whereas the FH/ZFC protocol shows the thermal stability of long-range state once frozen in [40]. The time dependence of the linear birefringence shows a number of discontinuous jumps approximately 500 s after the field was applied. The optically detected Barkhausen jumps were related to the depinning of microdomains, which in turn provide the evidence of the ferroelectric domain state.

In addition to the optical studies also some data obtained from dielectric permittivity measurements as a function of ac electric field were interpreted as an evidence of domain wall motion process [61, 62]. Recently, Fu et al. presented TEM and Raman scattering measurement data obtained on PMN single crystal oriented along [110] direction in favor of RF model [129]. The zero-field Raman scattering measurements show softening of observed frequency towards transition temperature $T_C \sim$ 225 K. In support to Raman scattering data, TEM measurements were presented which show some domain walls at $T < T_C$. Those finding seems to support the random field Ising model according to which system may order even in zero electric field [128]. Figure 26 shows the schematic $E - T$ phase diagram according to the random-field theory prediction. In this case, the line which separates the ferroelectric nanodomain and microscopic ferroelectric phase is a kind of conversion line at which the system goes from disordered into ordered state even at zero electric field. However, the RF model has some problems to explain the polarization behavior as a function of temperature and electric field [25, 27, 28, 29, 37, 48]. The absence of jumps in $P(T)$ measured at low constant electric fields gives rise to the suspicion of the existence of the ferroelectric nanodomain state in relaxors. If the relaxor ground state was ferroelectric nanodomain state, then one would expect to observe some jumps in the polarization due to the domain reorientation even at small electric fields at the conversion line. In contrast, one can observe only one discontinuous jump in the polarization if the applied electric field is high enough. The same story is repeated with the polarization evolution as a function of the electric field at constant temperature. Another problem of the RF model is the absence of the heat capacity anomaly at zero electric field at the conversion line tested in a wide temperature range [67]. If the ferroelectric nanodomain state is formed at some higher temperature, one should observe an anomaly in the heat capacity related to the onset of ferroelectric phase.

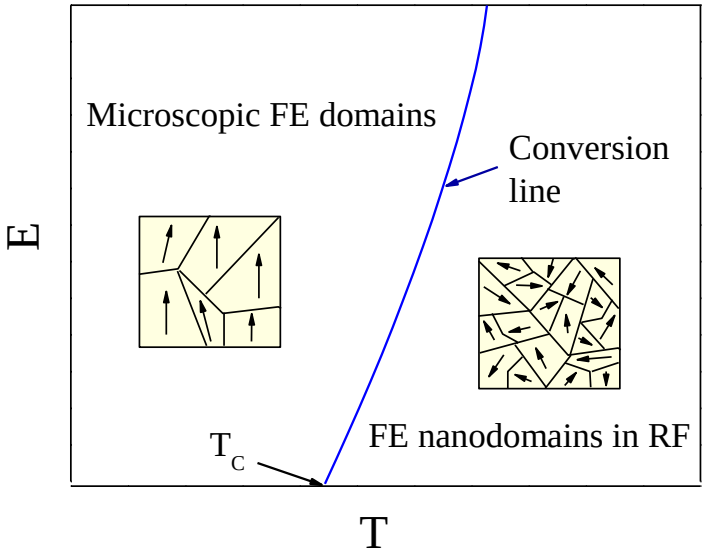

Figure 26: *Schematic $E-T$ phase diagram for RF scenario.* Theory predicts the formation of the microscopic ferroelectric (FE) state at T_C in zero electric field. The solid line represents schematically conversion line where nanodomains are reoriented into long range microscopic FE state.

In contrast to RF model the SRBRF model describes the dielectric behavior of relaxor ferroelectric materials more adequate and rigorous [51]. The structurally inhomogeneous B site of relaxor materials is the origin of formation Nb rich polar clusters which are embedded in chemically ordered regions or chemical clusters [119]. The polar clusters have strong temperature and electric field dependence and are reorientable. As such they are responsible for the observed dielectric behavior [24, 28]. On the other hand the chemical clusters are temperature independent and essentially static. The charge imbalance within ordered chemical clusters is the source of random fields in relaxor materials [51]. SRBRF model describes the interactions between polar clusters via *"random-bonds"* and takes into account the influence of random fields. Each polar cluster C_i consists of number of cubic unit cell distorted by the shift of the ions on A and B sites from their equilibrium position. Let us say that $\vec{u}_k(il)$ is the displacement of the k-th ion with the charge $e_k(l)$ in l-th unit cell from its ideal perovskite cubic position in polar cluster C_i. The overall dipole moment of the cluster C_i is then

$$\vec{p}_i = \sum_l \sum_k e_k(l)\vec{u}_k(il) \approx n_i \vec{p}_0(i), \tag{78}$$

where n_i is the number of all unit cells inside one polar cluster. For the sake of simplicity, in order to calculate the dipolar moment of the polar cluster, two assumptions were made. The first assumption is that only cells with Nb ion contribute to the dipole moment, and n_i is actually the number of Nb-type of cells inside the cluster. The second assumption is that each Nb cell in the polar cluster has the same dipole moment $\vec{p}_0(i)$ [51, 108].

SRBRF model is based on randomly competing interactions between reorientable polar clusters in the presence of random fields. The experimental study based on the quadrupole perturbed NMR technique show that the probability distribution of the local polarization in PMN remain Gaussian at all temperatures [45]. This suggests that in a relaxor, the order parameter field is described as a continuous vector field of variable length. Thus, a

dimensionless order parameter field $\vec{S}_i$ is introduced, which is proportional to the dipolar moment of the cluster and the number of Nb-type cells, which has a large number of equilibrium orientations [51]. Therefore it is assumed that each component $S_{i\mu}(\mu = x, y, z)$ varies in the range $-\infty < S_{i\mu} < +\infty$. If the order parameter field satisfies the closure relation

$$\sum_i \left(\vec{S}_i\right)^2 = 3N, \tag{79}$$

this then leads to a spherical vector model or SRBRF model [51].

The total energy/Hamiltonian of a SRBRF model of a relaxor system is then written as

$$\mathcal{H} = -\frac{1}{2}\sum_{i,j} J_{ij}\vec{S}_i \cdot \vec{S}_j - \sum_i \vec{h}_i \cdot \vec{S}_i - g\sum_i \vec{E}_i \cdot \vec{S}_i, \tag{80}$$

where J_{ij} are random interactions or bonds and $\vec{h}_i$ random local electric fields. By analogy to spin and dipolar glasses it is assumed that the random bonds are infinitely ranged with a Gaussian probability distribution characterized by the mean value $\left[J_{ij}\right]_{av}^{C} = \frac{J_0}{N}$ and the variance $\left[J_{ij}^2\right]_{av}^{C} = \frac{J^2}{N}$ [30, 31, 32, 33]. Similar assumption as for random interaction is taken for random electric fields which obey an independent Gaussian distribution with the average mean value of zero $\left[h_{i\mu}\right]_{av}^{C} = 0$ and the variance $\left[h_{i\mu}h_{j\nu}\right]_{av}^{C} = \Delta\delta_{ij}\delta_{\mu\nu}$. The third part of equation (80) is related to the interaction between polar clusters and applied external electric field $\vec{E}_i$, where g is effective dipole moment [51]. By applying the replica method random averages over J_{ij} and $h_{i\mu}$ are performed to write down the expression for the free energy. In the expression of the free energy of the system, two order parameters appear. The first one is polarization

$$P_\mu = \frac{1}{N}\sum_i \langle \vec{S}_{i\mu} \rangle, \tag{81}$$

and the second one is the Edwards-Anderson order parameter for a special kind of dipolar glass/spherical glassy state

$$q_\mu = \frac{1}{N}\sum_i \langle \vec{S}_{i\mu} \rangle^2. \tag{82}$$

For the reason of simplicity it is assumed that the external electric field is applied along [111] direction, hence the order parameters are independent of direction. With the minimization of the free energy the following equation for order parameters are obtained [51]

$$P = \beta(1-q)(J_0 P + gE), \tag{83}$$

$$q = \beta^2(1-q)^2(J^2 q + \Delta) + P^2, \tag{84}$$

where $\beta = \frac{1}{kT}$, and k is the Boltzmann constant set here to $k = 1$.

Now, let us discuss the case when the external applied electric field is zero in the presence of random electric fields $(\Delta \neq 0)$. The equations (83) and (84) have two sets of solutions: (i) $P = 0$ and $q \neq 0$ and (ii) $P \neq 0$ and $q \neq 0$. The first pair of solutions corresponds to a dipolar glass state without long-range order, whereas the second pair of solution belongs to ferroelectric state with long-range order. The ferroelectric phase can

be established only if $J_0^2 > J^2 + \Delta$ where the random field strength should not exceed some critical value which would prevent the formation of long-range order at any temperature. If the condition for long-range order is satisfied, then a ferroelectric phase appears below the critical temperature

$$T_c = J_0 \left(1 - \frac{\Delta}{J_0^2 - J^2}\right) \theta \left(\frac{J_0}{J-1}\right), \tag{85}$$

where $\theta(x)$ is the unit step function [51].

By applying the external electric field larger than the critical field of relaxor system, a ferroelectric phase is induced. This implies that J_0 is a function of external electric field and therefore the SRBRF model can be applied to other relaxor ferroelectric materials by using proper $J_0(E)$ relation as this was shown in the case of 6.5/65/35 hot pressed PLZT ceramics [130]. The validity of SRBRF model was tested by the investigation of the nonlinear dielectric response in dipolar glassy (DG) phase and ferroelectric (FE) phase. Because of easier discrimination between the DG and FE behavior the scaled nonlinear response $a_3(E) = \frac{\chi_3(E)}{\chi_1^4}$ was introduced. The a_3 in DG phase exhibits a divergent behavior, whereas in FE phase a_3 should not diverge. In experiments, a_3 behavior was measured for PMN and PLZT ceramics at higher temperatures where the dielectric dispersion is weak [37, 48, 50]. In both cases data show a quasidivergent behavior which is in good agreement with the SRBRF model prediction. However, the nonlinear dielectric measurements were performed at high temperatures where the impact of the dynamic effects is negligible and the quasidivergent behavior was assumed on the basis of the fitting results. For this reason, the nonlinear dielectric response does not give strong enough evidence to confirm the existence of the glassy state.

3.2 Experimental results

From the discussion above, it is obvious that the nature of the relaxor ground state is not resolved yet and due to lack of arguments it is difficult to discern between two competing models favoring either glassy or random-field ferroelectric state. The main question that arises is which experimental approach would be most suitable to distinguish between the glassy and ferroelectric state. In the case of the ferroelectric nanodomains ground state the ferroelectric nanodomains should exhibit a rhombohedral symmetry [41]. According to the X-ray studies, this would imply that the relaxor ground state has the same structural symmetry as the electric field-induced long-rage ordered ferroelectric phase [131, 132]. This leads to the conclusion that in the case of the ferroelectric nanodomain state, the applied external electric field does not induce a structural phase transition at which the symmetry is changed, but only a reorientation of nanodomains via domain wall motion to establish long-range ordered ferroelectric macrodomain state. Thus, the solid line in $E - T$ phase diagram (see Figure 11) does not represent a true phase transition line but rather a kind of conversion line resembling a coercive field line at which the system transforms from the short-range ordered ferroelectric nanodomain state into the long-range ordered ferroelectric macrodomain state. On the other hand, if the relaxor ground state is a glassy state with average cubic structure, the applied electric field would induce a break of symmetry and consequently formation of a rhombohedral ferroelectric phase. Therefore, the best way to discern the nature of the relaxor ground state is to study the thermodynamic properties of the phase transition line separating the low and high electric field regions of the $E - T$ phase diagram. If the transition line represents a true phase transition line, critical or discontinuous anomalies should be observed in thermodynamic quantities, such as the heat capacity and polarization order parameter. In the case that the

phase transition is of the first-order, a latent heat should be observed by calorimetric measurements. In the following sections, the experiments dealing with the question about the nature of the transition line will be presented. All experimental data shown in this chapter were obtained on annealed [110] PMN sample to avoid the history effects of previous treatment.

3.2.1 Polarization measurements

The measurement of the polarization as a function of the temperature and electric field is the basic experiment to determine the unusual ordering properties since the polarization plays a role of the order parameter [4, 20, 22, 25, 27, 28, 29, 37, 54, 55, 56]. Typically, a sharp and discontinuous jump of order parameter indicates a first-order phase transition whereas a continuous evolution of the order parameter indicates a second-order phase transition.

The quasi-static polarization measurements via charge accumulation technique under isofield and isothermal condition were conducted on PMN single crystal oriented along [110] direction. Figure 27 shows temperature evolution of the polarization at various constant electric fields between 100 and 340 K, i.e., isofield measurements [57]. The discontinuous jump in the polarization appears at critical electric field $(E \geq E_C)$ necessary to induce the phase transition, denoted by a line in the $E - T$ phase diagram. The step in the polarization mark the onset of long-range ordered ferroelectric phase and can be related to the first-order phase transition due to the observed discontinuity. With increasing electric field the discontinuous step moves towards higher temperatures and gets less sharp. Around 8 kV/cm the discontinuous step disappears and the polarization response gets continuous and smooth. Similar behavior of the polarization was observed in the PMN single crystal oriented in [111] direction and PMN-PT system [55, 56]. In [111] PMN single crystal the electric field at which the discontinuous step disappears was found at 4 kV/cm which is slightly lower as in [110] direction [55]. However, this is expected since the [111] axis is expected to be the polar axis of the electric field-induced ferroelectric phase.

The crossover from discontinuous to continuous evolution of the polarization was interpreted as a consequence of the existence of the liquid vapor type critical point in the system [55, 56, 57]. The electric field-induced first-order relaxor to ferroelectric transition line ends in a critical point which is the only second-order transition point. Above the critical point the symmetry difference between the different phases disappears and the response function such as polarization, dielectric constant, and heat capacity exhibit a continuous supercritical evolution. The crossover in the polarization behavior is a strong indication of the presence such of critical point also in the [110] PMN system.

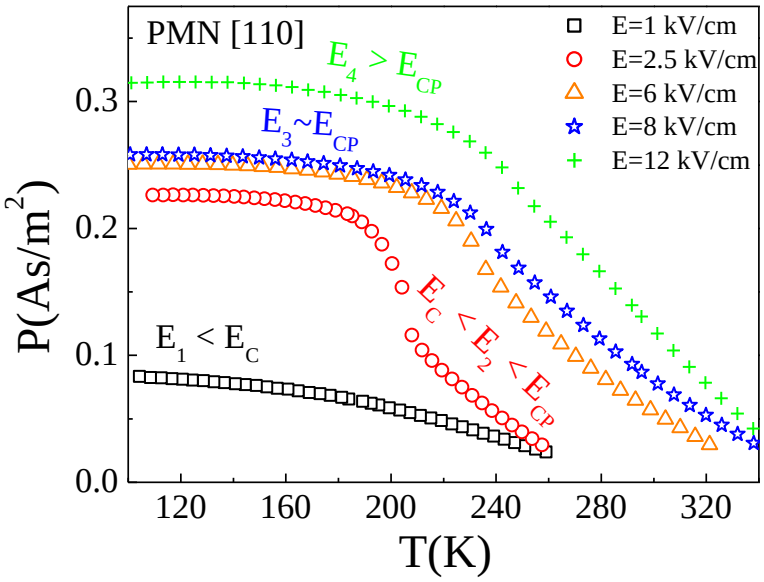

Figure 27: *Quasi-static polarization.* The temperature evolution of the polarization at several different constant electric fields.

The isothermal polarization measurements, i.e., hysteresis loop measurements reveal similar behavior of the polarization as isofield measurements. The obtained hysteresis loops are shown in Figure 28.

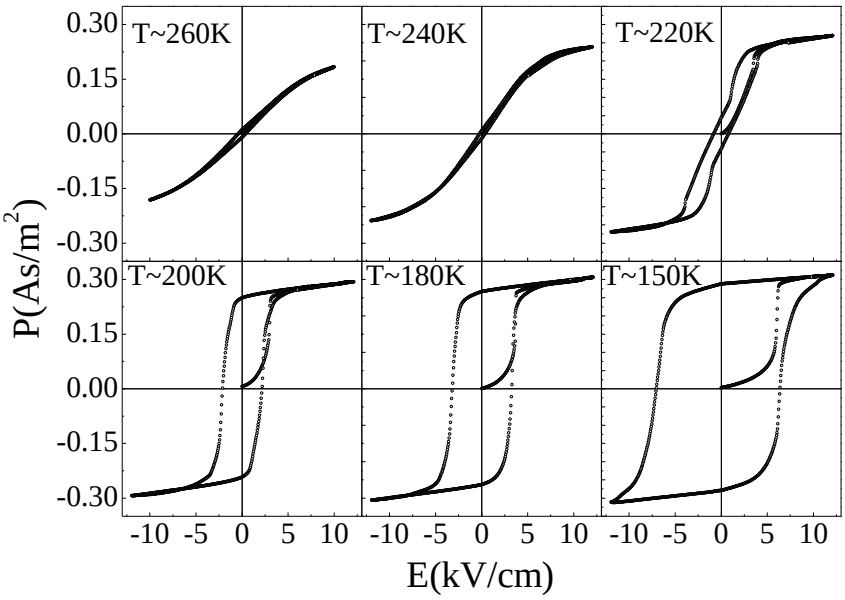

Figure 28: *Hysteresis loops for [110] PMN*. Typical relaxors slim hysteresis loop observed at higher temperature starts to broadened with decreasing temperature. A discontinuous jump of the polarization marks a first-order phase transition.

In high temperature/ergodic phase slim hysteresis loops are observed which is typical for relaxors. By cooling the system towards the freezing temperature at ~ 224 K and below, in the so-called nonergodic phase, the hysteresis loops start to broaden.

Broadening of the hysteresis loops is a consequence of the slowing down of the polarization relaxation processes [37, 38, 54]. However, the polarization electric-field dependence exhibits a sharp discontinuous step in the range of electric fields between the E_C and $\sim$ 8 kV/cm. Here, in contrast to isofield measurements the increasing of discontinuous step together with the increase of critical electric field is observed with decreasing temperature. Therefore, the value of the critical electric field E_C at particular temperature depends on the way how the ferroelectric phase is approached, i.e., along the isofield direction ($E =$ const. and $T \neq$ const.) or along the isothermal direction ($T =$ const. and $E \neq$ const.) [52, 54- 57].

Although the discontinuity observed in the polarization temperature or electric field profile may suggest a behavior typical for a first-order phase transition as expected for the glass-to-ferroelectric phase transition, one should also consider a possibility that such a sharp increase of polarization could be the result of rather rapid domain switching around a very sharply defined coercive field. In this case, discontinuous steps would not represent the actual ferroelectric phase transition but merely the collective switching of already established randomly frozen ferroelectric domains according to the RF picture [40, 81]. Despite the very indicative critical behavior of the polarization, which favors a glassy scenario, it is obvious that the polarization studies alone cannot provide a definitive answer about the ground state of relaxors.

3.2.2 Calorimetric study of electric-field-induced ferroelectric phase transition

As already discussed above, the behavior of thermodynamic properties like heat capacity, enthalpy, and latent heat in the vicinity of the glassy to ferroelectric transition line should provide more information about the ground state of the PMN relaxor. In the case of the RF picture the ferroelectric order should be established already at some higher temperatures even in the absence of the electric field and consequently only switching and coalescence of the randomly frozen domains should be observed when crossing the conversion line either by increasing the electric field at constant temperature or decreasing the temperature at constant field. In such case no latent heat (L) and only very minute change of enthalpy should be observed at the $E_C(T)$ conversion line. In contrast, in the glassy picture the conversion line represents the true phase transition between the dipolar glassy and long range ferroelectric state. In this case, significant change in the enthalpy and the latent heat should be observed when crossing the relaxor to ferroelectric line. In order to detect the enthalpy changes, the ac and relaxation measurements of the heat capacity (C_p) were conducted.

The temperature and the electric field dependence of the excess heat capacity (ΔC_p) obtained from the ac measurements in the PMN [110] single crystal are displayed in Figure 29(a) and Figure 29(b), respectively [57]. The temperature evolution of C_p at various bias electric fields clearly shows an excess heat capacity only if $E \geq E_C$ (see Figure 29(a)). At much higher electric field, $E =$ 14 kV/cm, the C_p anomaly is suppressed indicating supercritical behavior. The obtained behavior of the excess heat capacity is similar to that observed at the cubic to tetragonal (C-T) phase transition in PMN-PT [55]. The isofield excess heat capacity anomalies therefore represent direct evidence of a long-range ferroelectric state formation when crossing the long-range ferroelectric transition line (solid line in Figure 11). Additional proof that the excess heat capacity is truly connected with the established ferroelectric order is provided by the isothermal heat capacity measurements in which C_p is measured as a function of the electric field at constant temperature (see Figure 29(b)). The overlapping discontinuous steps in the

polarization and excess ac heat capacity presented in Figure 29(b) indicate that the observed sharp steps in the polarization are indeed the consequence of a first-order ferroelectric transition. Thus one may expect that latent heat will be observed when crossing the ferroelectric transition line, which in the case of isothermal experiments, presented in Figure 29(b), will result in a sharp sudden heating of the sample and vice versa if the field is reduced. From measurements of such a sharp electrocaloric increase (decrease) of the sample temperature it is possible to estimate the released (absorbed) latent heat.

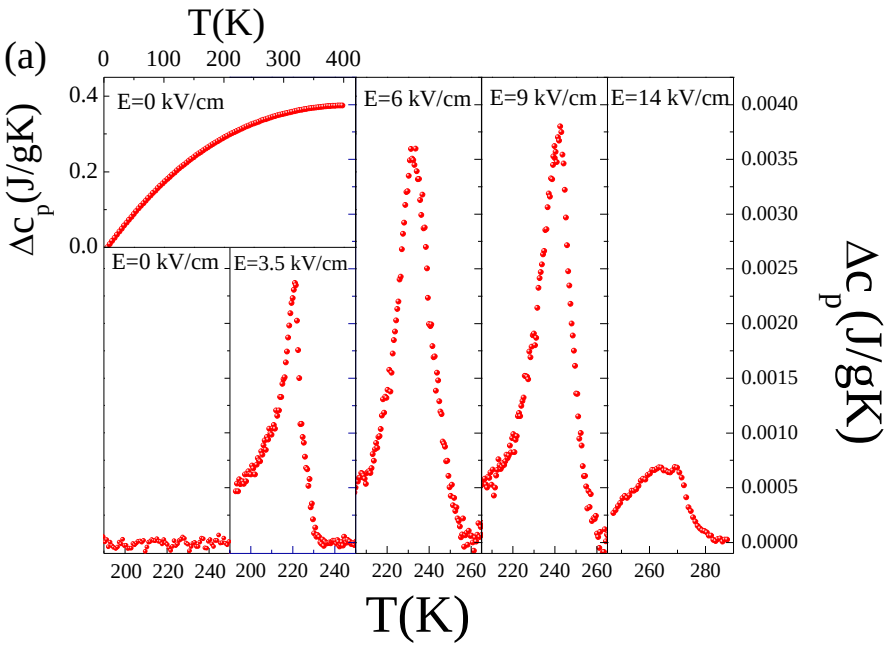

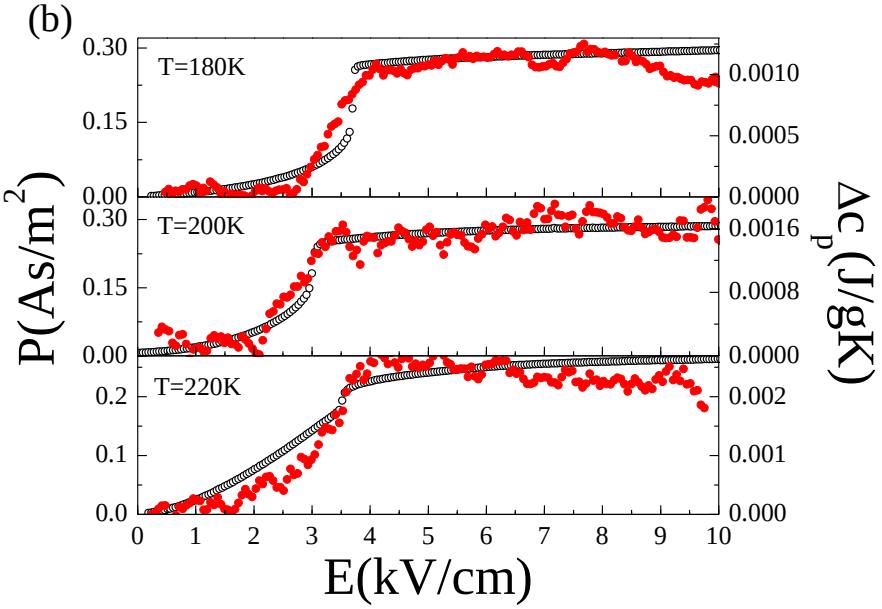

Figure 29*: Isofield and isothermal measurements of the excess specific heat obtained in the ac measurements.* (a) The temperature dependence of the excess heat capacity obtained at different constant electric fields shows a peak at electric field-induced phase transition. The inset shows an absence of the peak anomaly in a broad temperature range at zero electric field. (b) Overlap of discontinuous steps in polarization (open circles) and specific heat (solid circles) observed when crossing the ferroelectric transition line.

In order to prove the existence of the latent heat, a modified relaxation calorimetry, which is sensitive to the released latent heat at the phase transition, was utilized. The relaxation technique was adopted and modified in such a way that we could apply linearly ramped electric field. The measurements were performed as follows. The sample was annealed at 380 K for 15 min and cooled down to particular stabilized temperature to satisfy the isothermal condition. During the measurement, the electric field was linearly increased in time from 0-10 kV/cm in 250 s and at the peak the field was linearly reduced back to zero again with the same rate. The same was repeated for negative fields giving the total period of 1000 s for the complete field cycle. Within this period around 1500 temperature $T(t)$ data points were recorded with accuracy within 0.1 mK with the bath temperature being stabilized. Figure 30(a) and 30(b) show the variation of the sample temperature for the complete field cycle at two different bath temperatures 180 and 220 K, respectively.

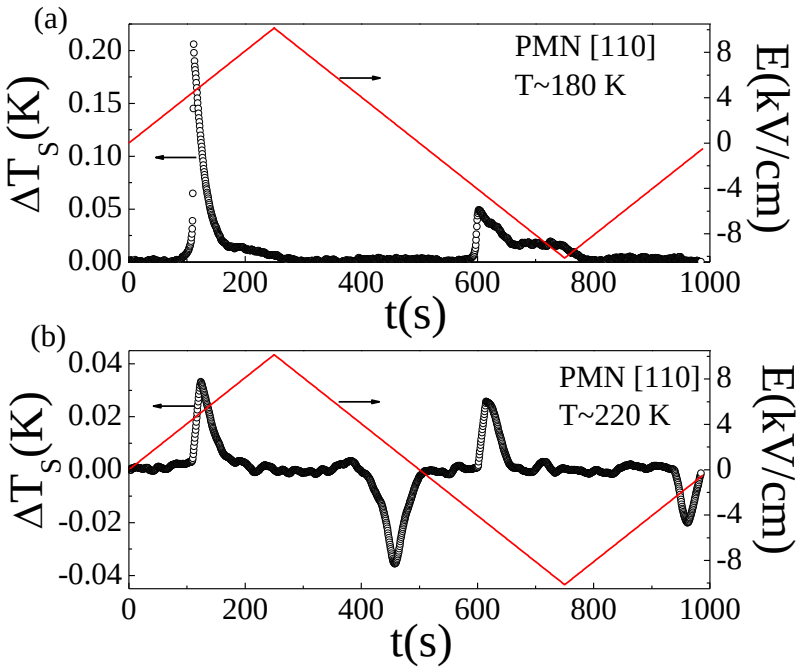

Figure 30: *Quasi-isothermal measurements.* The quasi-isothermal measurements at 180 and 220 K show a sharp anomaly of the sample temperature. The peaks in the temperature are related to the field-induced phase transition into the ferroelectric ordered state, whereas the dips are related to the onset of the glassy state when the field is reversed. The solid lines show the time dependence of the linearly changing bias electric field.

At $E \geq E_C$, an extremely sharp increase of the sample temperature ΔT_S exceeding 0.2 K at lower temperatures is clearly visible (see Figure 31(a)). The released latent heat is subsequently dissipated into the surrounding bath resulting in an exponential decay of the sample temperature back to the initial bath temperature. With increasing bath temperature the magnitude of ΔT_S gradually decreases with increasing E_C, indicating that the latent heat decreases and finally vanishes at the critical point (see Figure 31(a)) [55, 56, 57]. In a first approximation$\Delta T_S(t)$ can be fitted by the simple exponential decay ansatz $\Delta T_S(t) = \Delta T_S e^{\left(-\frac{t}{\tau_{ext}}\right)}$. From such experiments, ΔT_S and thus the latent heat $L = c_p \Delta T(t = 0)$ can be determined within a few percent accuracy. The calculation of the latent heat at the temperature 180 K using $c_p = 0.25$ J/gK (see Figure 31(b)) gives latent heat $L = 61 \pm 3$ J/kg.

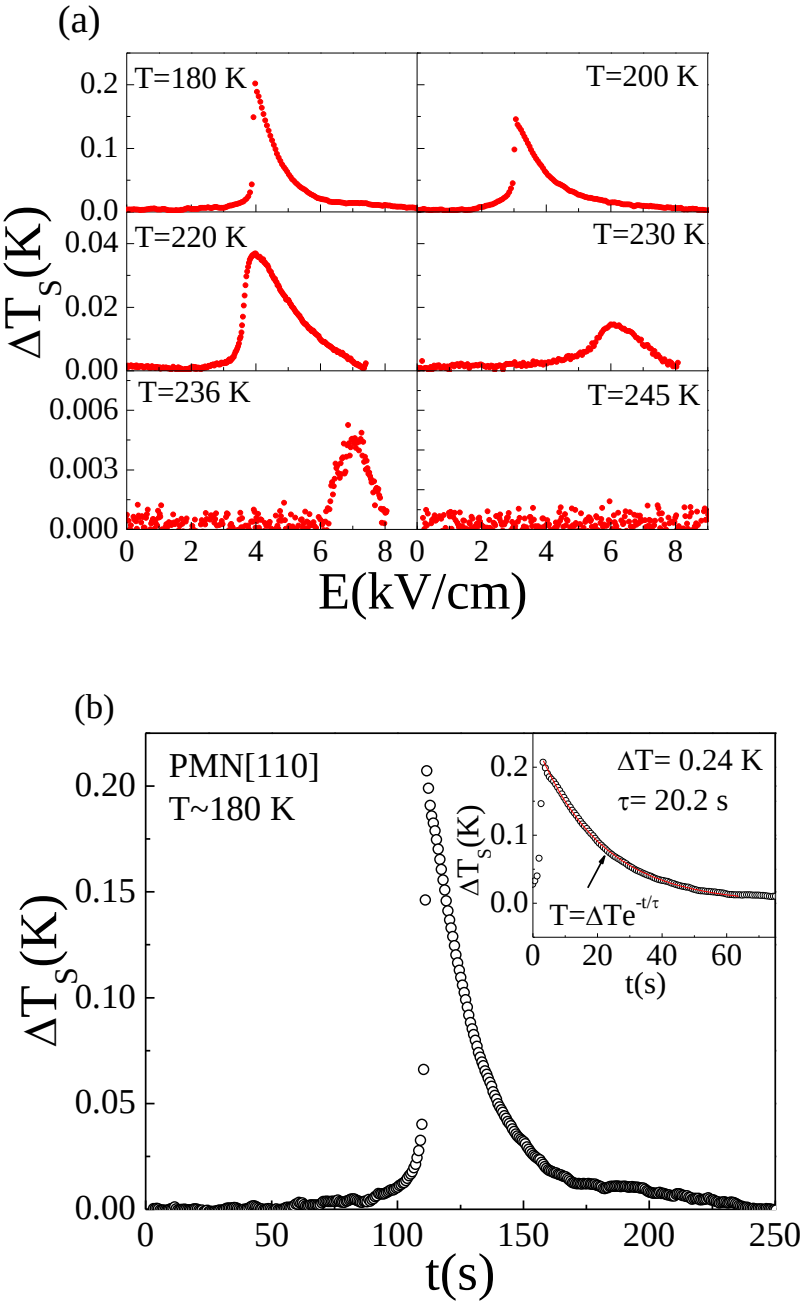

Figure 31: *The change of the sample temperature.* (a) Change of the sample temperature for the PMN [110] single crystal as a consequence of the released latent heat at the field-induced ferroelectric transition measured at several constant bath temperatures. (b) Details of the sharp anomaly in the thermal response of the sample temperature observed at the electric field of 4.5 kV/cm with temperature bath stabilized at 180 K. The temperature anomaly is a consequence of the released latent heat at the field-induced ferroelectric transition.

The temperature dependence of the estimated released latent heat and the total enthalpy change at the ferroelectric transition for PMN [110] is shown in Figure 32 [57]. The presence of the latent heat at the ferroelectric transition demonstrates the existence of a first-order transition line separating the glassy from the ferroelectric state. The latent heat vanishes at $T_{CP} \cong 240$ K and $E_{CP} \cong 8$ kV/cm, which corresponds to an isolated critical point. For fields above E_{CP} the broadened evolution of the polarization and C_p

indicates the supercritical regime. The value of the total enthalpy change at the glassy to ferroelectric transition reaches a maximum in the vicinity of the critical point.

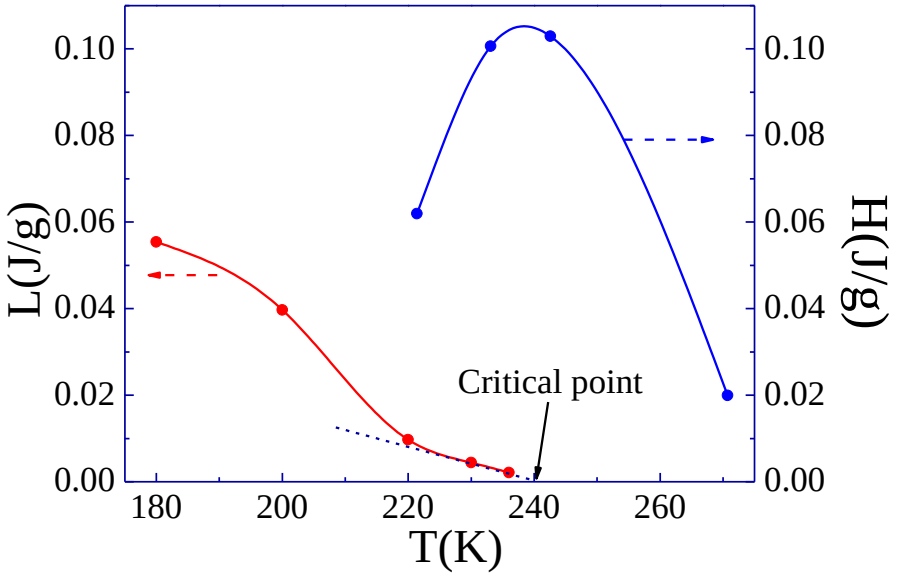

Figure 32: *Latent heat and total enthalpy.* Released latent heat and total enthalpy change at the ferroelectric conversion as determined by high resolution calorimetry.

3.2.2.1 Hysteresis of field-induced ferroelectric transition in PMN

As shown in Figure 30(a) and 30(b), the temperature of the sample exhibits the sharp discontinuous jump as a consequence of the released latent heat at the first-order phase transition from the glassy to FE state [55, 56, 57]. At 180 K two sharp changes of the ΔT_S are observed related to the onset of the FE order with different polarization orientations as the field is changing sign. One would expect that on reducing the field, the glassy phase would reappear and this should result in a negative ΔT_S anomaly. However, only positive but greatly reduced ΔT_S anomaly can be observed at 180 K. This can be explained in the following way.

The experimental time scale at which we exceed the electric field necessary to induce the FE phase transition at 180 K gets comparable or even shorter as the relaxation times. Because of this, transitions into the intermediate glassy state and FE ordered state with different polarization orientation merge together. The observed second anomaly at 180 K is actually the sum of the released and absorbed latent heat in this interplay of merged phase transitions. This results in practical cancellation of positive and negative ΔT_S, thus strong asymmetry in peaks magnitude. At higher temperatures, the relaxation times gets shorter allowing observation within the experimental time scale of the phase transition sequence from one FE state to another via the intermediate glassy state (see Figure 30(b)) at which the negative ΔT_S is observed due to the absorbed latent heat, i.e., electrocaloric effect. Because there is almost no merging of the transition anomalies the observed ΔT_S peaks are much more symmetric (see Figure 33).

The hysteresis of the phase transition from the glassy state into the FE state and back is clearly shown in Figure 33(a) and 33(b). With increasing temperature and the electric field the system becomes more and more continuous because of the approaching critical point. This results in slow disappearance of the hysteresis between the onset of the FE order with increasing electric field (positive ΔT_S in Figure 33) and the onset of the glassy state with decreasing electric field (negative ΔT_S in Figure 33), thus positive and negative

ΔT_S slowly merge with increasing temperature. Such behavior is related to the presence of a critical point at which the FE transition becomes continuous and which was found to be around ~ 240 K in the PMN single crystal oriented in the [110] direction [57]. The anisotropy of the electric field-induced phase transition in ergodic and merging of phase transitions in nonergodic region as a consequence of the freezing processes was some time ago discerned from the polarization data [54]. Here, the calorimetric data provide additional support for the freezing-dynamics origin of the hysteresis effect.

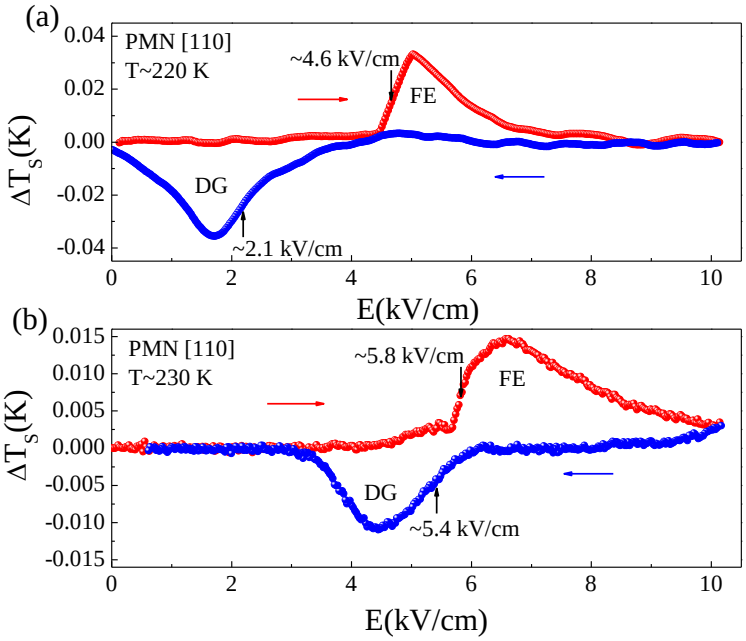

Figure 33: *Phase transition hysteresis.* The onset of the ferroelectric (FE) and the glassy (DG) state are reflected in the positive and negative ΔT_S, respectively. The red and blue solid circles represents data obtained at linear increasing and reduction of the electric field denoted by the red and blue arrows, respectively. (a) Shows ΔT_S anomalies observed at 220 K exhibit an hysteresis. The DG-FE transition is induced around 4.6 kV/cm, whereas the FE-DG transition is observed around 2.1 kV/cm. (b) Shows ΔT_S anomalies observed at 230 K. The DG-FE transition is induced around 5.8 kV/cm, whereas the FE-DG transition is observed around 5.4 kV/cm.

3.2.3 The heat capacity response in PMN: experiments and theory

As mentioned above, the polarization and calorimetric techniques were utilized to investigate the relaxor to ferroelectric phase transition line in order to get an answer to the question of the relaxors ground state, the existence of the critical point in [110] PMN, and to discern between the proposed theoretical models. Both polarization and calorimetric experimental results coincide with each other and confirm the existence of the real phase transition line in $E-T$ phase diagram. The presence of the latent heat confirms the first-order nature of the phase transition line which ends in the liquid vapor type of critical point at 240 K and 8 kV/cm [57]. The $E-T$ phase diagram of PMN single crystal oriented in [110] direction is represented in Figure 34. It should be stressed that our results also exclude any ferroelectric ordering which would take place in zero field below 400 K, because no specific heat or enthalpy anomalies as well as no latent heat were observed in the zero-field experiments between 4 and 400 K (see the inset to Figure 29(a)) in contrast to predictions of random field models.

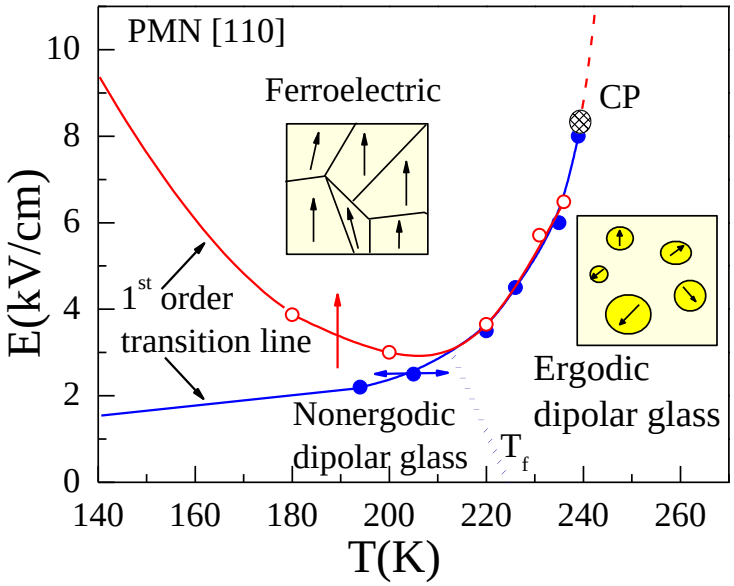

Figure 34: *$E-T$ phase diagram for relaxor PMN [110]*. Blue solid line with horizontal arrows represents the first-order phase transition line between the nonergodic relaxor and the ferroelectric phase as observed in isofield measurements. Solid circles denote data obtained from polarization and heat capacity anomalies (cf. Figure 27 and Figure 29(a)). Red solid line with vertical arrow represents the same first-order phase transition line but for isothermal experiments. Open circles denote data obtained from polarization and calorimetric measurements (cf. Figure 28 and Figure 31(a)). CP and dashed line denote the critical point and the Widom line, respectively. Dotted line represents the freezing line between the ergodic and nonergodic state at which the longest relaxation time diverges.

These experimental findings strongly support the physical picture of a dipolar glass for the canonical relaxor ferroelectric PMN and are in good agreement with the basic ideas of the SRBRF model. From this point of view it is only reasonable to apply the SRBRF model to describe the observed heat capacity behavior. In order to do this and to describe the observed anisotropy in dielectric properties of PMN, the improved version of SRBRF model the so-called compressible spherical dipolar glass model (CSDG) was adopted [54, 133]. The CSDG model includes the coupling terms between the polarization and strain. Due to this, additional elastic energy term are introduced in the Landau free energy expansion [17, 133]

$$f = f_0 + \frac{1}{2}aP^2 + \frac{1}{4}bP^4 + \frac{1}{6}cP^6 + \frac{1}{2}XC^{-1}X + XQP^2 + \cdots. \tag{86}$$

Here, X is a stress tensor, C is the elastic constant tensor and Q electrostriction tensor. Taking into account the relation between the strain x and polarization $x = \left(\frac{\partial f}{\partial X}\right) = QP^2$ and Hook's law $x = C^{-1}X$, one can rewrite the equation (86)

$$f = f_0 + \frac{1}{2}(a + QX)P^2 + \frac{1}{4}(b + 2QCQ)P^4 + \cdots \tag{87}$$

where $B = 2QCQ$ is a fourth range tensor [133]. Thus the resulting value of $(b + 2QCQ)$ for a symmetry direction can either be positive or negative depending on the relation between the coefficients B and $b = b_{rigid}$, where b_{rigid} means the Landau coefficient used in SRBRF model for an ideal isotropic relaxor system. The Landau coefficient $b^{[p]}$

for different symmetry direction $[p]$ =[100], [110] and [111] is now $b^{[p]} = b_{rigid}^{[p]} + B^{[p]}$, where $b^{[p]}$ is expressed as follows [133]:

$$b^{[100]} = b_{11}, \tag{88}$$

$$b^{[110]} = \frac{1}{2}(b_{11} + b_{12} + 2b_{44}), \tag{89}$$

$$b^{[111]} = \frac{1}{3}(b_{11} + 2b_{12} + 4b_{44}). \tag{90}$$

Therefore, Pirc et al. show that the new term $B^{[p]}$ is in general anisotropic and calculated corresponding values of $B^{[p]}$ for PMN [133]. The anisotropy of the new term can change the sign of the Landau coefficient $b^{[p]}$ which has important consequences for the existence of the field-induced critical points for fields along the direction $[p]$.

Figure 35 show the polarization as a function of the electric field calculated from the SRBRF for $b < 0$. The polarization shows a discontinuous jump at some value of E at low temperatures. As T increases, the jump becomes smaller and finally disappears at the critical point E_{CP}, T_{CP}. The calculated polarization shows qualitatively the same behavior as experimentally obtained data. A similar behavior of $P(T)$ had been obtained earlier for PMN [111] [56]. The excess specific heat $\Delta C_E(T)$, which is due to the contribution of the dipolar degrees of freedom, namely, PNRs can be derived from the free energy by applying the thermodynamic relation for the entropy $S = -\left(\frac{\partial f}{\partial T}\right)_E$. The dipolar part S_{dip} is defined as the contribution of all P-dependent terms in the free energy. The temperature dependence of the excess of the heat capacity at constant fields is given by $\Delta C_E^{sing} \cong T\chi(E,T)(a_1 P)^2$, where a_1 is a temperature derivative of $\chi_1(T)$ derived from SRBRF model [133]. Figure 36 shows the theoretical prediction of $\Delta C_E^{sing}(T)$ behavior which qualitatively agrees with the experimental values $\Delta C_E(T)$ (see Figure 29(a)).

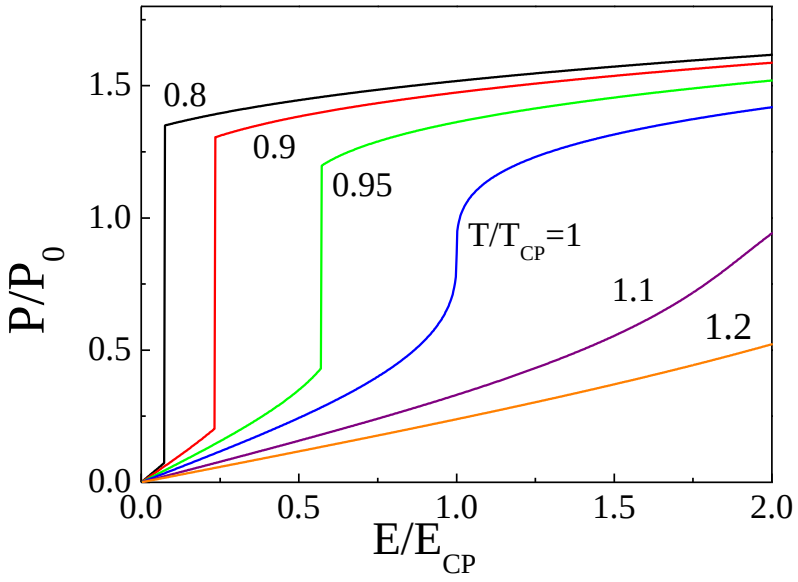

Figure 35: *Theoretical calculation of* $P(E)$. Field dependence of $P(E)$ for a relaxor with $b < 0$ and several values of temperature T close to the critical temperature T_{CP}, obtained by minimizing the free energy. Note that these calculations are only valid in the ergodic region above the freezing line shown in Figure 34.

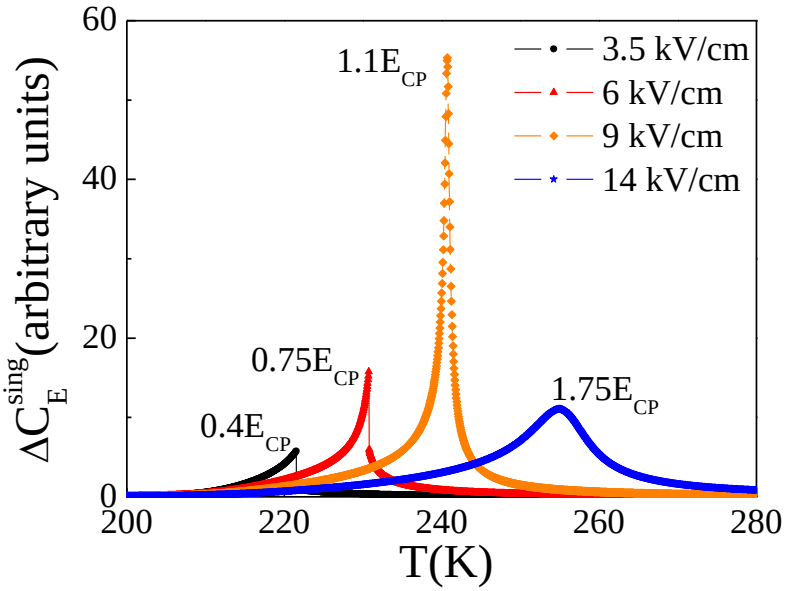

Figure 36: *Theoretical calculation of* $\Delta C_E^{sing}(T)$. Calculated temperature dependence of the singular part of the excess specific heat ΔC_E^{sing} for a relaxor with $b = -0.2$ and $c = 0.08$ at the same field values as used in the experiment (see Figure 29(a)).

3.3 Critical point in PLZT ceramic

Perovskite structured lead zirconate titanate (PZT) is an important ferroelectric material used in numerous modern applications due to its excellent dielectric and electromechanical properties. These properties can be significantly changed by doping PZT with lanthanum (La) which forms a solid solution lead lanthanum zirconate titanate, $Pb_{(1-x)}La_x(Zr_yTi_{(1-y)})_{(1-x/4)}O_3$ (denoted as PLZT). PLZT ceramic material is very interesting due to its memory properties and extraordinary electro-optical properties suitable for various applications of memory and electro-optical devices [2, 78]. The substituted La^{3+} ion on A-site brings a valence difference into the structure. In order to satisfy electrical neutrality, a vacancies on A-site or B-site are created. The structural disorder and the presence of defects are important factors in the exhibited properties of PLZT ceramics which can be easily changed by variation of the Zr/Ti ratio and ingredient of lanthanum. Certain composition of the PLZT ceramics like, $x = 0.09$ and $y = 0.65$ labeled as 9/65/35 PLZT, shows relaxor-like behavior and belongs to the family of the relaxor ferroelectrics. Detailed investigations of the x/65/35 PLZT ceramics show that the PLZT ceramics with the La content varying between 4 and 12 % belongs to the relaxor ferroelectric systems [2, 134, 135]. Broad frequency dispersion of the dielectric constant, broadening of the relaxation spectrum, divergence of the longest relaxation time, increasing of nonlinear dielectric coefficient when approaching the freezing temperature, logarithmic polarization decay and the absence of the ferroelectric transition in zero electric field are typical relaxor features and characteristics of 9/65/35 PLZT ceramics [48, 50, 130, 136, 137, 138, 139, 140]. The linear and nonlinear dielectric susceptibility as a function of the ac and dc bias electric field has been measured, yielding an $E - T$ phase diagram (Figure 37) [48, 130, 136].

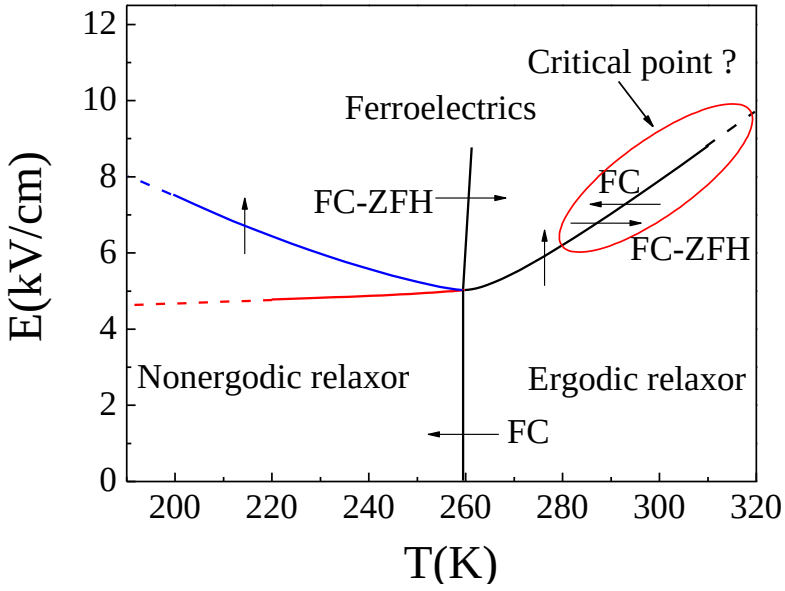

Figure 37: *Schematic $E - T$ phase diagram.* Schematic E-T phase diagram of 9/65/35 PLZT ceramics. Arrows indicate the direction of crossing the phase transition lines.

$E - T$ phase diagram for 9/65/35 PLZT is qualitatively similar to that observed for PMN relaxor ferroelectric (see Figure 34). However, in PLZT ceramics no investigations were performed so far to confirm or reject the presence of the critical point. It is

interesting to expose the complex dielectric constant data as a function of electric field shown in Ref. 130. The real part of the complex dielectric constant shows a discontinuous jump at $E \geq E_C$ related to the field-induced phase transition. The discontinuous jump above the freezing temperature ~ 259 K move towards higher electric fields with increasing temperature and gets less pronounced. Above ~ 270 K the step in the real part of the complex dielectric constant vanishes [130]. Such behavior of the complex dielectric constant suggests the presence of the critical point in the system. As already discussed in the case of PMN the only real proof of the existence of the critical point can be provided by the quasi-isothermal measurements of the latent heat at the ferroelectric transition line induced by the linearly changing electric field. Figure 38 shows the electrocaloric change of the sample temperatureΔT_S in the vicinity of the field-induced ferroelectric transition at several fixed temperatures for 9/65/35 PLZT ceramic.

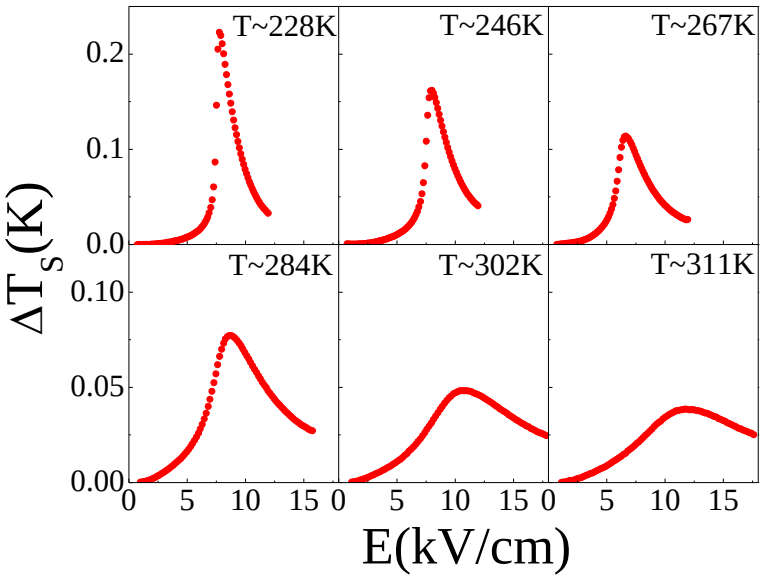

Figure 38: $\Delta T_S(E)$ *for ferroelectric relaxor ceramic.* Isothermal change of the sample temperature as a function of the electric field obtained in the 9/65/35 PLZT. The ΔT_S anomaly related to the released L persists up to higher temperatures.

The anomaly ΔT_S in the sample temperature observed at the phase transition line is a consequence of the released latent heat at the first-order phase transition from the glassy to ferroelectric phase. The ΔT_S anomaly decreases with increasing temperature and moves towards higher electric fields as expected when approaching the critical point. According to complex dielectric constant results the latent heat should vanish above 270 K where a supercritical region is expected. However, the quasi-isothermal measurements of the latent heat show that the sample temperature anomaly persist up to higher temperatures. The decreasing of the ΔT_S indicates that latent heat is slowly vanishing, but the latent heat does not disappear completely at well-defined temperature [55, 56, 57].

The fact that the latent heat does not vanish completely can be explained with the anisotropy of the critical point position in the $E-T$ phase diagram. The experimental results show that the position (T_{CP}, E_{CP}) of the critical points in the $E-T$ phase diagram for PMN depends on the crystal orientation with respect to the external electric field. For instance, in PMN single crystal oriented in [111] direction the critical point was found at (T_{CP}~ 220 K, E_{CP}~ 4 kV/cm), and in [110] direction at (T_{CP}~ 240 K, E_{CP}~ 8 kV/cm),

whereas in [100] direction no critical point was found. [52, 54, 55, 56, 57]. The 9/65/35 PLZT ceramic is a polycrystalline material which contains small randomly oriented monocrystals. For this reason it is assumed that the orientational heterogeneity of the ceramic materials can lead to a smearing of the critical point position in the $E-T$ phase diagram with absence of the sharp definition of $(T_{CP},\ E_{CP})$. The smearing of the critical point position in the $E-T$ phase diagram also explains the observed smeared anomalies ΔT_S of the sample temperature and the presence of the latent heat at higher temperatures.

3.4 Critical point in $BaTiO_3$ ferroelectric crystal

In contrast to relaxor PMN single crystal and 9/65/35 PLZT ceramics, barium titanate ($BaTiO_3$ or shortly BT) belongs to a family of ferroelectric materials and exhibits a clear first-order ferroelectric transition already at zero external bias electric field. The history of BT goes back in the time of World War II, when the first BT ceramic material was prepared [1, 141]. The growth of $BaTiO_3$ crystals and increased availability of the material contributed to the fundamental understanding of the dielectric anomaly at the ferroelectric transition, ferroelectric domain switching and structures, electro-optical and electromechanical properties, and the nature of ferroelectric phase transitions [3, 11, 13, 14, 17, 142]. BaTiO3 is an especially suitable material for investigating the influence of the electric field on the ferroelectric transition because of its specific structural ferroelectric transition sequence at $E=0$: high temperature paraelectric cubic phase $\xrightarrow{405\ K}$ ferroelectric tetragonal $\xrightarrow{281\ K}$orthorhombic $\xrightarrow{193\ K}$ rhombohedral phase [3]. Recently, a theoretically calculated $E-T$ phase diagram based on a Ginzburg-Landau model was presented for cubic to tetragonal phase transition for the single crystal barium titanate [92]. In order to verify the phase diagram and the existence of the electric-field-induced critical point terminating the line of first-order ferroelectric (tetragonal) to paraelectric (cubic) phase transitions, the dielectric and calorimetric experiments were carried out on [001] BT single crystal [93]. Figure 39 shows temperature dependence of the real part of the complex dielectric constant at different constant bias electric fields. A sharp and narrow discontinuous step in the dielectric constant at 405 K signals a strong first-order character of the phase transition in the absence of the electric field. With increasing electric field up to 10 kV/cm, the discontinuous dielectric anomaly moves towards higher temperatures and the value of the dielectric constant increases. In addition, the shape of the dielectric anomaly becomes more and more continuous. At 12 kV/cm and above, the dielectric anomaly starts to decrease and becomes increasingly suppressed as an indication of supercritical behavior.

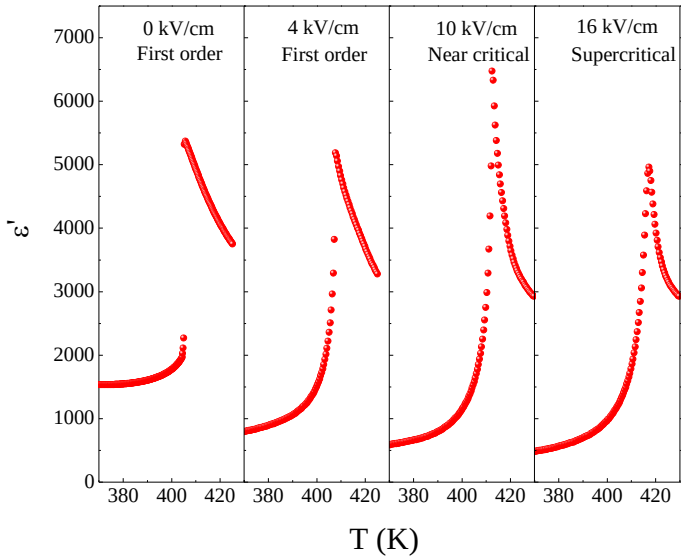

Figure 39: *Dielectric measurements for $BaTiO_3$.* The real part of the complex dielectric constant shows a discontinuous step at the C-T phase transition. With increasing electric field the dielectric constant increases and the T_C moves towards higher temperatures. Above 10 kV/cm the dielectric constant decreases and gets more continuous.

It should be mentioned that the linear birefringence also exhibits a crossover from the sharp discontinuous to continuous evolution between 10 and 12 kV/cm [142]. At higher fields the birefringence anomaly becomes smeared and suppressed, as typical for the supercritical regime [142].

The temperature dependence of the excess specific heat of $BaTiO_3$ single crystal obtained in the vicinity of the cubic to tetragonal phase transition is displayed in Figure 40 for three different bias electric fields. Similar to the dielectric response, the specific heat shows a sharp and discontinuous anomaly at the transition temperature. By increasing the bias electric field the transition temperature shifts from ~ 405 K at zero field to ~ 412 K at 10 kV/cm and the heat capacity anomaly becomes increasingly rounded and less pronounced.

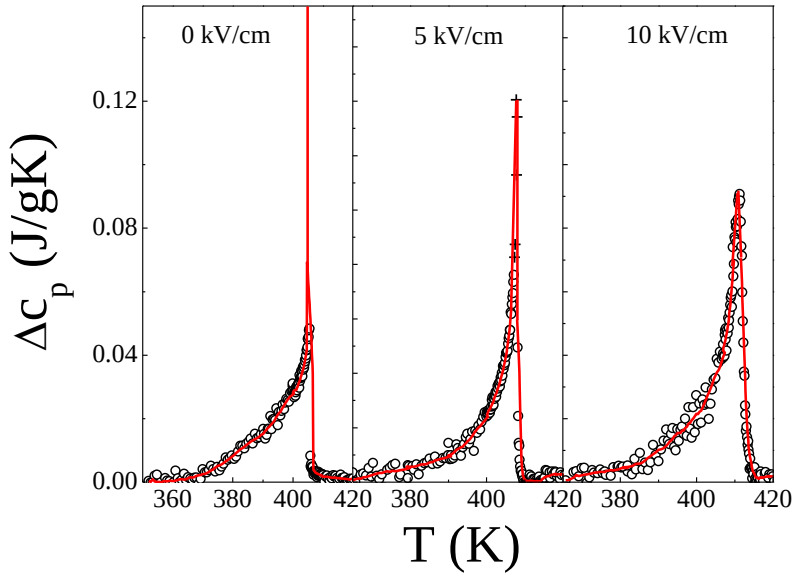

Figure 40: *The ac calorimetry of $BaTiO_3$.* Temperature evolution of the excess specific heat data obtained in the ac mode at various constant electric fields. The solid line is a guide to the eye, whereas open circles and crosses are the c_p data obtained outsite and inside the coexistence range, respectively. In the first panel the anomalous response of c_p in the coexisting range is so huge that it is out of the drawing range.

However, the ac measurements cannot quantitatively detect a latent heat and thus cannot provide enough information about the crossover from the first-order to second-order phase transition induced by the applied electric field. In order to detect the latent heat, the quasi-isothermal measurements of the latent heat on a ferroelectric transition line with linearly changing electric field were utilized. The variation of the sample temperature (ΔTs) as a function of the electric field is presented in Figure 41. At the field-induced ferroelectric transition a sharp increase in the sample temperature is observed as a consequence of the released latent heat. The amplitude of the variation of the sample temperature exceeds the value of 1 K at lower temperatures. The estimated amount of the released latent heat responsible for this rather big change of the sample temperature is ~ 400 J/kg which is almost a magnitude higher as detected in PMN and PLZT relaxors. With increasing the bath temperature the magnitude of ΔTs gradually decreases, whereas the electric field necessary to induce the transition increases. The decreasing of ΔTs also indicates the decreasing of latent heat. It is interesting to note that ΔTs does not vanish completely. The continuous anomaly observed at higher temperatures is most likely related to the residual electrocaloric effect related to continuous changes of the polarization which will be addressed in the next chapter. The dielectric and calorimetric data obtained in BT [001] single crystal at the cubic to tetragonal phase transition line shows the existence of the critical point. The $E-T$ phase diagram constructed from dielectric and quasi-isothermal latent heat data (see Figure 42) shows the first-order transition line terminated at the critical point at $T_{CP} \cong 412$ K and $E_{CP} \cong 10$ kV/cm [93]. The experimentally estimated coordinates of the critical point are in good agreement with the theoretical prediction by Porta et al. [92]. They calculated the critical point for ordered crystal and for a crystal with small amount of disorder to be at $T_{CP} = 414.32$ K, $E_{CP} = 14.6$ kV/cm and $T_{CP} = 415$ K, $E_{CP} = 9.55$ kV/cm, respectively [92].

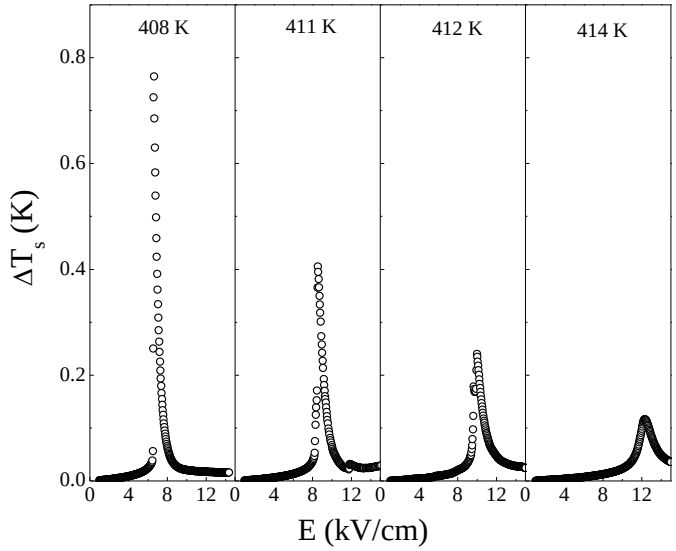

Figure 41: $\Delta T_S(E)$ *for ferroelectric* $BaTiO_3$. Change of the sample temperature for the $BaTiO_3$ single crystal as a consequence of the released latent heat at the field-induced cubic to tetragonal phase transition, measured at several constant bath temperatures.

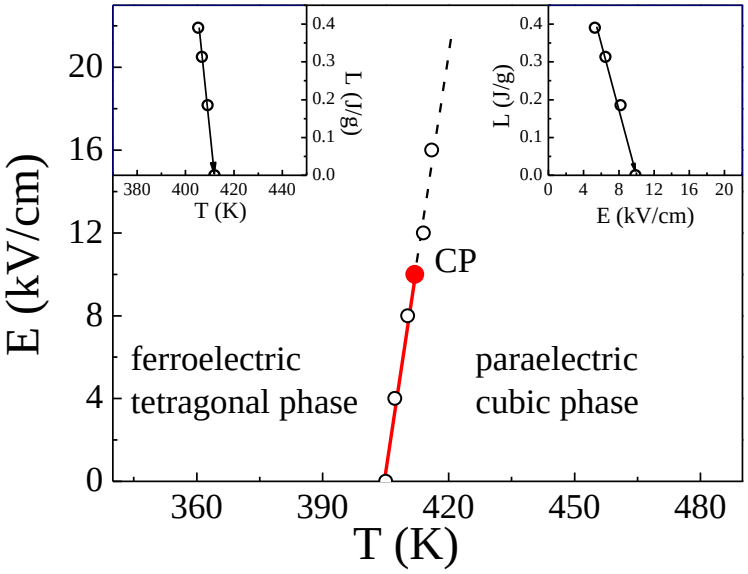

Figure 42*: $E-T$ phase diagram for $BaTiO_3$ single crystal*. $E-T$ phase diagram for the BT single crystal constructed from the calorimetric and dielectric data. Solid line represents the electric-field-induced first-order transition line between the cubic and tetragonal phases, which ends in a critical point at $T_{CP} \cong 412$ K and $E_{CP} \cong 10$ kV/cm. The dashed line denotes the Widom line, a region of supercritical behavior emanating from the critical point. The two insets represent the temperature and electric field variation of the latent heat.

4 Influence of the critical point on electromechanical and electrocaloric properties

Of special interest are the studies of the electromechanical and electrocaloric properties in the vicinity of the liquid-vapor type critical point, which has been shown to play an important role in the enhancement of the piezoelectric coefficient and electrocaloric responsivity [55, 56, 88, 95, 97, 98, 117]. On approaching the critical point the response functions such as the dielectric susceptibility and heat capacity exhibit a maximum value which leads to the enhancement of the piezoelectric and electrocaloric response [55, 56, 95]. In this chapter the studies of the influence of the critical point on electromechanical behavior in relaxor PMN-PT and ferroelectric $BaTiO_3$ single crystal as well as electrocaloric response of $BaTiO_3$ are presented.

4.1 Enhancement of electromechanical properties at critical point

4.1.1 Relaxor ferroelectric PMN-xPT

The perovskite solid solution PMN is characterized by site and charge disorder which are the origin of relaxor behavior. The ferroelectric behavior can be induced by applying electric field or reduction of disorder [25, 118]. This can be done by changing the composition with adding ferroelectric $PbTiO_3$ (PT) which forms a crystalline solution with PMN, i.e., the PMN-xPT solution. Pure PMN retain its average cubic symmetry down to temperatures as low as 5 K [63]. Small amount of PT content $x > 0.05$ change the PMN-xPT system into ferroelectric rhombohedral symmetry at low temperature [80, 143]. At sufficiently high PT concentration, PMN-xPT solid solution undergoes several phase transitions in the vicinity of the morphotropic phase boundary. On cooling a typical phase sequence cubic (C) – tetragonal (T) - monoclinic (M) – rhombohedral (R) is observed close to the C-T-R triple point [143]. As already pointed out in chapter 1.5 the proximity of critical point is a new driving mechanism for polarization rotation and the enhancement of the piezoelectric responses [55, 56]. In the case of PMN-0.295PT single crystal oriented in [111] direction it was shown that the largest piezoelectric coefficient is observed at electric field corresponding to the electric field of the critical point [55]. The enhancement of the piezoelectric coefficient is a direct consequence of the nearby critical point fluctuations which are reflected in the divergence of the dielectric susceptibility, i.e., dielectric constant which is directly proportional to the piezoelectric coefficient,

$$d_{im} = \sum_{jk} 2\varepsilon_{ij} Q_{mjk} P_k \tag{91}$$

[56]. In addition it was shown that the necessary electric field and required enthalpy for the polarization rotation decrease in the proximity of the critical point [55]. As discussed already for PMN, the existence and position of the critical point depends on the orientation of the crystal. The enhancement of the piezoelectric coefficient at critical point was shown for PMN-0.295PT oriented in [111] and [110] direction but not for [100].

Figure 43 shows the real part of the complex dielectric constant ε' in the PMN-0.26PT single crystal measured in [100] direction at frequency 20 Hz and various bias electric

fields. Dielectric constant clearly shows anomalous behavior around 368 K at sufficiently high electric field. The observed dielectric anomaly is similar to that reported in PMN-0.295PT for [111] and [110] direction and is related to the monoclinic phase sequence inserted between tetragonal and rhombohedral phases [55, 56, 143, 144].

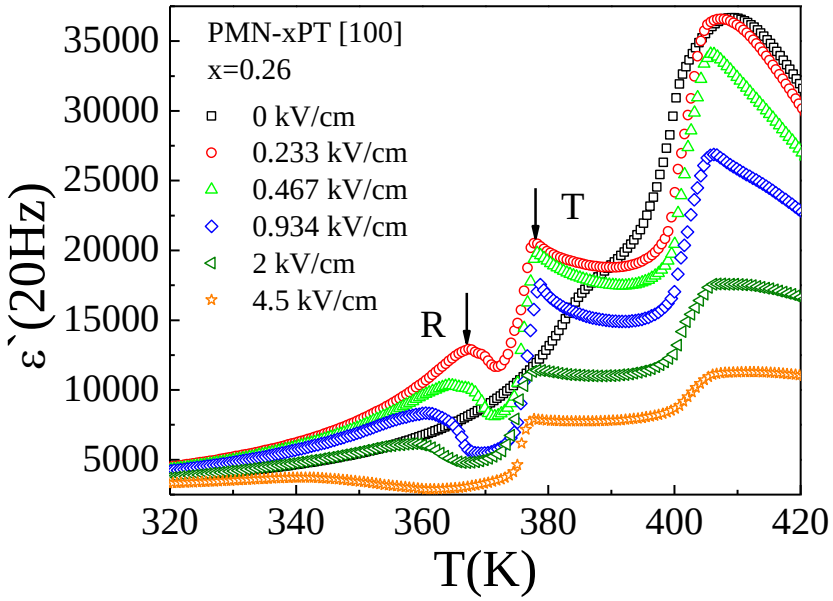

Figure 43: *Dielectric response of PMN-PT solid solution.* Temperature dependence of the dielectric constant measured for PMN-PT [100] with $x = 0.26$ crystal at various bias electric fields. It shows the evolution of monoclinic phase sequence between rhombohedral (R) and tetragonal (T) (denoted by the arrows) under the electric field.

The monoclinic phase sequence appeared first at $E = 0.1$ kV/cm and with increasing electric field the anomaly becomes sharper. Based on previous reports for PMN-xPT system, the monoclinic phase sequence shown in Figure 44 at $E = 0.233$ kV/cm is as follows, rhombohedral (R) → monoclinic (M_B) → orthorhombic (O) → monoclinic (M_C) → tetragonal (T) → cubic (C) [143, 144]. The influence of the bias electric field on the evolution of the monoclinic phase sequence (Figure 43) shows that these transitions get suppressed and smeared out at higher electric fields above $E = 0.467$ kV/cm.

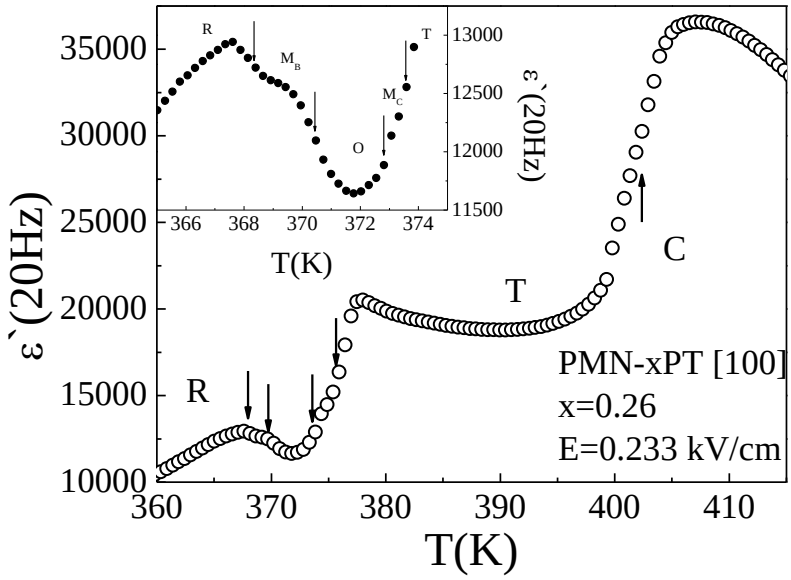

Figure 44: *Dielectric anomalies of the phase transitions.* Steps in the dielectric constant represent the phase transitions between different monoclinic and orthorhombic phases between the ferroelectric rhombohedral phase and the paraelectric cubic phase. The inset shows zoom in of the monoclinic phase sequence between the rhombohedral and tetragonal phases.

The temperature dependence of the heat capacity measured at three different electric fields exhibits similar behavior as the dielectric constant (Figure 45). In the absence of the electric field, only a smeared anomalies in the excess of specific heat can be observed related to the R→T and T→C phase transitions. With increasing electric field the transitions become sharper and the lower anomaly related to the R→T splits into two anomalies now representing the transition to monoclinic and rhombohedral phases [56]. With increasing the electric field the $R \rightarrow M_B$ enthalpy decreases significantly resulting in further suppression of the anomaly, as shown in Figure 45 for the $E = 4.672$ kV/cm [55, 56, 88].

The dielectric and heat capacity data obtained in PMN-0.26PT [100] single crystal resemble closely data obtained in PMN-0.295PT single crystal for [111] and [110] orientations implying the possibility of existence of the critical point for both C→T and $T \rightarrow M_C$ phase transitions [55, 56]. Due to small enthalpy variations the situation is much less clear for the monoclinic phase sequence. According to the theoretical calculations the orthorhombic and monoclinic phases can disappear at high electric fields and do not terminate in a critical point [145].

The linear electromechanical response or piezoelectric response was studied via the dielectric resonant method described in chapter 2.1.1 Figure 46 shows the temperature dependence of transverse (d_{31}) piezoelectric coefficient of PMN-0.26PT [100] single crystal at different electric fields. The piezoelectric coefficient d_{31} exhibits a peak in the rhombohedral phase which is much smaller than that reported for electric fields applied along [111] and [110] direction in the PMN-0.295PT single crystal [55, 56]. This is due to the fact that the direction of the electric field is further away from the [111] polar axis direction. Nevertheless, it is interesting that the piezoelectric coefficient peak was observed below monoclinic phase sequence (~ 362 K) and not in the temperature range of monoclinic phase sequence (see inset in Figure 44), as one would expect according to the theory of polarization rotation via intermediate monoclinic phases [81]. Fitting by

using the simple power law ansatz shows that observed critical dependence of the d_{31} is actually related to critical behavior of the phase transitions above the monoclinic phase sequence [56]. This suggests that the monoclinic phase sequence is actually responsible for prior cut-off of the critical dependence of d_{31} and not for enhancement of d_{31}. With increasing electric field the cut-off temperature and peak values of d_{31} are decreasing. This is due to the shift of $M_B \rightarrow R$ phase transition towards low temperatures and increasing of $M_C \rightarrow T$ phase transition temperature with increasing electric field [56, 88]. This suggests that the piezoelectric response could be even larger if it would be possible to create a material with very narrow temperature range of intermediate monoclinic phase sequence close to the T→C transition. Nevertheless, the increase of d_{31} in the rhombohedral phase, similar to that observed in [111] and [110] axis indicate the critical enhancement of the piezoelectric response [55, 56, 88].

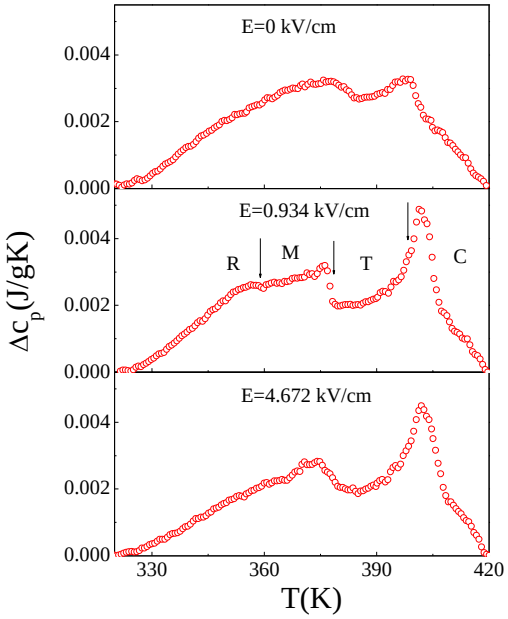

Figure 45: *Electric field-induced monoclinic phase sequence*. Temperature dependence of the excess specific heat Δc_p at different bias electric fields of the PMN-xPT [100] with $x = 0.26$. The Δc_p anomaly related to the transition from the monoclinic to the rhombohedral phase is clearly visible (denoted by an arrow) at the electric field of 0.934 kV/cm.

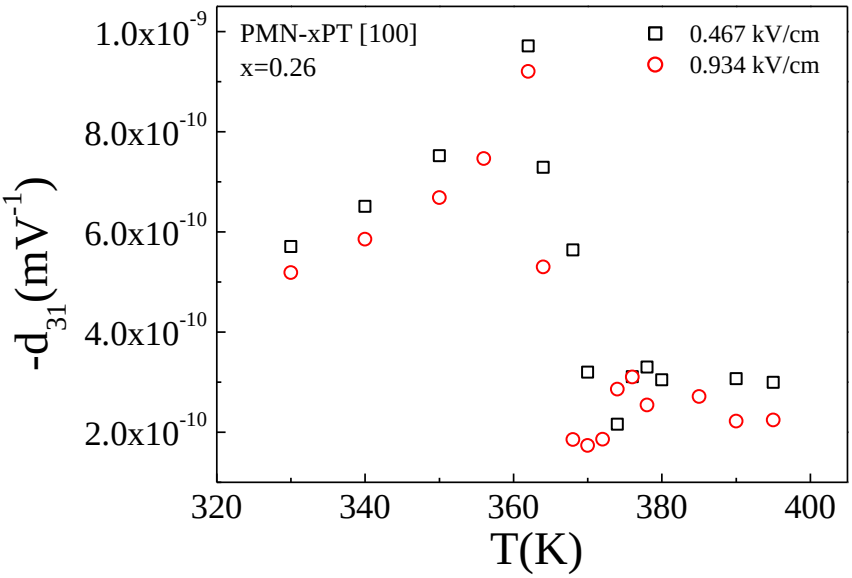

Figure 46: *Piezoelectric response of PMN-PT solid solution.* The temperature dependence of the piezoelectric coefficient d_{31} obtained in a PMN-xPT single crystal with $x = 0.26$ poled along [100] at two different electric fields.

4.1.2 Ferroelectric $BaTiO_3$

The suggestion that the proximity of critical point is perhaps even more responsible for the enhancement of the piezoelectric coefficient than the morphotropic phase boundary is strongly supported by the large piezoelectric response found in materials without MPB [77, 91]. Ferroelectric $BaTiO_3$ is a material without MPB region, which on the other hand possess a critical point as it was shown theoretically and recently confirmed experimentally [92, 93]. The theoretical calculations presented by Porta et al. predict also the enhancement of the piezoelectric responses in the vicinity of the critical point [92]. This theoretical prediction and previous experimental work on PMN-0.295PT and PMN put the proximity of the critical point as a driving mechanism for the enhancement of the piezoelectric responses [55, 56].

In order to verify this prediction, the experimental study of piezoelectric coefficient d_{31} in the vicinity of the critical point at cubic to tetragonal phase transition in $BaTiO_3$ single crystal poled along [001] direction was performed by using the resonance method described in the chapter 2.1.1 Figure 47 shows the temperature evolution of the piezoelectric coefficient d_{31} at several different constant electric fields. The value of d_{31} found at room temperature is in good agreement with previous reported values [81, 146, 147]. The observed peaks in the piezoelectric coefficient are related to the ferroelectric phase transition at which the dielectric susceptibility exhibits a maximum due to the critical fluctuations. So it is reasonable to expect enhancement or even divergence of the piezoelectric tensor and thus also d_{31} at the phase transition which at which the dielectric susceptibility exhibits a maximum or even diverges (see equation (91)). By plotting the maximum values of $d_{31}(T)$ obtained at a specific bias field as a function of that field, one can follow the evolution of d_{31} along the phase transition line in the $E - T$ phase diagram (see the inset in Figure 47). Both plots show that the obtained piezoelectric response clearly exhibit a maximum at the temperature and electric field close to the critical point, i.e., 412 ± 3 K and 10 ± 2 kV/cm, respectively [93]. These findings of the piezoelectric

response enhancement at the critical point in $BaTiO_3$ [001] single crystal are in a good qualitative agreement with the theoretical predictions of the piezoelectric tensor divergence at the critical point in $BaTiO_3$ due to the divergence of the dielectric susceptibility [92]. The obtained results strongly support the idea that the mechanism for the enhancement of the piezoelectric response is most likely governed by the proximity of critical point and not necessary only by the presence of the MPB.

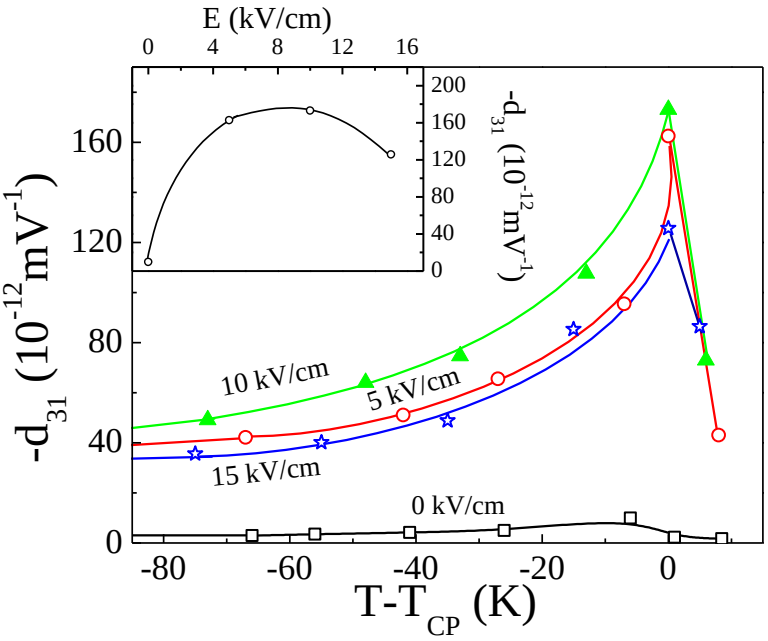

Figure 47: *Piezoelectric response of $BaTiO_3$ ferroelectric*. The temperature dependence of the piezoelectric coefficient d_{31} obtained in a $BaTiO_3$ single crystal poled along the [001] direction at four different values of the bias electric field below and above E_{CP}. The inset shows the electric field dependence of the piezoelectric coefficient d_{31} at $T = T_{CP}$, which exhibits a maximum at the critical field E_{CP}.

4.2 Enhancement of electrocaloric properties at critical point

4.2.1 Electrocaloric effect in $BaTiO_3$ ferroelectric

Recently, the electrocaloric effect attracted significant attention due to the prediction of a giant ECE in some organic and inorganic materials [73, 74]. Later the direct measurements of the ECE confirm the giant ECE in polymer based organic ferroelectric and relaxor materials, and inorganic relaxors materials [75, 95, 97, 98, 99, 100]. Most of the direct ECE studies were performed on inorganic relaxor materials such as PMN, PMN-xPT with different PT concentration, and 8/65/35 PLZT ceramics [117]. However, there is a lack in experimental studies of relaxor single crystal materials and only few experiments were performed on ferroelectric single crystals mostly on $BaTiO_3$ [101, 102, 103]. In fact most of the EC experiments were carried out solely by using the indirect method via measurements of the electric polarization as a function of the electric field and temperature and not by direct measurements of the ECE itself [73].

The experiments and theoretical calculations show that the maximum of the ECE responsivity $\Delta T_{EC}/E$, in bulk relaxor ferroelectrics is obtained near the critical point [95, 96]. The observed behavior of the ECE near the critical point in relaxors can be understood by considering the entropy density of the system $S(E,T) = S_{dip}(E,T) +$

$S_{ph}(T)$, as a function of the applied field E and the temperature T [95, 96]. As already discussed in the section 1.5 the entropy change of the dipolar subsystem ΔS_{dip} is a function of the dielectric polarization $P(E,T)$, which depends on the electric field E. The second term S_{ph} is a field independent contribution of phonons, electrons, etc. In the ECE cycle the electric field is changed from E_1 to E_2 which causes the change in temperature. If the process is adiabatic, then the total entropy change must be zero and one obtains [96]

$$S_{ph}(T_2) - S_{ph}(T_1) = -\big[S_{dip}(E_2, T_2) - S_{dip}(E_1, T_1)\big]. \tag{92}$$

Thus the corresponding entropy change can be evaluated as an integral over the lattice heat capacity $C_{ph}(T)$ from which the electrocaloric temperature change is obtained [95, 96]

$$\Delta T_{EC} = \frac{T_1}{C_{ph}}\big[S_{dip}(E_1, T_1) - S_{dip}(E_1, T_1 + \Delta T)\big]. \tag{93}$$

The dipolar entropy density S_{dip} can be written as

$$S_{dip} = S_0 + S_1(P), \tag{94}$$

where $S_0 = -\left(\frac{\partial f_0}{\partial T}\right)_0$, is the contribution at zero field and does not contribute to ΔS_{dip} and $S_1(P) = -\left(\frac{\partial f(P)}{\partial T}\right)_E$ is the contribution related to the polarization change due to the applied electric field [95, 96]. Using the expression for the density of the free energy of ferroelectrics written in equation (2) one obtains

$$S_1(P) = -\frac{1}{2}a_1P^2 - \frac{1}{4}b_1P^2 - \frac{1}{6}c_1P^6 + \cdots, \tag{95}$$

where $a_1 = \frac{da}{dT}$, $b_1 = \frac{db}{dT}$, etc. By assuming that b and c are temperature independent, follows that $b_1 = c_1 = \cdots = 0$. Taking into account equations (92) one can rewrite equation (93) [95, 96]

$$\Delta T_{EC} = \frac{1}{2}\frac{T_1}{C_{ph}}a_1(T + \Delta T)P^2(E, T + \Delta T). \tag{96}$$

According to the above theory the electrocaloric change of the sample temperature is therefore proportional to the square of the polarization $\Delta T_{EC} \sim P^2$ [95, 96, 97]. The applied electric field or phase transition significantly influences the electrocaloric effect due to the change of the polarization. One would expect that the largest ECE would be observed at the phase transition where beside the polarization change also the released/absorbed latent heat at the first-order transition contributes to the ECE. The EC responsivity is a sum of the discontinuous part related to the latent heat and the continuous part of the polarization change due to the applied electric field. In relaxor systems the phase transition is induced with electric field and the released/absorbed latent heat is rather small [55, 57]. In contrast, the ferroelectric $BaTiO_3$ undergoes the first-order ferroelectric phase transition at which much bigger amount of the latent heat is released/absorbed [93]. The ECE responsivity of $BaTiO_3$ as a function of the electric field obtained via direct ECE measurements is shown as a solid line in Figure 48. The electrocaloric responsivity shows a shift of the maximum away from the critical point towards lower electric fields (see the difference between the solid and dashed line in Figure 48). Here, the dashed line in Figure 48 is a schematic representation of the EC responsivity for a system with vanishingly small latent heat, like bulk relaxor systems. The influence of the latent heat in

those systems is negligible or zero which means that the main contribution to the ECE response is due to the continuous changes of the polarization which results in the responsivity maximum near the critical point [96].

The shift of the EC responsivity is a consequence of the released latent heat at the phase transition. The huge amount of the latent heat which is present at lower electric fields decreases fast when approaching the critical point and both solid and dashed line merges.

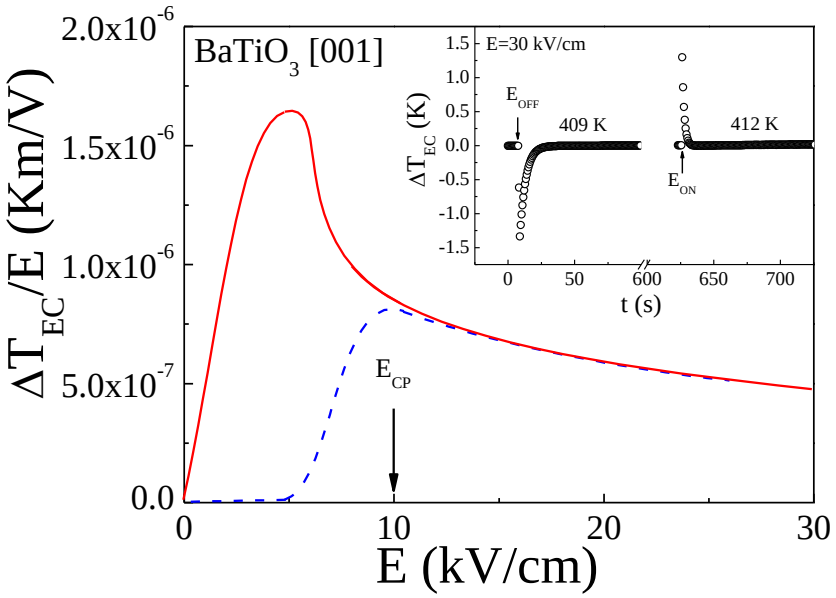

Figure 48: *EC responsivity*. The electric-field dependence of the electrocaloric responsivity $\Delta T_{EC}/E$ determined along the ferroelectric transition line shown in the $E-T$ phase diagram (Figure 42) for $BaTiO_3$ [001] single crystal. Solid line is obtained from the direct electrocaloric measurements (example shown in the inset) at different temperatures and magnitudes of the electric field. Dashed line is a schematic representation of the field dependence of the electrocaloric responsivity for a system with vanishingly small latent heat; in such a case, the maximum of $\Delta T_{EC}/E$ occurs near the critical field E_{CP} [96].

5 Conclusions

The enigma of the relaxor ferroelectrics ground state is as old as the first report about these materials. The question whether the relaxor phase is: (i) a ferroelectric phase broken up into nanodomains under the constraint of quenched random electric fields, or (ii) a special kind of dipolar glass state with randomly interacting polar nanoregions in the presence of random fields, is one of the basic unsolved tasks in the ferroelectric community. Until now, the X-ray, neutron scattering and TEM structural studies could not provide a final answer due to the surface effects which were found to have strong influence on these measurement methods and a small size of the polar nanoregions which is below the resolution possibility of these methods. In addition, several others studies like optical, dielectric, polarization or Raman studies were interpreted either in favor of the ferroelectric nanodomain or a dipolar glass concept. For these reasons, the main purpose of this work was to present additional experimental data which will contribute to the better understanding of the relaxor ferroelectric materials behavior and its ground state.

In particular, the electric field-induced phase transition was investigated in a canonical relaxor ferroelectric $Pb(Mg_{1/3}Nb_{2/3})O_3$ single crystal oriented along [110] direction. In order to distinguish between the ferroelectric nanodomain and dipolar glass concept, the nature of the phase transition line in $E-T$ phase diagram was studied.

For this purpose, several different experimental techniques have been utilized. Specifically, the isofield and isothermal measurements of the quasi-static polarization measurements $P(T)$ and heat capacity were done.

The polarization measurements show a discontinuous step at high enough electric field which is a typical sign of first-order phase transition. The isofield ac measurements of the excess of the heat capacity show an anomaly corresponding to the field-induced phase transition, whereas at zero electric field no anomaly was observed in a broad temperature range. Even more, the isothermal heat capacity measurements show a jump which overlaps with isothermal polarization measurements. The electric field-induced anomalies observed in the polarization and heat capacity data suggest the existence of the real phase transition from the relaxor glassy to ferroelectric state in PMN [110] single crystal. The quasi-isothermal latent heat study reveals the presence of the latent heat at the phase transition. This gives final proof that the transition line in the $E-T$ phase diagram is not a kind of conversion line at which the ferroelectric nanodomain aligned into a long-range ordered macrodomain state, but is rather the real first-order phase transition line between a dipolar glass phase and long-range ordered ferroelectric phase. The polarization and heat capacity anomalies together with the detected latent heat strongly support the dipolar glassy concept in PMN [110] single crystal. The detailed study of the latent heat also shows that the first-order transition line ends in a liquid-vapor type of the critical point at $T_{CP} \cong 240$ K and $E_{CP} \cong 8$ kV/cm. In contrast to sharp exhibited critical point in the single crystal the studies on PLZT relaxor ceramics do not exhibit a sharp definition of the critical point. The persistence of the latent heat at high temperatures suggests a smeared position of the critical point as a consequence of material isotropy. The existence of the critical point was also tested at the cubic to tetragonal phase transition in the ferroelectric $BaTiO_3$ single crystal oriented in [001] direction. The latent heat and dielectric studies

show that the field-induced paraelectric to ferroelectric phase transition line ends in the critical point at $T_{CP} \cong 412$ K and $E_{CP} \cong 10$ kV/cm.

The study of the critical point in the system is very important due to the strong enhancement of electromechanical and electrocaloric responses near the critical point. The investigated piezoelectric coefficient d_{31} as a function of temperature in relaxor ferroelectric PMN-0.26PT single crystal oriented in [100] and ferroelectric $BaTiO_3$ single crystal oriented in [001] show a critical behavior related to the proximity of the critical point. The d_{31} response obtained in [100] PMN-0.26PT is more complicated due to the presence of monoclinic phases. The presence of monoclinic phases which should act as an enhancement mechanism according to the theory of polarization rotation via intermediate monoclinic phases is actually responsible for prior cut-off of d_{31} critical response. On the other hand, the enhancement of d_{31} in $BaTiO_3$ which does not possess the morphotropic phase boundary, is a consequence of the proximity of the critical point. This implies that the enhancement of the piezoelectric response is most likely governed by the proximity of critical point and not necessarily only by the presence of the MPB.

The influence of the critical point on the electrocaloric responsivity was also investigated in $BaTiO_3$. In contrast to the bulk relaxor system where the maximum of the EC responsivity was observed near the critical point, the $BaTiO_3$ system exhibits the maximum of the EC responsibility slightly below the critical point. The shift of the maximum is a result of the interplay between two electrocaloric contributions related to: (i) the released latent heat and (ii) the continuous polarization change due to the applied electric field.

To conclude, the basic research of some canonical relaxors and ferroelectric materials was presented here. The investigation of electromechanical and electrocaloric properties could contribute to their better understanding and to engineer new even more improved advanced materials.

6 Acknowledgements

At first I would like to acknowledge the financial support of the Slovenian Ministry of Education, Science, Culture and Sport through the Young Researcher educational program.

Great thanks go also to my mentor Prof. Dr. Zdravko Kutnjak, who gave me a chance to be a member of Laboratory for Calorimetry and Dielectric Spectroscopy. I would like to thank him for his support and expert guidance and for his expert advice and assistance during the educational program.

Many thanks go also to my colleagues, George, Brigita, Vid, Cene, Andreja, and Adrijan who were responsible for a pleasant and social atmosphere within the research group.

In the end I would like to thank my family and friends, for their patience and support during the process of education.

7 References

[1] Cross, L. E.; Newnham, R. E. History of Ferroelectrics. In: Kingery, W.D. (ed.) *Ceramics and civilization III: High-technology ceramics-Past, present and future* (The American Ceramic Society, Westerville, Ohio, 1987).

[2] Heartling, G. H. Ferroelectric Ceramic: History and Technology. *Journal of American Ceramic Society* **82**, 798 (1999).

[3] Jona, F.; Shirane, G. Ferroelectric Crystals. In: Smoluchowski, R. and Kurti, N. *International Series of Monographs on Solid State Physics* (Pergamon Press, Oxford, 1962).

[4] Lines, M. E.; Glass, A. M. *Principles and Applications of Ferroelectric Materials* (Clarendon, Oxford, 1977).

[5] Whatmone, R. Ferroelectric material. In: Kasap, S.; Capper, P. (eds.) *Springer Handbook of Electronic and Photonic Material*. 597-623 (Springer, New York, 2007).

[6] Kittel, C. Dielectrics and Ferroelectrics. In: Johnson, S. (ed.) *Introduction to Solid State Physics 8^{-th}edition*. 453-486 (John Wiley & Sons, New York, 2005).

[7] Blinc, R. On the isotopic effects in the ferroelectric behavior of crystals with short hydrogen bonds. *Journal of Physical and Chemistry of Solids* **13**, 204 (1960).

[8] Ichikawa, M.; Motida, K.; Yamada N. Negative evidence for a proton-tunneling mechanism in the phase transition of KH_2PO_4-tyape crystals. *Physical Review B* **36**, 874 (1987).

[9] Nelmes, R. J. On the structural evidence for a direct proton tunnelling effect in the KH_2PO_4-type transition. *Journal of Physics C: Solid State Physics* **21**, L881 (1988).

[10] Reiter, G. F.; Mayers, J.; Platzman, P. Direct observation of tunneling in KDP using Neutron Compton Scattering. *Physical Review Letters* **89**, 135505 (2002).

[11] Devonshire, A. F. Theory of Barium Titanate. *Philosophical Magazine* 40, 1040 (1949).

[12] Valasek, J. Piezo-Electric Activity of Rochelle Salt under Various Conditions. *Physical Review* **19**, 478 (1922).

[13] von Hippel, A. Ferroelectricity, Domain Structure, and Phase Transitions of Barium Titanate. *Review of Modern Physics* **22**, 221 (1950).

[14] Merz, W. J. Duble Hysteresis Loop of $BaTiO_3$ at the Curie Point. *Physical Review* **91**, 513 (1953).

[15] Merz, W. J. Domain Formation and Domain Wall Motions in Ferroelectrics $BaTiO_3$ Single Crystals. *Physical Review* **95**, 690 (1954).

[16] Arlt, G. Review Twinning in ferroelectric and ferroelastic ceramics: stress relief. *Journal of Materials Science* **25**, 2655 (1990).

[17] Damjanović, D. Ferroelectric dielectric and piezoelectric properties of ferroelectric thin films and ceramics. *Reports on Progress in Physics* **61**, 1267 (1998).

[18] Samara, G. A. Ferroelectricity Revisited-Advances in Materials and Physics. In: Ehrenreich, H.; Spaepen, F. (eds.) *Solid State Physics Advances in Research and Applications* 59, 240-483 (Academic Press, New York, 2001).

[19] Bobnar, V.; Vodopivec, B.; Levstik, A.; Kosec, M.; Hilczer, B.; Zhang, Q. M.

Dielectric Properties of Relaxor-like Vinylidene Fluoride-Trifluoroethylene-Based Electroactive Polymers. *Macromolecules* **36**, 4436 (2003).

[20] Smolenskii, G. A.; Agranovskaya, A. I. Dielectric polarization of a number of complex compounds. *Soviet Physics Solid State* **1**, 1429 (1959).

[21] Cross, L. E. Relaxor Ferroelectrics. In: Heywang, W.; Lubitz, K.; Wersing, W. (eds.) *Springer Series in Material Science: Piezoelectricity* **114**, 131-155 (Springer, Berlin, 2008).

[22] Cross, L. E. Relaxor Ferroelectrics. *Ferroelectrics* **76**, 241 (1987).

[23] Kersten, O.; Rost, A.; Schmidt, G. Dielectric dispersion of relaxor ferroelectrics (SBN 75 and PLZT 8/65/35). *Physica Status Solidi a* **75**, 495 (1983).

[24] Viehland, D.; Jang, S. J.; Cross, L. E.; Wuttig, M. Deviation from Curie-Weiss behavior in relaxor ferroelectrics. *Physical Review B* **46**, 8003 (1992).

[25] Schmidt, G.; Arndt, H.; Borchhardt, G.; von Cieminski, J.; Petzsche, T.; Borman, K.; Sternberg, A.; Zirnite, A.; Isupov, V. A. Induced Phase Transitions in Ferroelectrics with Diffuse Phase Transition. *Physica Status Solid (a)* **63**, 501 (1981).

[26] Viehland, D.; Li, J. F.; Jang, S. J.; Cross, L. E.; Wuttig, M. Dipolar-glass model for lead magnesium niobate. *Physical Review B* **43**, 8316 (1991).

[27] Burns, G.; Dacol, F. H. Glassy polarization behavior in ferroelectric compounds $Pb(Mg_{1/3}Nb_{2/3})O_3$ and $Pb(Zn_{1/3}Nb_{2/3})O_3$. *Solis State Communications* **48**, 853 (1983).

[28] Viehland, D.; Jang, S. J.; Cross, L. E.; Wuttig, M. Freezing of the polarization fluctuation in lead magnesium niobate relaxor. *Journal of Applied Physics* **68**, 2916 (1990).

[29] Sommer, R.; Yushin, N. K.; van der Klink, J. J. Polar metastability and an electric-field-induced phase transition in the disordered perovskite $Pb(Mg_{1/3}Nb_{2/3})O_3$. *Physical Review B* **48**, 13230 (1993).

[30] Binder, K.; Young, A. P. Spin glasses: Experimental facts, theoretical concepts, and open questions. *Review of Modern Physics* **58**, 801 (1986).

[31] Fiory, A. T. Electric Dipole Interactions Among Polar Defects in Alkali Halides. *Physical Review B* **4**, 614 (1971).

[32] Höchli, U. T.; Knorr, K.; Loidl, A. Orientational glasses. *Advances in Physics* **39**, 405 (1990).

[33] Pirc, R.; Tadić, B.; Blinc, R. Random-field smearing of the proton-glass transition. *Physical Review B* **36**, 8607 (1987).

[34] Kutnjak, Z.; Filipič, C.; Levstik, A.; Pirc, R. Glassy Dynamics of $Rb_{0.40}(ND_4)_{0.60}D_2PO_4$. *Physical Review Letters* **70**, 4016 (1993).

[35] Colla, E. V.; Koroleva, E. Y.; Okuneva, N. M.; Vakhrushev, S. B. Low-frequency dielectric response of $PbMg_{1/3}Nb_{2/3}O_3$. *Journal Physics of Condensed Matter* **4**, 3671 (1991).

[36] Smolensky, G. Ferroelectrics with diffuse phase transition. *Ferroelectrics* **53**, 129 (1984).

[37] Levstik, A.; Kutnjak, Z.; Filipič, C.; Pirc, R. Glassy freezing in relaxor ferroelectric lead magnesium niobate. *Physical Review B* **57**, 11204 (1998).

[38] Colla, E. V.; Koroleva, E. Y.; Okuneva, N. M.; Vakhrushev, S. B. Long-Time Relaxation of the Dielectric Response in Lead Magnoniobat. *Physical Review Letters* **74**, 1681 (1995).

[39] Imry, Y.; Ma, S. Random Field Instability of the Ordered State of Continuous Symmetry. *Physical Review Letters* **35**, 1399 (1975).

[40] Westphal, V.; Kleemann, W.; Glinchuk, M. D. Diffuse Phase Transition and Random-Field-Induced Domain States of the "Relaxor" Ferroelectric

$PbMg_{1/3}Nb_{2/3}O_3$. *Physical Review Letters* **68**, 847 (1992).
[41] de Mathan, N.; Hussont, E.; Calvarint, S. G.; Gavarris, J. R.; Hewat, A. W.; Morell, A. A structural model for the relaxor $PbMg_{1/3}Nb_{2/3}0_3$ at 5 K. *Journal Physics of Condensed Matter* **3**, 8159 (1991).
[42] Husson, E.; Chubb, M.; Morell, A. Superstructure in $PbMg_{1/3}Nb_{2/3}O_3$ ceramics revealed by high resolution electron microscopy. *Materials Research Bulletin* **23**, 357 (1988).
[43] Vugmeister, B.E.; Glinchuk, M. D. Dipole glass and ferroelectricity in random-site electric dipole systems. *Reviews of Modern Physics* **62**, 993 (1990).
[44] Vugmeister, B. E.; Rabitz, H. Dynamics of interacting clusters and dielectric response in relaxor ferroelectrics. *Physical Review B* **57**, 7581 (1998).
[45] Blinc, R.; Dolinšek, J.; Gregorovič, A.; Zalar, B.; Filipič, C.; Kutnjak, Z.; Levstik, A.; Pirc, R. Local Polarization Distribution and Edwards-Anderson Order Parameter of Relaxor Ferroelectrics. *Physical Review Letters* **83**, 424 (1999).
[46] La-Orauttapong, D.; Toulouse, J.; Robertson, J. L.; Ye, Z.-G. Diffuse neutron scattering study of a disordered complex perovskite $Pb(Zn_{1/3}Nb_{2/3})O_3$ crystal. *Physical Review B* **64**, 212101 (2001).
[47] Hirota, K.; Ye, Z.-G.; Wakimoto, S.; Gehring, P. M.; Shirane, G. Neutron diffuse scattering from polar nanoregions in the relaxor $Pb(Mg_{1/3}Nb_{2/3})O_3$. *Physical Review B* **65**, 104105 (2002).
[48] Kutnjak, Z.; Filipič, C.; Pirc, R.; Levstik, A.; Farhi, R.; El Marssi, M. Slow dynamics and ergodicity breaking in a lanthanum-modified lead zirconate titanate relaxor system. *Physical Review B* **59**, 294 (1999).
[49] Chen, J.; Chan, H. M.; Harmer, M. P. Ordering Structure and Dielectric Properties of Undoped and La/Na-Doped $Pb(Mg_{1/3}Nb_{2/3})O_3$. *Journal of the American Ceramic Society* **72**, 593 (1989).
[50] Bobnar, V.; Kutnjak, Z.; Pirc, R.; Blinc, R.; Levstik, A. Crossover from Glassy to Inhomogeneous-Ferroelectric Nonlinear Dielectric Response in Relaxor Ferroelectrics. *Physical Review Letters* **60**, 6420 (1999).
[51] Pirc, R.; Blinc, R. Spherical random-bond-random-field model of relaxor ferroelectrics. *Physical Review B* **60**, 13470 (1999).
[52] Zhao, X.; Qu, W.; Tan, X.; Bokov, A. A.; Ye, Z.-G. Electric field-induced phase transitions in (111)-, (110)-, and (100)-oriented $Pb(Mg_{1/3}Nb_{2/3})O_3$ single crystals. *Physical Review B* **75**, 104106 (2007).
[53] Raevskaya, S. I.; Emelyanov, A. S.; Savenko, F. I.; Panchelyuga, M. S.; Raevski, I. P.; Prosandeev, S. A.; Colla, E. V.; Chen, H.; Lu, S. G.; Blinc, R.; Kutnjak, Z.; Gemeiner, P.; Dkhil B.; Kamzina, L. S. Quasivertical line in the phase diagram of single crystals of $PbMg_{1/3}Nb_{2/3}O_3$-$xPbTiO_3$ (x=0.00, 0.06, 0.13, and 0.24) with a giant piezoelectric effect. *Physical.. Review B* **76**, 060101 (2007).
[54] Kutnjak, Z.; Vodopivec, B.; Blinc, R. Anisotropy of electric field freezing of the relaxor ferroelectric $Pb(Mg_{1/3}Nb_{2/3})O_3$. *Physical Review B* **77**, 054102 (2008).
[55] Kutnjak, Z.; Petzelt, J.; Blinc, R. The giant electromechanical response in ferroelectric relaxors as a critical phenomenon. *Nature* **441**, 956 (2006).
[56] Kutnjak, Z.; Blinc, R.; Ishibashi, Y. Electric field induced critical points and polarization rotations in relaxor ferroelectrics. *Physical Review B* **76**,104102 (2007).
[57] Novak, N.; Pirc, R.; Wencka, M.; Kutnjak, Z. High-Resolution Calorimetric Study of $Pb(Mg_{1/3}Nb_{2/3})O_3$ Single Crystal. *Physical Review Letters* **109**, 037601 (2012).
[58] Durand, D.; Denoyer, F.; Lefur, D.; Currat, R.; Bernard, L. Neutron diffraction study of sodium nitrite in an applied electric field. *Journal de Physique Letters* **44**, L207 (1983).
[59] Yao, H.; Chan, T.; Garland, C. W. Smectic-C–-smectic-I critical point in a liquid

crystal mixture: Static and dynamic thermal behavior. *Physical Review E* **51**, 4585 (1995).

[60] Kutnjak, Z.; Garland, C. W.; Schatz, C. G.; Collings, P. J.; Booth, C. J.; Goodby, J. W. Critical point for the blue-phase-III—Isotropic phase transition in chiral liquid crystals. *Physical Review E* **53**, 4955 (1996).

[61] Glazounov, A. E.; Tagantsev, A. K.; Bell, A. J. Evidence for domain-type dynamics in the ergodic phase of the $PbMg_{1/3}Nb_{2/3}O_3$ relaxor ferroelectric. *Physical Review B* **53**, 11281 (1996).

[62] Tagantsev, A. K.; Glazounov, A. E. Mechanism of polarization response in the ergodic phase of a relaxor ferroelectric. *Physical Review B* **57**, 18 (1998).

[63] Bonneau, P.; Garnier, P.; Calvarin, G.; Husson, E.; Gavarri, J. R.; Hewat, A. W.; Morell, A. X-Ray and Neutron-Diffraction Studies of the Diffuse Phase-Transition in $PbMg_{1/3}Nb_{2/3}O_3$ Ceramics. *Journal of Solid State Chemistry* **91**, 350 (1991).

[64] Xu, G.; Zhong, Z.; Bing, Y.; Ye, Z.-G.; Stock, C.; Shirane, G. Ground state of the relaxor ferroelectric $Pb(Zn_{1/3}Nb_{2/3})O_3$. *Physical Review B* **67**, 104102 (2003).

[65] Conlon, K. H.; Luo, H.; Viehland, D.; Li, J. F.; Whan, T.; Fox, J. H.; Stock, C.; Shirane, G. Direct observation of the near-surface layer in $Pb(Mg_{1/3}Nb_{2/3})O_3$ using neutron diffraction. *Physical Review B* **70**, 172204 (2004).

[66] Bidaulty, O.; Licheronyz, M.; Hussonyz, E.; Morellx, A. The onset of an electric field-induced ferroelectric-like phase in the perovskite $PbMg_{1/3}Nb_{2/3}O_3$. *Journal Physics of Condensed Matter* **8**, 8017 (1996).

[67] Goreva,M. V.; Flerova, I. N.; Bondareva, V.S.; Sciaub, P. Heat Capacity Study of Relaxor $PbMg_{1/3}Nb_{2/3}O_3$ in a Wide Temperature Range. *Journal of Experimental and Theoretical Physics* **96**, 531 (2003).

[68] Goreva,M. V.; Bondareva, V.S.; Aleksandrov, K. S. Heat Capacity Study of PMN Near Field-Induced Phase Transition. *Ferroelectrics* **360**, 37 (2007).

[69] Tachibana, M.; Takayama-Muromachi, E. Thermal conductivity and heat capacity of the relaxor ferroelectric $[PbMg_{1/3}Nb_{2/3}O_3]_{1-x}[PbTiO_3]_x$. *Physical Review B* **79**, 100104 (2009).

[70] Park, S.-E.; Shrout, T. R. Ultrahigh strain and piezoelectric behavior in relaxor based ferroelectric single crystals. *Journal of Applied Physics* **82**, 1804 (1997).

[71] Noheda, B.; Cox, D. E.; Shirane, G.; Gonzalo, J. A.; Cross, L. E.; Park, S.-E. A monoclinic ferroelectric phase in the $Pb(Zr_{1-x}Ti_x)O_3$ solid solution. *Applied Physical Letters* **74**, 2059 (1999).

[72] Kelly, J.; Leonard, M.; Tantigate, C.; Safari, A. Effect of Composition on the Electromechanical Properties of $(1-x)Pb(Mg_{1/3}Nb_{2/3})O_3–xPbTiO_3$ Ceramics. *Journal of American Ceramic Society* **80**, 957 (1997).

[73] Mischenko, A. S.; Zhang, Q. M.; Scott, J. F.; Whatmore, R. W.; Mathur, N. D. Giant electrocaloric effect in thin-film $Pb_{0.95}Ti_{0.05}O_3$. *Science* **311**, 1270 (2006).

[74] Scott, J. F. Application of modern ferroelectrics. *Science* **315**, 954 (2007).

[75] Rožič, B.; Malič, B.; Uršič, H.; Holc, J.; Kosec, M.; Neese, B.; Zhang, Q. M.; Kutnjak, Z. Direct measurements of the giant electrocaloric effect in soft and solid ferroelectric materials. *Ferroelectrics* **405**, 26 (2010).

[76] Kholkin, A. L.; Pertsev, N. A.; Goltsev, A. V. Piezoelectricity and Crystal Symmetry. In: Safari, A.; Akdogan, E. K. (eds.) *Piezoelectric and Acoustic Materials for Transducer Applications.* 17-38 (Springer, New York, 2008).

[77] Damjanović, D. Comments on Origins of Enhanced Piezoelectric Properties in Ferroelectrics. *IEEE Transactions on Ultrasonics, Ferroelectrics, and Frequency Contrl* **56**, 1574 (2009).

[78] Uchino, K. *Piezoelectric Actuators and Ultrasonic Motors* (Kluwer Academic, Boston, 1996).

[79] Noheda, B.; Gonzalo, J. A.; Cross, L. E.; Guo, R.; Park, S.-E.; Cox, D. E.; Shirane, G. Tetragonal-to-monoclinic phase transition in a ferroelectric perovskite: The structure of $PbZr_{0.52}Ti_{0.48}O_3$. *Physical Review B* **61**, 8687 (2001).
[80] Xu, G.; Viehland, D.; Li, J. F.; Gehring, P. M.; Shirane, G. Evidence of decoupled lattice distortion and ferroelectric polarization in the relaxor system PMN-xPT. *Physical Review B* **68**, 212410 (2003).
[81] Fu, H.; Cohen, R. E. Polarization rotation mechanism for ultrahigh electromechanical response in single crystal piezoelectrics. *Nature* **403**, 281 (2000).
[82] Ahart, M.; Somayazulu, M.; Cohen, R. E.; Ganesh, P.; Dera, P.; Mao, H.-K.; Hemley, R. J.; Ren, Y.; Liermann, P.; Wu, Z. Origin of morphotropic phase boundaries in ferroelectrics. *Nature* **451**, 545 (2008).
[83] Davis, M.; Damjanović, D.; Setter, N. Electric-field-, temperature-, and stress-induced phase transitions in relaxor ferroelectric single crystals. *Physical Review B* **73**, 014115 (2006).
[84] Wada, S.; Suzuki, S.; Noma, T.; Suzuki, T.; Osada, M.; Kakihana, M.; Park, S.-E.; Cross, L. E.; Shrout, T. R. Enhanced Piezoelectric Property of Barium Titanate Single Crystals with Engineered Domain Configurations. *Japan Journal of Applied Physics* **38**, 5505 (1999).
[85] Kuwata, J.; Uchino, K.; Nomura, S. Dielectric and Piezoelectric Properties of $0.91Pb(Zn_{1/3}Nb_{2/3})O_3$-$0.09PbTiO_3$ Single Crystals. *Japan Journal of Applied Physics* **21**, 1298 (1982).
[86] Wada, S.; Kakemoto, H.; Tsurumi, T. Enhanced Piezoelectric Properties of Piezoelectric Single Crystals by Domain Engineering. *Materials Transactions* **45**, 178 (2004).
[87] Liu, D.; Li, J.-Y. The enhanced and optimal piezoelectric coefficients in single crystalline barium titanate with engineered domain configurations. *Applied Physics Letters* **83**, 1193 (2003).
[88] Novak, N.; Cordoyiannis, G.; Kutnjak, Z. Dielectric and Heat Capacity Study of $(Pb(Mg_{1/3}Nb_{2/3})O_3)_{0.74}$-$(PbTiO_3)_{0.26}$ Ferroelectric Relaxor Near the Cubic-Tetragonal-Rhombohedral Triple Point. *Ferroelectrics* **428**, 43 (2012).
[89] Bellaiche, L.; Garcia, A.; Vanderbilt, D. Electric-field induced polarization paths in $Pb(Zr_{1-x}Ti_x)O_3$ alloys. *Physical Review B* **64**, 060103 (2001).
[90] Iwata, M.; Ishibashi, Y. Phenomenological theory of morphotropic phase boundary with monoclinic phase in solid-solution systems of perovskite-type oxide ferroelectrics. *Japan Journal of Applied Physics* **44**, 3095 (2005).
[91] von Arx, A.; Bantle, W. Der Inverse Piezoeffekt des seignetteelektrischen Kristalls KH_2PO_4. *Helvetica Physica Acta* **17**, 298 (1944).
[92] Porta, M.; Lookman, T.; Saxena, A. Effects of criticality and disorder onpiezoelectric properties of ferroelectrics. *Journal Physics of Condensed Matter* **22**, 345902 (2010).
[93] Novak, N.; Pirc, R.; Kutnjak Z. Impact of critical point on piezoelectric and electrocaloric response in barium titanate. (submitted).
[94] Neese, B.; Chu, B.; Lu, S.-L.; Wang, Y.; Furman, E.; Zhang, Q. M. Large electrocaloric effect in ferroelectric polymers near room temoperature. *Science* **321**, 821 (2008).
[95] Rožič, B.; Kosec, M.; Uršič, H.; Holc, J.; Malič, B.; Zhang, Q. M.; Blinc, R.; Pirc, R.; Kutnjak, Z. Influence of the critical point on the electrocaloric response of relaxor ferroelectrics. *Journal of Applied Physics* **110**, 064118 (2011).
[96] Pirc, R.; Kutnjak, Z.; Blinc, R.; Zhang, Q. M. Electrocaloric effect in relaxor ferroelectrics. *Journal of Applied Physics* **110**, 074113 (2011).
[97] Lu, S.-G.; Rožič, B.: Zhang, Q. M.; Kutnjak, Z.; Li, X.; Furman, E.; Gorny, L. J.;

Lin, M.; Malič, B.; Kosec, M.; Blinc, R.; Pirc, R. Organic and inorganic relaxor ferroelectrics with giant electrocaloric effect. *Applied Physics Letters* **97**, 162904 (2010).

[98] Rožič, B.; Malič, B.; Uršič, H.; Holc, J.; Kosec, M.; Kutnjak, Z. Direct measurements of the electrocaloric effect in bulk $PbMg_{1/3}Nb_{2/3}O_3$ (PMN) ceramics. *Ferroelectrics* **421**, 103 (2011).

[99] Rožič, B.; Kutnjak, Z.; Neese, B.; Lu, S.-G.; Zhang, Q. M. Electrocaloric effect in the relaxor in the relaxor ferroelectric polymer composition $P(VDF\text{-}TrFE)_{0.90}$-$P(VDF\text{-}CTFE)_{0.10}$. *Phase Transitions* **83**, 819 (2010).

[100] Lu, S.-G.; Rožič, B.; Zhang, Q. M.; Kutnjak, Z.; Neese, B.; Enhanced electrocaloric effect in ferroelectric poly(vinylidene-fluoride/trifluoroethylene) 55/45 mol% copolymer at ferroelectric-paraelectric transition. *Applied Physics Letters* **98**, 122906 (2011).

[101] Akcay, G.; Alpaya, S. P.; Mantese, J. V.; Rossetti, G. A. Magnitude of the intrinsic electrocaloric effect in ferroelectric perovskite thin films at high electric fields. *Applied Physics Letters* **90**, 252909 (2007).

[102] Bai, Y.; Ding, K.; Zheng, G.-P.; Shi, S.-Q.; Cao, J.-L.; Qiao, L. The electrocaloric effect around the orthorhombictetragonal first-order phase transition in $BaTiO_3$. *American Institute of Physics Advances* **2**, 022162 (2012).

[103] Bai, Y.; Ding, K.; Zheng, G.-P.; Shi, S.-Q.; Qiao, L. Entropy-change measurement of electrocaloric effect of $BaTiO_3$ single crystal. *Physica Status Solidi A* **209**, 941 (2012).

[104] Hill, N. E. *Dielectric properties and molecular behavior* (Van Nostrand, London, 1969).

[105] Kremer, F.; Schönhals, A. *Broadband Dielectric Spectroscopy* (Springer-Verlag Berlin, Heidelberg, Germany, 2003).

[106] Cole, K. S.; Cole, R. H. Dispersion and Absorption in Dielectrics. *Journal of Chemical Physics* **9**, 341 (1941).

[107] Okada, K.; Sekino, T. *Agilent Technologies Impedance Measurement Handbook* (Agilent Technologies Co. Ltd, USA, 2003).

[108] Vodopivec, B. The glassy phase and induced ferroelectricity in relaxor systems. *Doctoral dissertation* (University of Ljubljana Faculty of Mathematics and Physics, Ljubljana, 2005).

[109] Damjanović, D. An equivalent electric circuit of a piezoelectric bar resonator with a large piezoelectric phase angle. *Ferroelectrics* **110**, 129 (1990).

[110] Bobnar, V.; Kutnjak, Z.; Levstik, A. Temperature Dependence of Piezoelectric, Dielectric, and Elastic Properties of Lead Lanthanum Zirconate Titanate Ceramics. *Japan Journal of Applied Physics* **37**, 5634 (1998).

[111] Garland, C. W.; Nounesis, G. Critical-behavior at nematic smectic A phase transitions. *Physical Review E* **49**, 2964 (1994).

[112] Djurek, D.; Baturic-Rubcic, J.; Franulovic, K. Specific-Heat Critical Exponents near the Nematic-Smectic-A Phase Transition. *Physical Review Letters* **33**, 1126 (1974).

[113] Cordoyiannis, G.; Lebar, A.; Zalar, B.; Žumer, S.; Finkelmann, H.; Kutnjak, Z. Criticality Controlled by Cross-Linking Density in Liquid Single-Crystal Elastomers. *Physical Review Letters* **99**, 197801 (2007).

[114] Garland, C. W. Calorimetric studies. In Kumar, S. (ed.) *Experimental Study of Physical Properties and Phase Transitions.* 240−294 (Cambridge University Press, Cambridge, 2001) and references cited therein.

[115] Yao, H.; Ema, K.; Garland, C.W. Nonadiabatic scanning calorimeter. *Review of Scientific Instruments* **69**, 172 (1998) and references cited therein.

[116] Chan, T. Smectic Phase Transitions in Chiral Liquid Crystals. *Doctoral dissertation* (Massachusetts Institute of Technology, Boston, 1995).
[117] Rožič, B. Giant energy-conversion effects in soft and solid advanced materials. *Doctoral dissertation* (Jožef Stefan International Postgraduate School, Ljubljana, 2012).
[118] Setter, N.; Cross, L. E. The role of B-site cation disorder in diffuse phase transition behavior of perovskite ferroelectrics. *Journal of Applied Physics* **51**, 4356 (1980).
[119] Boulesteix, C.; Varnier, F.; Llebaria, A.; Husson, E. Numerical Determination of the Local Ordering of $PbMg_{1/3}Nb_{2/3}O_3$ (PMN) from High-Resolution Electron-Microscopy Images. *Journal of Solid State Chemistry* **108**, 141 (1994).
[120] Akbas, M. A.; Davies, P. K. Domain Growth in $Pb(Mg_{1/3}Ta_{2/3})O_3$ Perovskite Relaxor Ferroelectric Oxides. *Journal of American Ceramic Society* **80**, 2933 (1997).
[121] Toulouse, J.; Jiang, F.; Svitelskiy, O.; Chen, W.; Ye, Z.-G. Temperature evolution of the relaxor dynamics in $Pb(Zn_{1/3}Nb_{2/3})O_3$: A critical Raman analysis. *Physical Review B* **72**, 184106 (2005).
[122] Gehring, P. M.; Hiraka, H.; Stock, C.; Lee, S.-H.; Chen, W.; Ye, Z.-G.; Vakhrushev, S. B.; Chowdhuri, Z. Reassessment of the Burns temperature and its relationship to the diffuse scattering, lattice dynamics, and thermal expansion in relaxor $Pb(Mg_{1/3}Nb_{2/3})O_3$. *Physical Review B* **79**, 224109 (2009).
[123] Bobnar, V.; Filipič, C.; Levstik, A.; Kutnjak, Z. High-temperature dielectric response of $(1-x)Pb(Mg_{1/3}Nb_{2/3})O_3-xPbTiO_3$: Does Burns temperature exist in ferroelectric relaxors?. *Journal of Applied Physics* **107**, 084104 (2010).
[124] Kleemann, W.; Random-Field Induced Antiferromagnetic, Ferroelectric and Structural Domain State. *International Journal of Modern Physics B* **7**, 2469 (1993).
[125] Nattermann, T. Theory of the Random Field Ising Model. In: Young, A. P. (ed.) *Spin Glasses and Random Fields* 277 (World Scientific, Singapore, 1998).
[126] Kleemann, W. Random fields in dipolar glasses and relaxors. *Journal of Non-Crystalline Solids* **307-310**, 66 (2002).
[127] Imry, Y.; Ma, S.-K. Random-Field Instability of the Ordered State of Continuous Symmetry. *Physical Review Letters* **35**, 1399 (1975).
[128] Imbrie, J. Z. Lower Critical Dimension of the Random-Field Ising Model. *Physical Review Letters* **53**, 1747 (1984).
[129] Fu, D.; Taniguchi, H.; Itoh, M.; Koshihara, S.-Y.; Yamamoto, N.; Mori, S. Relaxor $PbMg_{1/3}Nb_{2/3}O_3$: A Ferroelectric with Multiple Inhomogeneities. *Physical Review Letters* **103**, 207601 (2009).
[130] Bobnar, V.; Kutnjak, Z.; Pirc, R.; Levstik, A.; Electric-field–temperature phase diagram of the relaxor ferroelectric lanthanum-modified lead zirconate titanate. *Physical Review B* **60**, 6420 (1999).
[131] Vakhrushev, S. B.; Kiatb, J.-M.; Dkhilb, B. X-Ray Study of the Kinetics of Field Induced Transition from the Glass-like to the Ferroelectric Phase in Lead Magnoniobate. *Solid State Communications* **103**, 477 (1997).
[132] Ye, Z.-G. Relaxor Ferroelectric Complex Perovskites: Structure, Properties and Phase Transitions. *Key Engineering Materials* **155-156**, 81 (1998).
[133] Pirc, R.; Kutnjak, Z.; Novak, N. Compressible spherical dipolar glass model of relaxor ferroelectrics. *Journal of Applied Physics* **112**, 114122 (2012).
[134] Farhi, R.; El Marssi, M.; Dellis, J-L.; Picot, J-C.; Morell, A. On the nature of the glassy state in 9/65/35 PLZT ceramics. *Ferroelectrics* **176**, 99 (1996).
[135] Vodopivec, B., Filipič, C.; Levstik, A.; Holc, J.; Kutnjak, Z.; Beige, H. Dielectric properties of partially disordered lanthanum-modified lead zirconate titanate relaxor

ferroelectrics. *Physical Review B* **69**, 224208 (2004).
[136] Bobnar, V.; Kutnjak, Z.; Pirc, R., Levstik, A. Relaxor freezing and electric-field induced ferroelectric transition in a lanthanum lead zirconate titanate ceramics. *Europhysics Letters* **48**, 326 (1999).
[137] Bobnar, V.; Kutnjak, Z.; Levstik, A. Nonlinear dielectric response of relaxor PLZT ceramics in a dc bias electric field. *Journal of the European Ceramic Society* **21**, 1319 (2001).
[138] Kutnjak, Z.; Filipič, C.; Levstik, A. Nonlinear dielectric constant as function of bias electric field in relaxor material. *Journal of the European Ceramic Society* **21**, 1313 (2001).
[139] Viehland, D.; Li, J. F.; Jang, S. J.; Cross, L. E.; Wuttig, M. Glassy polarization behavior of relaxor ferroelectrics. *Physical Review B* **46**, 8013 (1992).
[140] Bovtun, V.; Petzelt, J.; Porokhonskyy, V.; Kamba, S.; Yakimenko, Y.; Structure of the dielectric spectrum of relaxor ferroelectrics. *Journal of the European Ceramic Society* **21**, 1307 (2001).
[141] Thurnaurer, H.; Deaderick, J. U.S. Patent No. 2, 429, 588, Oct. 21, 1947; filed (1941).
[142] Meyerhofer, D. Transition to the Ferroelectric State in Barimin Titanate. *Physical Review* **112**, 413 (1958).
[143] Noheda, B.; Cox, D. E., Shirane, G.; Gao, J.; Ye, Z.-G. Phase diagram of the ferroelectric relaxor (1-x)$PbMg_{1/3}Nb_{2/3}O_3$-x$PbTiO_3$. *Physical Review B* **66**, 054104 (2002).
[144] Singh, A. K.; Pandey, D. Evidence for M_B and M_C phases in the morphotropic phase boundary region of (1-x)[$Pb(Mg_{1/3}Nb_{2/3})O_3$]-xPbTiO3: A Rietveld study. *Physical Review B* **67**, 064102 (2003).
[145] Iwata, M.; Kutnjak, Z.; Ishibashi, Y.; Blinc, R. Theoretical Analysis of the Temperature–Field Phase Diagrams of Perovskite-Type Ferroelectrics. *Journal of the Physical Society of Japan* **77**, 034703 (2008).
[146] Zgonik, M.; Bernasconi, P.; Duelli, M.; Schlesser, R.; Gunter, P.; Garrett, M. H.; Rytz, D.; Zhu, Y.; Wu, X. Dielectric, elastic, piezoelectric, electro-optic, and elasto-optic tensors of $BaTiO_3$ crystals. *Physical Review B* **50**, 5941 (1994).
[147] Li, Y. L.; Cross, L. E.; Chen, L. Q. A phenomenological thermodynamic potential for $BaTiO_3$ single crystals. *Journal of Applied Physics* **98**, 064101 (2005).

Index of Figures

Appendix: Personal bibliography for the period of 2009–2013

Publications related to this thesis

I. Scientific articles (first author)

1. Novak, N.; Pirc, R.; Kutnjak, Z. Impact of the electric field on the freezing dynamics of $Pb(Mg_{1/3}Nb_{2/3})O_3$. *Ferroelectrics* **426**, 31 (2012).
2. Novak, N.; Rožič, B.; Holc, J.; Kosec, M.; Pirc, R.; Kutnjak, Z. Thermal response at the dipolar-glassto ferroelectric transition in structuraly disordered ferroelectric materials. *Ferroelectrics* **426**, 223 (2012).
3. Novak, N.; Cordoyiannis, G.; Kutnjak, Z. Dielectric and Heat Capacity Study of $(Pb(Mg_{1/3}Nb_{2/3})O_3)_{0.74}$-$(PbTiO_3)_{0.26}$ Ferroelectric Relaxor Near the Cubic-Tetragonal-Rhombohedral Triple Point. *Ferroelectrics* **428**, 43 (2012).
4. Novak, N.; Pirc, R.; Wencka, M.; Kutnjak, Z. High-Resolution Calorimetric Study of $Pb(Mg_{1/3}Nb_{2/3})O_3$ Single Crystal. *Physical Review Letters* **109**, 037601 (2012).
5. Novak, N.; Kutnjak, Z. Calorimetric study of field-induced ferroelectric transition in $Pb(Mg_{1/3}Nb_{2/3})O_3$ relaxor ferroelectrics. in: *ISAF ECAPD PMF 2012*. Danvers: IEEE, 2012, str. 1-4. http://ieeexplore.ieee.org/xpl/articleDetails.jsp;jsessionid=NGGvQZVhxvCYy4l5xGXLBDYPWWy2ln7Nk1wzFxkZ2Kyd2tVYzwTW!58582823?arnumber=6297770&contentType=Conference+Publications

II. Scientific articles (co-author)

6. Pirc, R.; Kutnjak, Z.; Novak, N. Compressible spherical dipolar glass model of relaxor ferroelectrics. *Journal of Applied Physics* **112**, 114122 (2012).

ACCEPTED ARTICLES

SUBMITTED ARTICLES

7. Novak, N.; Pirc, R.; Kutnjak Z. Impact of critical point on piezoelectric and electrocaloric response in barium titanate.

8. Novak, N.; Kutnjak, Z. Hysteresis of field-induced ferroelectric transition in $Pb(Mg_{1/3}Nb_{2/3})O_3$ relaxor ferroelectrics.

ARTICLES IN PREPARATION FOR PUBLICATION

9. Novak, N.; Pirc, R.; Kutnjak Z. Critical point 9/65/35 PLZT ceramic.

COBISS Co-operative Online Bibliographic system & services COBISS

NIKOLA NOVAK [32160]

ARTICLES AND OTHER COMPONENT PARTS

1.01 Original scientific article

1. Novak, N.; Pirc, R.; Kutnjak, Z. Impact of the electric field on the freezing dynamics of Pb(Mg[sub](1/3)Nb[sub](2/3))O[sub]3 : special issue : professor Wolfgang Kleemann in honor of his 70th birthday. *Ferroelectrics* **426**, 31–37 (2012).

2. Novak, N.; Rožič, B.; Holc, J.; Kosec, M.; Pirc, R.; Kutnjak, Z. Thermal response at the dipolar-glass to ferroelectric transition in structuraly disordered ferroelectric materials : special issue : professor Wolfgang Kleemann in honor of his 70th birthday. *Ferroelectrics* **426**, 223–229 (2012).

3. Novak, N.; Cordoyiannis, G.; Kutnjak, Z. Dielectric and heat capacity study of (Pb(Mg[sub](1/3)Nb[sub](2/3))O[sub]3)[sub](0.74) ferroelectric relaxor near the cubic-tetragonal-Rrombohedral triple point. *Ferroelectrics* **428**, 43–48 (2012).

4. Viršek, M.; Novak, N.; Filipič, C.; Kump, P.; Remškar, M.; Kutnjak, Z. Transport properties in MoS[sub]2 selective morphology system. *Journal of Applied Physics* **112**, 103710-1-103710-6 (2012).

5. Novak, N.; Pirc, R.; Wencka, M.; Kutnjak, Z. High-resolution calorimetric study of Pb(Mg[sub](1/3)Nb[sub](2/3)O[sub]3 single crystal. *Physical Review Letter*. **109**, 037601-1-037601-5 (2012).

6. Pirc, R.; Kutnjak, Z.; Novak, N. Compressible spherical dipolar glass model of relaxor ferroelectrics. *Journal of Applied Physics* **112**, 114122-1-114122-5 (2012).

7. Kralj, S.; Cordoyiannis, G.; Jesenek, D.; Zidanšek, A.; Lahajnar, G.; Novak, N.; Amenitsch, H.; Kutnjak, Z. Dimensional crossover and scaling behavior of a smectic liquid crystal confined to controlled-pore glass matrices. *Soft matter* **8**, 2460–2470 (2012).

1.08 Published scientific conference contribution

8. Novak, N.; Kutnjak, Z. Calorimetric study of field-induced ferroelectric transition in Pb(Mg[sub](1/3)Nb[sub](2/3))O[sub]3 relaxor ferroelectrics. V: *ISAF ECAPD PMF 2012*, 1–4 (Danvers: IEEE, 2012).

9. Novak, N.; Kutnjak, Z. Basic study of relaxors : materials for high technological devices. V: Petelin, D. (ur.); Tavčar, A. (ur.); Kaluža, B. (ur.). *Zbornik 4. študentske konference Mednarodne podiplomske šole Jožefa Stefana* (Mednarodna podiplomska šola Jožefa Stefana, Ljubljana, 2012).

10. Novak, N.; Kutnjak, Z. Enhancing the materials for new generation of piezoelectric devices. V: Petelin, D. (ur.); Tavčar, A. (ur.); Rožič, B. (ur.); Pogorelc, B. (ur.). *Zbornik prispevkov 3. študentske konference Mednarodne podiplomske šole Jožefa Stefana*. 183–189 (Mednarodna podiplomska šola Jožefa Stefana, Ljubljana, 2011).

1.10 Published scientific conference contribution (invited lecture)

11. Pirc, R.; Rožič, B.; Novak, N.; Kutnjak, Z. Field-induced phase transitions in relaxor ferroelectrics : theory and experiment. V: *International Workshop on Relaxor Ferroelectrics : Edesheim.* 26 (Technische Universität, Darmstadt, Germany, 2012).

1.12 Published scientific conference contribution abstract

12. Novak, N.; Pirc, R.; Wencka, M.; Kutnjak, Z. Calorimetric study of ferroelectric transition in [110] PMN relaxor ferroelectric. V: ISAF ECAPD PFM 2012, 21st International Symposium on Applications of Ferroelectrics, 11th European Conference on Applications of Polar Dielectrics, 4th Conference Piezoresponse Force Microscopy and Nanoscale Phenomena in Polar Materials, *Abstract book.* 464 (IEEE Ultrasonics, Ferroelectrics, and Frequency Control Society, Aveiro, Portugal, 2012).

13. Novak, N.; Kutnjak, Z.; Holc, J. Study of thermodynamic phase transition line in PLZT ceramic. V: ISAF ECAPD PFM 2012, 21st International Symposium on Applications of Ferroelectrics, 11th European Conference on Applications of Polar Dielectrics,4th Conference Piezoresponse Force Microscopy and Nanoscale Phenomena in Polar Materials, *Abstract book*. 485 (IEEE Ultrasonics, Ferroelectrics, and Frequency Control Society, Aveiro, Portugal, 2012).

14. Novak, N.; Pirc, R.; Wencka, M.; Kutnjak, Z. Advances in dielectric materials and electronic devices. V: MS&T'12, Materials Science & Technology 2012, Conference and Exhibition, *Final program*. 1 (elektronski vir, Pittsburgh, USA, 2012).

15. Novak, N.; Pirc, R.; Wencka, M.; Kutnjak, Z. The ground state and the enhancement of the electromechanical effect in ferroelectric relaxor materials. V: MS&T'12, Materials Science & Technology 2012, Conference and Exhibition, *Final program*. 1 (Elektronski vir, Pittsburgh, USA, 2012).

16. Kralj, S.; Cordoyiannis, G.; Jesenek, D.; Zidanšek, A.; Lahajnar, G.; Novak, N.; Amenitsch, H.; Kutnjak, Z. Dimensional crossover and scaling behavior of a smectic liquid crystal confined to controlled-pore glass matrices. V: 18th Symposium on Thermophysical Properties, *Program*. 1 (Elektronski vir, Boulder, Colorado, USA, 2012).

17. Jesenek, D.; Cordoyiannis, G.; Novak, N.; Kutnjak, Z.; Amenitsch, H.; Kralj, S. Phase behavior character of strongly confined nematic and smectic liquid crystals. V: Repnik, R. (ur.) 11th European Conference on Liquid Crystals ECLC 2011, *Conference programme*. 1 (Faculty of Natural Sciences and Mathematics, Maribor, 2011).

18. Cordoyiannis, G.; Jesenek, D.; Zidanšek, A.; Novak, N.; Kutnjak, Z.; Lahajnar, G.; Amenitsch, H.; Nounesis, G.; Rosso, R.; Virga, E. G.; Kralj, S. Universal behaviour of liquid crystals confined in controlled-pore glasses. V: Repnik, Robert (ur.). 11th European Conference on Liquid Crystals ECLC 2011, *Conference programme*. 1 (Faculty of Natural Sciences and Mathematics, Maribor, 2011).

19. Novak, N.; Cordoyiannis, G.; Kutnjak, Z. Dielectric and heat capacity study of (Pb(Mg[sub](1/3)Nb[sub](2/3)O[sub]3)[sub](1-x)-(PbTiO[sub]3)[sub]x ferroelectric relaxor near the morphotropic phase boundary. V: 12th European Meeting on Ferroelectricity, *EMF 2011 program*. 33 (ICMCB-CNRS, Bordeaux, France, 2011).

20. Novak, N.; Blinc, R.; Kutnjak, Z. Enhancement of the electromechanical effect near the critical point in ferroelectric relaxor material. V: *Proceedings of the 20th IEEE International Symposium on Applications of Ferroelectrics, [and] International Symposium on Piezoresponse Force Microscopy & Nanoscale phenomena in Polar Materials*. 83 (IEEE Ultrasonics, Ferroelectrics, and Frequency Control Society, Vancouver, Canada, 2011).

21. Novak, N.; Cordoyiannis, G.; Kutnjak, Z. Improvement of piezoelectric response in (Pb(Mg[sub](1/3)Nb[sub](2/3))O[sub]3)[sub](0,74)-(PbTiO[sub]3)[sub](0,26) ferroelectric relaxor near the morphotropic phase boundary. V: *Proceedings of the International Symposium on Integrated Functionalities*. 133 (University of Cambridge, Cambridge, 2011).

22. Jesenek, D.; Cordoyiannis, G.; Kralj, S.; Lahajnar, G.; Zidanšek, A.; Novak, N.; Kutnjak, Z. Structural and phase properties of smectic liquid crystals strongly-confined in controlled-pore glass matrices. V: Perkowski, P. (ur.). V: *Programme & abstracts of the 19th* Conference *on Liquid Crystals (Chemistry, Physics & Applications)*. 1 (elektronski vir, Międzydroje, Poland, 2009).

23. Novak, N.; Cordoyiannis, G.; Kutnjak, Z.; Kamba, S. Study of the electromechanical response in (Pb(Mg[sub](1/3)Nb[sub](2/3))O[sub]3)[sub](0,74)[sup]-(PbTiO[sub]3)[sub](0,26) ferroelectric relaxor near the morphotropic phase boundary. V: *Proceedings of the 19th International Symposium on the Applications of Ferroelectrics, 10th European Conference on the Applications of Polar Dielectrics.* 131 (Heriot-Watt University Edinburgh, UK, 2010).

24. Novak, N.; Cordoyiannis, G.; Kutnjak, Z.; Kamba, S. Elektromehanski odziv (Pb(Mg[sub](1/3)Nb[sub](2/3))O[sub]3)[sub](0.74)-(PbTiO[sub]3)[sub](0.26) feroelektričnega relaksorja blizu morfotropne fazne meje. V: Humar, M. (ur.); Škarabot, M. (ur.). *Zbornik povzetkov 7. konference fizikov v osnovnih raziskavah, Portorož 2010*. 63 (DMFA - založništvo, Ljubljana, 2010).

MONOGRAPHS AND OTHER COMPLETED WORKS

2.11 Undergraduate thesis

25. Novak, N. *Fazna ločitev : diplomsko delo*, (Pedagoška fakulteta, Fizika, Maribor,2005).

26. Novak, N. *Gorivne celice : diplomsko delo*, (Pedagoška fakulteta, Tehniška vzgoja, Maribor, 2005).

PERFORMED WORKS (EVENTS)

3.15 Unpublished conference contribution

27. Kralj, S.; Cordoyiannis, G.; Jesenek, D.; Zidanšek, A.; Lahajnar, G.; Novak, N.; Amenitsch, H.; Kutnjak, Z. Dimensional crossover and scaling behavior of a smectic liquid crystal confined to controlled-pore glass matrices. *Paper presented at the 18th Symposium on Thermophysical Properties* (University of Colorado Boulder, Colorado, USA, 2012).

28. Novak, N. Enhancement of the electromechanical effect near the critical point in ferroelectric relaxor materials. *Paper presented at PAC RIM 9, 9th International Meeting of Pacific Rim Ceramic Societies*, (Pacific Rim Ceramic Societies, Cairns, Australia, 2011).

Unallocated

29. Novak, N. Fazna ločitev v naravi in družbi. *Življenje in tehnika* **60**, 10, 63–65 (2009).

Selected format of bibliographic unit: ISO 690
Source of bibliographic records: shared data base COBISS.SI/COBIB.SI